

BULGARIAN CHEMICAL COMMUNICATIONS

2022 Volume 54 / Special Issue A

*Journal of the Chemical Institutes
of the Bulgarian Academy of Sciences
and of the Union of Chemists in Bulgaria*



Preface

Dear reader,

This special issue of Bulgarian Chemical Communications contains a selection of full text articles from scientific investigations presented at the 8th National Crystallographic Symposium with international participation (NCS'21), which took place from 1st to 4th September at the Creativity House of the Bulgarian Academy of Sciences, Varna. The manuscript selection was based on the Journal's regular peer review criteria. The papers in the present issue outline the latest research interests of Bulgarian crystallographers. They cover a wide interdisciplinary range of topics including the preparation and investigation of already known advanced and newly emerging materials, as well as special attention is paid to the synthesis procedures, investigation of the structure and properties. We sincerely hope and believe that this issue reveals the high quality of Bulgarian crystallographers' research and that it will serve as a good foundation for provoking business interest in the investment in innovations and production of advanced materials.

The National Crystallographic Symposium is the principal forum of the Bulgarian Crystallographic Society and has become a regular meeting of the growing Bulgarian crystallographic community during the years. The former symposia became leading scientific events and opportunity to meet and share ideas not only for the Bulgarian crystallographers, but also for numerous participants coming from different countries worldwide. Major objective of these events is to gather the crystallographic community in Bulgaria and to exchange knowledge in the fields of structural crystallography, crystal chemistry, crystal physics, mineralogy and advanced materials science. The present meeting has also provided an excellent opportunity for young and experienced scientists from Bulgaria and abroad to exchange ideas and best practices, as well as to lay the foundations of new collaborations and initiate successful common projects

while enjoying the pleasant atmosphere near the Black Sea coast.

Two colleagues and outstanding scientists – Prof. Andrei Apostolov and Assoc. Prof. Venelin Krastev from the Faculty of Physics, Sofia University “St. Kl. Ohridski” were decorated with the special honorary sign of the Bulgarian Crystallographic Society for their overall activity as co-founders of the Bulgarian Crystallographic Society and for their contribution to the development of crystallography in Bulgaria, as well as for their dedicated scientific activity.

Lecturers at the NCS'21 were leading researchers and experts: Christian Rüssel, Friedrich Schiller University, Germany; Valentin Valtchev, ENSICAEN, University of Caen – CNRS, France; Valentina Ivanova, Institut List, CEA Saclay Nano-INNOV, Commissariat à l'énergie atomique et aux énergies alternatives, France; Ognyan Petrov, IMC-BAS, Bulgaria; Svetoslav Stankov, Institute for Photon Science and Synchrotron Radiation, Karlsruhe Institute of Technology, Germany; Tanya Vitova, Institute for Nuclear Waste Disposal, Karlsruhe Institute of Technology, Germany; Snejana Bakardjieva, Institute of Inorganic Chemistry of the Czech Academy of Sciences, Czech Republic; Plamen Tchoukov, TCH NanoSolutions, Edmonton, Canada; Martin Fabián, Institute of Geotechnics, Slovak Academy of Sciences, Slovakia; Venelin Krastev, Sofia University “St. Kl. Ohridski”, Bulgaria; Liliya Vladislavova, EMPA, Switzerland; Silvana Dimitrijević, Mining and Metallurgy Institute Bor, Serbia; Zara Cherkezova-Zheleva, IC-BAS, Bulgaria; Ruzha Harizanova, UCTM-Sofia, Bulgaria.

The investigations presented at the NCS'21 were focused on the current topics in materials design and preparation, as well as on various advanced characterization techniques. 18 oral and 59 poster presentations encompassing different topics and aspects of



crystallography were presented by 217 participants from 17 countries. 22 out of 77 reports were presented by PhD students and young scientists. They had the opportunity to disseminate their research results, to discuss problems, ask questions and to share their personal ideas and opinion. According to a long-term and well-established tradition, the organizers of the National Crystallographic Symposia encourage and support the initiation of successful scientific career of young researchers by

awarding the best young scientist poster presentations as recognition of their achievements.

The symposium NCS'21 has been organized with the kind financial support of our traditional partners and sponsors – Malvern-PANalytical, Aurubis-Bulgaria, Aquachim, Labexpert, InfoLab, ELTA'90 and Gravelita Ltd.

We are looking forward to welcome you at the 9th National Crystallographic Symposium, 2023.

*Prof. Zara Cherkezova-Zheleva,
Assoc. Prof. Ruzha Harizanova
Co-chairs of the Organizing Committee and
Guest editors of the Special issue of Bulgarian
Chemical Communications*

Tandem hydroxymethylation-acetal protection of phenols under Eschweiler-Clarke conditions. The activation role of phenyl-azo moiety

V. Kurteva^{1*}, R. Rusev², B. Shivachev², R. Nikolova²

¹ Institute of Organic Chemistry with Centre of Phytochemistry, Bulgarian Academy of Sciences, Acad. G. Bonchev str., bl. 9, 1113 Sofia, Bulgaria

² Institute of Mineralogy and Crystallography “Acad. Ivan Kostov”, Bulgarian Academy of Sciences, Acad. G. Bonchev str., bl. 107, 1113 Sofia, Bulgaria

Received November 09, 2021; Accepted January 16, 2022

A fast and efficient direct protocol for benzo[1,3]dioxin' synthesis *via* tandem hydroxymethylation–acetal protection of phenols under Eschweiler-Clarke conditions is developed. The scope of the reaction is studied and is found that the presence of azo-dye fragment is crucial for effective conversion. The structures of the products are assigned on the basis of NMR spectra and confirmed by single crystal XRD.

Keywords: benzo[1,3]dioxin; Eschweiler-Clarke; 4-(phenylazo)phenol; NMR; XRD.

INTRODUCTION

Compounds possessing a benzo[1,3]dioxin moiety have shown diverse biological activity profiles, like anti-inflammatory [1], analgesic [2, 3], antipyretic [4], effective treatment of thalassemia [5] and sleep [6] and cardiovascular [7] disorders. Such compounds are practically used as agrochemical fungicides [8], pesticides [9, 10], herbicides [11, 12], biocides [13], fragrances [14], in animal husbandry to improve animal rate of growth or feed efficiency [15, 16], etc. This structural motif is found in numerous natural [17–23] and synthetic [24, 25] bioactive compounds and is widely exploited as key intermediate in multi-step sequences [26–29].

The protocols used to date for the synthesis of benzo[1,3]dioxins suffer from serious shortcomings. Indirect methods include multi-stage procedures with heavy and time-consuming purifications [30]. The direct conversion, known as Borsche-Berkhout reaction [31], is achieved firstly by treating phenols with formaldehyde in the presence of a mineral acid, hydrochloric or sulphuric [32], and is further modified by varying the acid component [33–38]. These procedures usually operate at high temperatures and/or pressure, lead to complex mix-

tures of products, and the yields are unsatisfactory. However, high activation by nitro group in *p*-position is observed and the product is isolated in unusually high yield of 84%, while no transformation or very low conversion is detected with the rest of phenols studied [39].

Herein, we report on the tandem hydroxymethylation-acetal protection of phenols under Eschweiler-Clarke conditions, where significant activation role of phenyl-azo moiety is observed.

RESULTS AND DISCUSSION

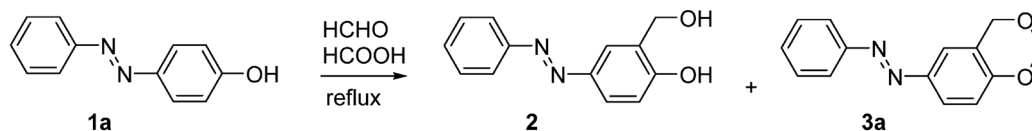
In an attempt to obtain *N*-methyl derivative of 4-phenylazo-phenol (**1a**), the latter was exposed to methylation under Eschweiler-Clarke conditions; refluxing in a mixture of formaldehyde and formic acid. However, instead of desired *N*-methyl derivative an approximately 1:2.5 mixture of known diol **2** [40] and its unknown acetal **3a** were isolated in moderate total yield (Scheme 1). The structures of the products are assigned by mono- and two-dimensional NMR spectra and are confirmed by single crystal XRD (Fig. 1, Table 1).

Isolation of diol **2** and its acetal protected derivative **3a** is an indication that the hydroxymethylation is the first step followed by its partial acetal protection. In order to accomplish complete protection, the reagents proportions were varied and it was found

* To whom all correspondence should be sent:
E-mail: vanya.kurteva@orgchem.bas.bg

Table 1. Most important crystal data and refinement parameters for compound **2**, **3a** and **3b** [41]

<i>Crystal data compound 2</i>	<i>Crystal data compound 3a</i>	<i>Crystal data compound 3b</i>
C ₁₃ H ₁₂ N ₂ O ₂ MW = 228.25 Monoclinic, <i>P</i> 2 ₁ / <i>c</i> <i>a</i> = 15.9679 (9) Å <i>b</i> = 5.5706 (3) Å <i>c</i> = 12.9979 (5) Å β = 91.628 (5)° <i>V</i> = 1155.70 (10) Å ³ <i>Z</i> = 4 <i>F</i> (000) = 480 <i>D</i> _x = 1.312 Mg m ⁻³ Mo K α radiation, λ = 0.71073 Å	C ₁₄ H ₁₂ N ₂ O ₂ MW = 240.26 Monoclinic, <i>P</i> 2 ₁ / <i>c</i> <i>a</i> = 26.2690 (17) Å <i>b</i> = 5.8234 (4) Å <i>c</i> = 7.6118 (5) Å β = 96.529 (6)° <i>V</i> = 1156.85 (13) Å ³ <i>Z</i> = 4 <i>F</i> (000) = 504 <i>D</i> _x = 1.379 Mg m ⁻³ Mo K α radiation, λ = 0.71073 Å	C ₁₀ H ₁₁ NO ₃ MW = 193.20 Monoclinic, <i>P</i> 2 ₁ / <i>a</i> <i>a</i> = 9.3244 (14) Å <i>b</i> = 10.1750 (16) Å <i>c</i> = 9.8241 (12) Å β = 92.098 (16)° <i>V</i> = 931.4 (2) Å ³ <i>Z</i> = 4 <i>F</i> (000) = 408 <i>D</i> _x = 1.378 Mg m ⁻³ Mo K α radiation, λ = 0.71073 Å, Graphite monochromator
Cell parameters from 2675 reflections θ = 3.4–32.9° μ = 0.09 mm ⁻¹ <i>T</i> = 290 K Block, colorless 0.25 × 0.22 × 0.20 mm	Cell parameters from 2100 reflections θ = 3.6–28.6° μ = 0.09 mm ⁻¹ <i>T</i> = 150 K Prism, colourless 0.20 × 0.15 × 0.12 mm	Cell parameters from 25 reflections θ = 5.9–19.6° μ = 0.10 mm ⁻¹ <i>T</i> = 290 K Block, colourless 0.28 × 0.26 × 0.24 mm
Data collection		
SuperNova, Dual, Cu at zero, Atlas diffractometer <i>T</i> _{min} = 0.621, <i>T</i> _{max} = 1.000 18570 measured reflections θ _{max} = 37.7°, θ _{min} = 3.1° Detector resolution: 10.3974 pixels mm ⁻¹ / ω scans 5910 independent reflections 2336 reflections with <i>I</i> > 2 σ (<i>I</i>) <i>R</i> _{int} = 0.048	SuperNova, Dual, Cu at zero, Atlas diffractometer <i>T</i> _{min} = 0.727, <i>T</i> _{max} = 1.000 5288 measured reflections θ _{max} = 28.7°, θ _{min} = 3.1° Detector resolution: 10.3974 pixels mm ⁻¹ / ω scans 2406 independent reflections 1943 reflections with <i>I</i> > 2 σ (<i>I</i>) <i>R</i> _{int} = 0.036	Enraf Nonius CAD4 diffractometer intensity decay: -2% 3773 measured reflections θ _{max} = 30.0°, θ _{min} = 2.1° Radiation sdetector: Enraf Nonius FR590, SP NaI 1939 independent reflections 910 reflections with <i>I</i> > 2 σ (<i>I</i>) <i>R</i> _{int} = 0.062
Refinement		
Refinement on <i>F</i> ² Least-squares matrix: full <i>R</i> [<i>F</i> ² > 2 σ (<i>F</i> ²)] = 0.075 <i>wR</i> (<i>F</i> ²) = 0.256 <i>S</i> = 1.05 5910 reflections 162 parameters 0 restraints Primary atom site location: Difference Fourier map Secondary atom site location: Difference Fourier map Hydrogen site location: mixed H atoms treated by a mixture of independent and constrained refinement (Δ / σ) _{max} < 0.001 $\Delta\rho$ _{max} = 0.31 e Å ⁻³ $\Delta\rho$ _{min} = -0.23 e Å ⁻³ Extinction correction: none <i>w</i> = 1/[$\sigma^2(F_o^2) + (0.086P)^2 + 0.1393P$] where <i>P</i> = (<i>F</i> _o ² + 2 <i>F</i> _c ²)/3	Refinement on <i>F</i> ² Least-squares matrix: full <i>R</i> [<i>F</i> ² > 2 σ (<i>F</i> ²)] = 0.090 <i>wR</i> (<i>F</i> ²) = 0.244 <i>S</i> = 1.15 2406 reflections 211 parameters 0 restraints Primary atom site location: Difference Fourier map Secondary atom site location: Difference Fourier map Hydrogen site location: mixed H atoms treated by a mixture of independent and constrained refinement (Δ / σ) _{max} < 0.001 $\Delta\rho$ _{max} = 0.41 e Å ⁻³ $\Delta\rho$ _{min} = -0.34 e Å ⁻³ Extinction correction: none <i>w</i> = 1/[$\sigma^2(F_o^2) + (0.058P)^2 + 4.4222P$] where <i>P</i> = (<i>F</i> _o ² + 2 <i>F</i> _c ²)/3	Refinement on <i>F</i> ² Least-squares matrix: full <i>R</i> [<i>F</i> ² > 2 σ (<i>F</i> ²)] = 0.049 <i>wR</i> (<i>F</i> ²) = 0.122 <i>S</i> = 1.00 1939 reflections 161 parameters 0 restraints Primary atom site location: structure-invariant direct methods Secondary atom site location: Difference Fourier map Hydrogen site location: mixed H atoms treated by a mixture of independent and constrained refinement (Δ / σ) _{max} < 0.001 $\Delta\rho$ _{max} = 0.17 e Å ⁻³ $\Delta\rho$ _{min} = -0.15 e Å ⁻³ Extinction correction: none <i>w</i> = 1/[$\sigma^2(F_o^2) + (0.0396P)^2$] where <i>P</i> = (<i>F</i> _o ² + 2 <i>F</i> _c ²)/3



Scheme 1. Synthesis of compounds 2 and 3.

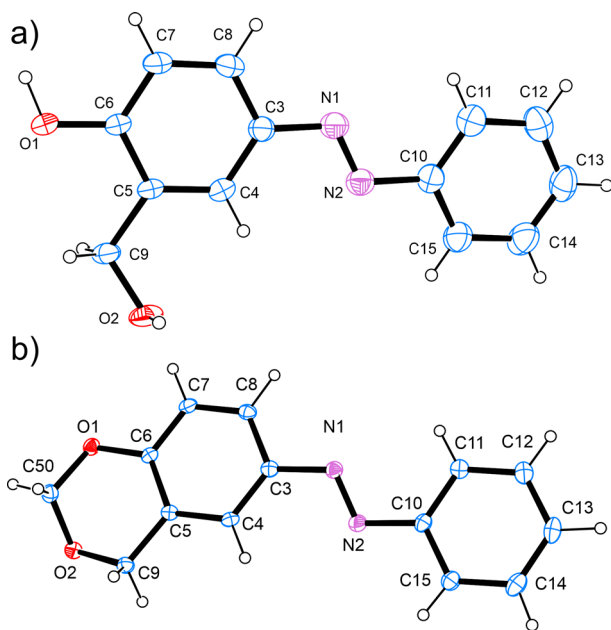


Fig. 1. ORTEP views of the molecules of compounds 2 (a) and 3a (b); atomic displacement parameters (ADP) are at 50% probability, hydrogen atoms are shown as small spheres with arbitrary radii.

that an increase in the amount of formaldehyde and formic acid from 1 ml each per mmol phenol to 7.5 ml leads to 71% yield of **3a** as a single reaction product (Table 2, entry 1).

The scope of the reaction is further extended toward variably substituted phenols, namely 4-acetylaminophenol (**1b**), 4-fluorophenol (**1c**), 3-fluorophenol (**1d**), 4-nitrophenol (**1e**), 3-nitrophenol (**1f**), 1-naphthol (**1g**), 1-hydroxypyridine (**1h**), and phloroglucinol (1,3,5-trihydroxybenzene, **1i**). Unfortunately, all attempts to achieve reaction with phenols **1e-1i** failed independently on the reagents' proportion and reaction prolongation. The known acetamido derivative **3b** [39] was isolated in very low yield after 8 h refluxing (Table 2, entry 2). Its structure is assigned by NMR spectra and confirmed by X-ray analyses (Fig. 2).

Despite the very low conversion achieved, the current protocol is comparable with the literature data for the preparation of **3b** [39], where 21% overall yield is reported after three steps. The results obtained with the regioisomeric fluorophenols are similar. The product **3c** was obtained in 19% yield within 8 h refluxing, while **1d** led to a mixture of

Table 2. Synthesis of acetals 3

Entry	Phenol	Time, h	Product	Yield, % ^a
1	1a	5.5	3a	71
2	1b	8	3b	17
3	1c	8	3c	19
4	1d	8	3d 3d'	11 ^b

^a After column chromatography purification; ^b Total for both products; **3d:3d'** 91:9 (1H NMR); not separated.

regioisomeric products **3d** and **3d'** in 91:9 ratio. The low total yield of 11% made the separation of the products irrelevant.

From structural (crystallographic) point of view the molecules of **2** and **3a** are quite similar (Fig. 3a). The angle between the mean planes of the aromatic rings (C3-C4-C5-C6-C7-C8 and C10-C11-C12-C13-C14-C15-C16) in **2** and **3a** is 4.578° and 2.628° respectively. The planarity of the molecules suggests a consistent propagation of the aromatic conjugation from one aromatic ring to the other. The hydrogen bonding interaction in **2** reveals that both O1 and O2 produce O—H...O hydrogen bonds. Based on the D...A distance O2-H...O1 is weaker than O1-H...O2, Figure 4, Table 3. As the hydroxyl O2 is slightly out of the conjugation plane we can speculate that O2 will be more accessible to formaldehyde for the initial (second) stage of acetal formation.

This is supported by the positioning of O2 in **3b** which also lays slightly outside of the aromatic plane (Fig. 5). The superposition of the 4*H*-benzo[*d*] [1,3]dioxin moiety of **3a** and **3b** (Figure 3b) shows a nearly conserved geometry (*rms* of 0.049). On the

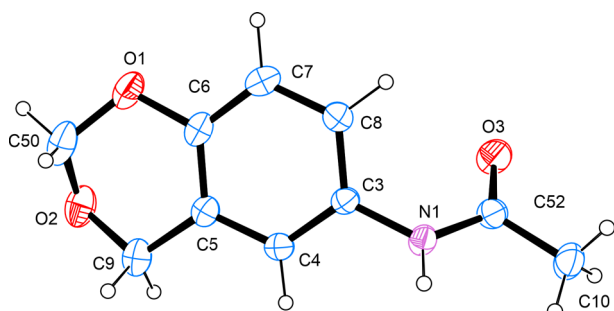


Fig. 2. ORTEP view of the molecule and atomic numbering scheme of compound **3b**.

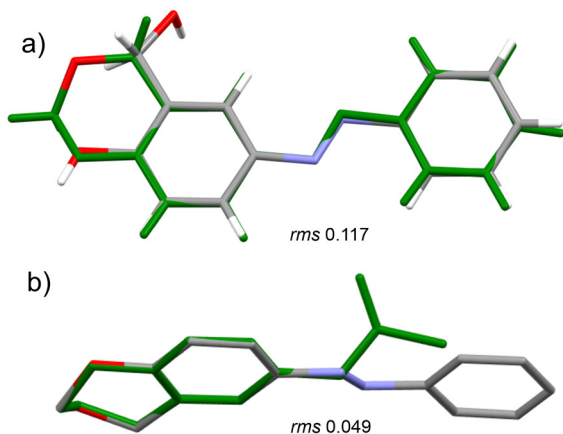


Fig. 3. Overlay of the molecules of a) **2** (grey) and **3a** (green); b) **3a** (grey) and **3b** (green).

other hand, the geometry/structural positioning of the substituent at position 4 does not seem to affect the outcome of the reaction, i.e. only the type of the substituent is important.

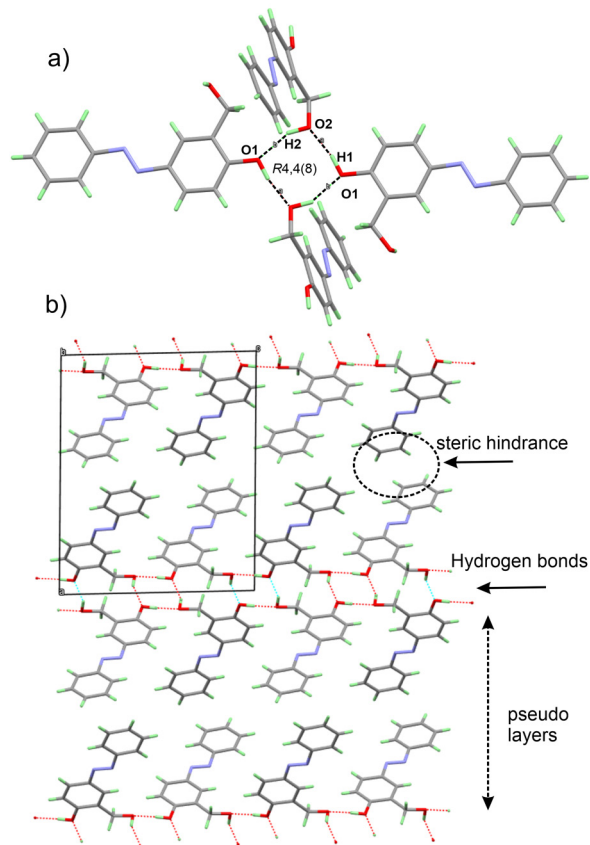


Fig. 4. Depiction of the hydrogen bonding interaction (a) and the three-dimensional arrangement of the molecules of **2** (b) disclosing the formation of pseudo layers.

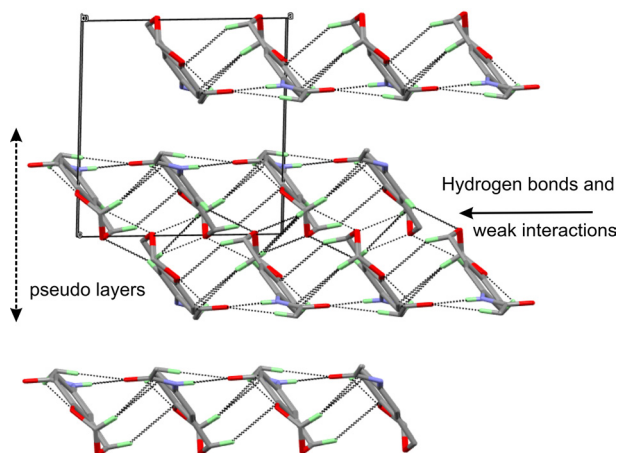


Fig. 5. A view along *b* of the three-dimensional arrangement of the molecules of **3b** disclosing the formation of pseudo layers and the positioning of O2.

Table 3. Observed Hydrogen bonding interactions in compound **2**, **3a** and **3b**

Compound 2				
$D-H \cdots A$	$D-H$ [Å]	$H \cdots A$ [Å]	$D \cdots A$ [Å]	$D-H \cdots A$ [°]
O1—H1 \cdots O2 ⁱ	0.95(3)	1.73(3)	2.6611(17)	168(2)
O2—H2 \cdots O1 ⁱⁱ	0.98(4)	1.89(4)	2.798(2)	153(3)
Symmetry codes: (i) $x, -y+5/2, z+1/2$; (ii) $-x, y-1/2, -z+1/2$				
Compound 3a				
$D-H \cdots A$	$D-H$ [Å]	$H \cdots A$ [Å]	$D \cdots A$ [Å]	$D-H \cdots A$ [°]
C9—H9A \cdots O2 ⁱ	0.97(4)	2.53(4)	3.427(5)	153(3)
C50—H50 \cdots O2 ⁱⁱ	1.01(4)	2.40(4)	3.397(5)	168(3)
C9—H9B \cdots O2 ⁱⁱⁱ	0.99(5)	2.56(5)	3.541(5)	170(4)
C50—H50 \cdots O2 ^{iv}	1.08(5)	2.46(5)	3.491(5)	160(4)
Symmetry codes: (i) $+x, 1/2-y, 1/2+z$; (ii) $-x, 1/2+y, 1/2-z$; (iii) $+x, -1+y, +z$; (iv) $+x, 3/2-y, 1/2+z$				
Compound 3b				
$D-H \cdots A$	$D-H$ [Å]	$H \cdots A$ [Å]	$D \cdots A$ [Å]	$D-H \cdots A$ [°]
N1—H1 \cdots O3 ⁱ	0.85(2)	2.03(2)	2.871(3)	172(2)
C10—H10A \cdots O3 ⁱ	0.96(4)	2.50(4)	3.353(5)	147(4)
Symmetry codes: (i) $1/2+x, -1/2-y, +z$				

CONCLUSIONS

A fast and efficient direct protocol for 6-(phenylazo)benzo[1,3]dioxin' synthesis *via* tandem hydroxymethylation-acetal protection of 4-phenylazo-phenol under Eschweiler-Clarke conditions is developed. The scope of the reaction is studied and is found that the presence of azo-dye fragment in phenol molecule is crucial for effective conversion. All other phenols examined lead to very low conversion or no transformation occurs. The single crystal XRD revealed that the 4*H*-benzo[*d*][1,3]dioxin part has a preserved conformation.

EXPERIMENTAL

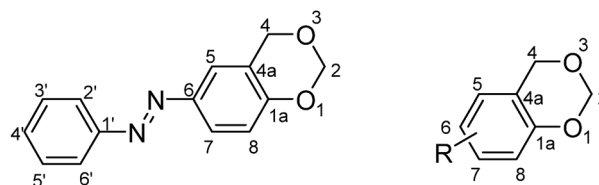
Synthesis

General: All reagents were purchased from Aldrich, Merck and Fluka and were used without any further purification. The deuterated solvents were purchased from Deutero GmbH. Fluka silica gel (TLC-cards 60778 with fluorescent indicator 254 nm) were used for TLC chromatography and R_f values determination. Merck Silica gel 60 (0.040–0.063 mm) was used for flash chromatography purification of the products. The melting points were determined in capillary tubes on SRS MPA100 OptiMelt (Sunnyvale, CA, USA) automated melting point system with heating rate of 1 °C per min. The NMR spectra were recorded on a Bruker Avance II+ 600 spectrometer (Rheinstetten, Germany) in $CDCl_3$; the chemical shifts were quoted in ppm

in δ -values against tetramethylsilane (TMS) as an internal standard and the coupling constants were calculated in Hz. The assignment of the signals is confirmed by applying two-dimensional COSY, NOESY, HSQC and HMBC techniques. The spectra were processed with Topspin 3.6.3 program. The mass spectra were recorded on a DFS high resolution magnetic sector instrument (Thermo Fisher Scientific GmbH, Bremen, Germany) operating in CI mode. The reaction prolongations and yields of the products **3** obtained by method B are listed on Table 2. The numeration scheme is given on Figure 6.

Method A: A solution of 4-phenylazo-phenol **1** (1 mmol) in HCHO (1 ml) and HCOOH (1 ml) was refluxed for 4 h. The products were partitioned between aq. K_2CO_3 and dichloromethane (DCM). The organic phase was washed with brine, dried over $MgSO_4$, evaporated to dryness, and purified by column chromatography on silica gel by using a mobile phase with a gradient of polarity from DCM to 5% acetone/DCM.

6-phenylazo-4*H*-benzo[*d*][1,3]dioxine 3a: 41% yield; R_f 0.78 (DCM); recrystallization from diiso-

**Fig. 6.** The numeration in compounds **3**.

propyl ether; m. p. 69.6-70.1 °C; NMR (CDCl₃) ¹H 5.001 (s, 2H, CH₂-4), 5.320 (s, 2H, CH₂-2), 7.012 (d, 1H, J 8.6, CH-8), 7.452 (tt, 1H, J 1.2, 7.3, CH-4'), 7.507 (ddd, 2H, J 1.2, 7.2, 7.8, CH-3'+CH-5'), 7.068 (d, 1H, J 2.3, CH-5), 7.819 (dd, 1H, J 2.3, 8.6, CH-7), 7.872 (dd, 2H, J 1.4, 7.7, CH-2'+CH-6'); ¹³C 66.33 (CH₂-4), 91.52 (CH₂-2), 117.46 (CH-8), 119.71 (CH-5), 121.45 (C_q-6), 122.62 (CH-2'+CH-6'), 123.78 (CH-7), 129.08 (CH-3'+CH-5'), 130.65 (CH-4'), 147.03 (C_q-4a), 152.56 (C_q-1'), 155.07 (C_q-1a); MS (m/z) 241 [M+1]⁺ (62), 211 [M-CH₂OH+1]⁺ (100), 163 [M-Ph]⁺ (4), 105 [PhN₂]⁺ (9).

2-hydroxymethyl-4-phenylazo-phenol 2: 16% yield; R_f 0.41 (10% acetone/DCM); recrystallization from benzene; m. p. 143.7-144.2 °C (lit 143-144 °C [40]).

Method B: A solution of starting phenol **1** (2 mmol) in HCHO (15 ml) and HCOOH (15 ml) was refluxed for 2-8 h (cf. Table 1). The work-up is analogous to that described in Method A.

6-acetamido-4H-benzo[d][1,3]dioxine 3b: R_f 0.39 (10% acetone/DCM); m. p. 128.5-128.8 °C (lit 129-130 °C [39]); NMR (CDCl₃) ¹H 2.142 (s, 3H, CH₃), 4.858 (s, 2H, CH₂-4), 5.214 (s, 2H, CH₂-2), 6.808 (d, 1H, J 8.7, CH-8), 7.051 (dd, 1H, J 2.5, 8.7, CH-7), 7.336 (d, 1H, J 2.4, CH-5), 7.468 (bs, 1H, NH); ¹³C 22.14 (CH₃), 66.02 (CH₂-4), 91.04 (CH₂-2), 116.86 (CH-8), 117.34 (CH-5), 120.16 (CH-7), 121.28 (C_q-4a), 131.23 (C_q-6), 149.14 (C_q-1a), 168.29 (C=O).

6-fluoro-4H-benzo[d][1,3]dioxine 3c: R_f 0.36 (DCM); m. p. 124.8-124.9 °C; NMR (CDCl₃) ¹H 4.852 (s, 2H, CH₂-4), 5.197 (s, 2H, CH₂-2), 6.661 (dd, 1H, J_{5,7} 2.8, J_{5,F} 8.3, CH-5), 6.814 (dd, 1H, J_{8,F} 4.7, J_{7,8} 8.9, CH-8), 6.855 (ddd, 1H, J_{5,7} 2.9, J_{7,F} 8.3, J_{7,8} 8.9, CH-7); ¹³C 65.91 (CH₂-4), 91.25 (CH₂-2), 111.45 (d, J_{5,F} 23.8, CH-5), 114.84 (d, J_{7,F} 23.3, CH-7), 117.97 (d, J_{8,F} 7.9, CH-8), 122.23 (d, J_{4a,F} 7.2, C_q-4a), 148.67 (d, J_{1a,F} 2.1, C_q-1a), 157.26 (d, J_{6,F} 239.9, C_q-6); MS (m/z) 155 [M+1]⁺ (71), 125 [M-CH₂OH+1]⁺ (100).

7-fluoro-4H-benzo[d][1,3]dioxine 3d: R_f 0.87 (DCM); NMR (CDCl₃) ¹H 4.864 (s, 2H, CH₂-4), 5.232 (s, 2H, CH₂-2), 6.601 (dd, 1H, J_{6,8} 2.5, J_{8,F} 9.9, CH-8), 6.655 (ddd, 1H, J_{6,8} 2.5, J_{5,6} 8.5, J_{6,F} 11.1, CH-6), 6.901 (dd, 1H, J_{5,F} 6.2, J_{5,6} 8.4, CH-5).

Crystallography

General: A crystal of compound **2**, **3a** or **3b** with suitable size was placed on a glass capillary and mounted on a Supernovadual or Enraf-Nonius CAD-4 diffractometer. X-ray data collection [41] was carried out at 290 or 150 K with graphite (for **3b**) or mirror monochromatized Mo-K α radiation (λ = 0.71073 Å) for compounds **2** and **3a**. The unit cell parameters were determined from 25 reflections

and refined employing 22 higher-angle reflections, $18 < \theta < 20^\circ$. The $\omega/2\theta$ technique was used for data collection using Nonius Diffractometer Control Software [42]. Lorentz and polarization corrections were applied to intensity data using the WinGX [43]. In the case of **2** and **3a** data collection and reduction was carried out using CrysAlispro [44]. The structure was solved by direct methods using SHELXS [45] and refined by full-matrix least-squares procedure on F^2 with SHELXL [45]. The hydrogen atom near oxygen's (O1 or O2) or nitrogen have been located from difference Fourier map. All remaining hydrogen atoms were placed in idealized positions ($C-H_{\text{aromatic}} = 0.93 \text{ \AA}$ and $C-H_{\text{methylene}} = 0.97 \text{ \AA}$) and were constrained to ride on their parent atoms, with $U_{\text{iso}}(H) = 1.2U_{\text{eq}}(C, N \text{ or } O)$. Experimental conditions are summarized in Table 2. Hydrogen bonds and weak interactions geometry are presented in Table 3. ORTEP [43] drawing diagram of the molecular structure with ADP 50% probability and the atom numbering scheme is shown in Figs. 1 and 4. The data for publication were prepared with WinGX [43], ORTEP [43], Mercury [46] and Olex2 [47] program packages.

REFERENCES

1. V. Dauksas, P. Gaidelis, A. Brukstus, J. Ramanauskas, L. Labanauskas, G. Gasperaviciene, I. Jautakiene, V. Lapinskas, N. Lauzikiene, *Khim-Farm. Zh.*, **23**, 942 (1989).
2. T. G. Tolstikova; A. V. Pavlova; E. A. Morozova; I. V. Ilina; K. P. Volcho; N. F. Salakhutdinov, *Russ. Pat. Appl.* RU2409353C1 (2011).
3. S. Kurbakova, I. Il'ina, A. Pavlova, D. Korchagina, O. Yarovaya, T. Tolstikova, K. Volcho, N. Salakhutdinov, *Med. Chem. Res.*, **23**, 1709 (2014).
4. A. Torre, *Eur. Pat. Appl.* EP272223 A1 (1988).
5. P. Roydeva, A.-M. Beckmann, M. Stirnberg, J. Cesar, D. Kikelj, J. Ilaš and M. Gütschow, *Pharmaceuticals*, **9**, 2 (2016).
6. R. L. Hudkins, J. A. Gruner, R. Raddatz, J. R. Mathiasen, L. D. Aimone, M. J. Marino, E. R. Bacon, M. Williams, M. A. Ator, *Neuropharmacology*, **106**, 37 (2016).
7. M. Nazaré, D. Kozian, M. Bossart, W. Czechtizky, A. Evers (Sanofi SA), *Eur. Pat. Appl.* EP2850070A1 (2015).
8. W. E. J. Simon, *Can. Pat. Appl.* CA 2117503 AA (1995).
9. M. Anderson, A. G. Brinnand, R. E. Woodall, *Eur. Pat. Appl.* EP469686 A1 (1992).
10. M. Anderson, A. G. Brinnand, R. E. Woodall, *Eur. Pat. Appl.* EP525877 A1 (1993).
11. M. Enomoto, H. Nagano, T. Haga, K. Morita, M. Sato, *Jpn. Pat. Appl.* JP63275580 A2 (1988).
12. U. J. Vogelbacher, J. Rheinheimer, E. Baumann, U. Kardorff, H. Walter, K.-O. Westphalen, U. Mislitz (BASF AG), *DE Pat. Appl.* DE19505181A1 (1996).

13. W. E. J. Simon, *Eur. Pat. Appl.* EP645373 A1 (1995).
14. J.-J. Chanot, J. Mane, C. Plessis, *Eur. Pat. Appl.* EP2459546A1 (2012).
15. F. T. Boyle, A. Davies, *US Pat. Appl.* US4232032A (1980).
16. F. T. Boyle, A. Davies, *US Pat. Appl.* CA1086744A (1980).
17. J. S. E. Holker, S. A. Kagal, L. J. Mulherin, P. M. White, *J. Chem. Soc., Chem. Commun.*, 911 (1966).
18. P. Roffey, M. V. Sargent, *J. Chem. Soc., Chem. Commun.*, 913 (1966).
19. J. Grandjean, *J. Chem. Soc., Chem. Commun.*, 1060 (1970).
20. R. G. Dushin and S. J. Danishefsky, *J. Am. Chem. Soc.*, **114**, 655 (1992).
21. J. L. Carr, D. A. Offermann, M. D. Holdom, P. Dusart, A. J. P. White, A. J. Beavil, R. J. Leatherbarrow, S. D. Lindell, B. J. Sutton and A. C. Spivey, *Chem. Commun.*, **46**, 1824 (2010).
22. L. Liu, *Mycology: Int. J. Fungal Biol.*, **2**, 37 (2011).
23. J. S. Yadav, C. D. Vani, M. Chowdeswari, K. Ananthalakshmi, N. Bhasker, B. V. S. Reddy, *Nat. Prod. Commun.*, **14**, 135 (2019).
24. S. W. Kang, C. M. Gothard, S. Maitra, A.-t. Wahab and J. S. Nowick, *J. Am. Chem. Soc.*, **129**, 1486 (2007).
25. F. Ayala-Mata, C. Barrera-Mendoza, H. A. Jiménez-Vázquez, E. Vargas-Díaz, L. G. Zepeda, *Molecules*, **17**, 13864 (2012).
26. J. Mal, A. Nath, R. V. Venkateswaran, *J. Org. Chem.*, **61**, 9164 (1996).
27. Y. Khaniani, H. Golchoubian, *Phosphorus Sulfur Silicon Relat. Elem.*, **181**, 2817 (2006).
28. M. Ghizzoni, A. Boltjes, C. de Graaf, H. J. Haisma, F. J. Dekker, *Bioorg. Med. Chem.*, **18**, 5826 (2010).
29. C. Glas, R. Wirawan, F. Bracher, *Synthesis*, **53**, 1943 (2021).
30. E. Kleinpeter, M. Sefkow, in: *Comprehensive Heterocyclic Chemistry*, Elsevier Ltd., 2008, chapter 8.11, p.739.
31. Z. Wang, Borsche-Berkhout reaction, *Comprehensive Organic Name Reactions and Reagents*, John Wiley & Sons, 2010, chapter 102, 468-470.
32. W. Borsche, A. D. Berkhout, *Ann.*, **330**, 82 (1904).
33. D. R. Mehta, P. R. Ayyar, *J. Univ. Bombay*, **8**, part 3, 176 (1939).
34. C. A. Buehler, G. F. Deebel, R. Evans, *J. Org. Chem.*, **6**, 216 (1941).
35. S. A. Harrison, *US Patent Appl.* US2789985 A (1957).
36. M. Ando, S. Emoto, *Bull. Chem. Soc. Jpn.*, **46**, 2903 (1973).
37. C. Li, Y. Wang, T. Wang, N. Li, Z. Yu, *Chem. J. Chinese U.*, **19**, 260 (1998).
38. J. Goswami, N. Borthakur, A. Goswami, *J. Chem. Res. (S)*, 200 (2003).
39. M. Yeh, F. Tang, S. Chen, W. Liu, L. Lin, *J. Org. Chem.*, **59**, 754 (1994).
40. E. Tummeley, *Ann.*, **251**, 174 (1889).
41. The crystallographic data for the product of **2**, **3a** and **3b** were deposited at the Cambridge Crystallographic Data Centre and allocated the deposition numbers CCDC 2120893, 2120894 and 2120895. Copies of the data can be obtained, free of charge, on application to CCDC, 12 Union Road, Cambridge CB2 1EZ, UK; tel: +44 1223 762910; fax: +44 1223 336033; e-mail: deposit@ccdc.cam.ac.uk; <http://www.ccdc.cam.ac.uk/deposit>.
42. K. Harms, S. Wocadlo. "XCAD4/PC." University of Marburg, Germany (1997).
43. L. Farrugia, WinGX and ORTEP for Windows: an update, *J. Appl. Crystallogr.*, **45**, 849-854 (2012).
44. CrysAlisPRO, Rigaku Oxford Diffraction Ltd., UK Ltd., Yarnton, England, 2021.
45. G. Sheldrick, *Acta Crystallogr. C*, **71**, 3 (2015).
46. C. F. Macrae, P. R. Edgington, P. McCabe, E. Pidcock, G. P. Shields, R. Taylor, M. Towler, J. van de Streek, *J. Appl. Cryst.*, **39**, 453 (2006).
47. O. V. Dolomanov, L. J. Bourhis, R. J. Gildea, J.A.K. Howard, H. Puschmann, *J. Appl. Crystallogr.*, **42**, 339 (2009).

Laccase-based optical biosensors for detection of phenol

S. A. Yaneva^{1*}, N. G. Rangelova¹, L. I. Aleksandrov², N. V. Savov¹

¹ *University of Chemical Technology and Metallurgy, Department of Industrial Safety, 8 Kl. Ohridski Blvd., 1756 Sofia, Bulgaria*

² *Institute of General and Inorganic Chemistry, Bulgarian Academy of Sciences, Acad. G. Bonchev str. bl. 11, 1113 Sofia, Bulgaria*

Received October 31, 2021; Accepted January 15, 2022

Hybrid carriers prepared by sol-gel method based on methyltriethoxysilane (MTES) or ethyltrimethoxysilane (ETMS) and cellulose acetate propionate with high molecule weight (CAPH) as precursors were used. Each carrier was examined by X-ray diffraction (XRD) analysis, Differential thermal (DTA/TG) analysis and Scanning electron microscopy (SEM). Laccase was immobilized by cross-linking using glutaraldehyde. The enzyme activity, catalytic properties and amount of bonded protein of immobilized systems were determined. The results were compared to free laccase. The most suitable matrix was used for design of optical biosensor for phenol detection. The operating parameters of the biosensors lifetime, linear range and limit of detection were described.

Keywords: sol-gel, biosensors, enzymes, toxic compounds.

INTRODUCTION

Regulation is becoming more and more severe regarding the release of pollutants in the environment. The management of industrial processes requires enhanced control of possible releases of hazardous chemicals. These facts should lead industry to develop new tools for selective and rapid responses to the release of hazardous chemicals in the environment [1].

As the common water contaminants, phenolic compounds are of high toxicity and difficulty to be degraded in natural conditions, which has seriously threatened human health. Phenol is a representative substance of phenolic pollutants and widely derived from different industries including coal chemical industry, plastics, textile, dyes and other fields [2].

Conventional detection techniques for environmental pollution using physical chemistry methods show a certain degree of sensitivity and specificity, there are still many challenges that limit their practical application, such as expensive equipment and complicated procedures, in addition to long waits for detection [3]. Hazard materials can be determined by application of classical analytical methods such as gas chromatography [4] or by highly

sensitive gas sensors constructed based on quartz crystal microbalance [5,6].

The specificity of every biosensor is due to the specificity of the bio receptor molecule used. Enzymes have been the most widely used bioreceptor molecules in biosensor applications. The growing field of biosensors represents an answer to this demand [7].

Optical biosensors have exhibited worthwhile performance in detecting biological systems and promoting significant advances in clinical diagnostics, drug discovery, food process control, and environmental monitoring. Without complexity in their pretreatment and probable influence on the nature of target molecules, these biosensors have additional advantages such as high sensitivity, robustness, reliability, and potential to be integrated on a single chip [8]. The degradative potential of fungi is mainly due to the production of different types of oxidases, of which laccases is one of the most prominent enzymatic activities [9]. A number of biosensors have been constructed using immobilized laccase to detect different compounds such as phenol [10], bisphenol A [11], azo-dye tartrazine [12], catechol [13] and others.

In previous studies we have immobilized laccase on various hybrid carriers and the potential of the biocatalytic system to degrade organic dyes or organochlorine pesticides has been studied [14,15].

* To whom all correspondence should be sent:
E-mail: sp_yaneva@uctm.edu

The results show that the amount of polysaccharides used in the hybrid materials is important in the immobilization of the enzyme. The advantages of these materials is that after immobilization, they are able to maintain catalytic activity of laccase even in hexane.

The aim of this work is sol-gel synthesis of hybrid membranes, enzyme immobilization and biosensor construction for phenol detection.

EXPERIMENTAL

Materials

CAPH (~25 000 m.w.), 2,2'-Azino-bis(3-ethylbenzothiazoline-6-sulfonic acid (ABTS) and Laccase (E.C. 1.10.3.2.), 0.5 U/mg from *Trametes versicolor* were purchased from Sigma-Aldrich. Ethanol, methanol, chloroform, MTES and ETMS, 25% Glutaraldehyde solution, Folin and Ciocalteu's solution, Phenol were provided by Merck, KH_2PO_4 , $\text{K}_2\text{HPO}_4 \cdot 3\text{H}_2\text{O}$ p.a. for 0.05 M buffers.

Hybrid preparation

In this study sol-gel derived hybrid carriers based on alkoxy silanes precursors MTES, ETMS and CAPH as organic part were used. The hybrids were prepared as we described previously [16].

Sample characterization

XRD patterns were used to investigate the crystallinity of the materials. For the XRD measurements a Bruker D8 Advance diffractometer was used at $\text{Cu K}\alpha$ radiation in $5 < 2\theta < 80$ range.

The morphology of the obtained structures was observed by SEM with a dual beam scanning electron/focused ion beam system LYRA I XMU, TESCAN after the samples were coated with a conductive thin gold film.

The thermal stability of synthesized amorphous hybrids was determined by DTA/TG analysis. A Seteram Labsysis Evo 1600 instrument was used for recording of thermo diagrams over the range from room temperature up to 600 °C. The heating rate was 10°/min in air atmosphere.

Laccase immobilization

The immobilization of laccase was performed using cross-linking method for immobilization with glutaraldehyde and the procedure was done using the immobilizer as described in previous study [17].

Determination of enzyme activity and protein content

Laccase activity was determined spectrophotometrically (VWR UV-1600 PC Spectrophotometer, Germany) at $\lambda = 420$ nm for 5 min, using 0.5 mM ABTS ($\epsilon = 36\ 000\ \text{M}^{-1}\ \text{cm}^{-1}$) as a substrate. Reaction mixture contained 0.1 ml enzyme solution with concentration mg/ml, 1 ml ABTS, 1 ml buffer and 0.9 ml distilled water. For immobilizes enzyme was used 100 mg carrier. One unit of laccase activity was defined as the amount of enzyme required to oxidize 1 μmol of ABTS per minute at 25 °C. The total protein content in immobilized system was determined by the modified Lowry method [18].

pH and temperature optimum

For determination of the pH optimum for laccase, the residual activities of free and immobilized enzymes were determined in the potassium phosphate buffer with pH range from 3.0 to 9.0 with a retention of 10 minutes.

The temperature optimum, of free and immobilized enzyme in the range from 30 °C to 80 °C with retention of 10 minutes was determined.

All determinations were referred to the specific activity of the immobilized enzyme. The amount of the bonded protein and the kinetic parameters were performed three times.

Biosensor construction and determination of work parameters

100 mg immobilized membrane was immersed in 2 ml of tested phenol solution by different concentrations from $1 \cdot 10^{-4}$ to $9 \cdot 10^{-3}$ M (phenol was dissolved in $5 \cdot 10^{-3}$ M potassium acetate buffer with pH = 5.0) and subsequent vigorous stirring was applied. The solution spectra were measured in the range from 200 to 600 nm at 0 to 40 min., to control of the linearity and stability of the received signal. The lifetime of biosensor was measured once a week on the same conditions described above.

RESULTS AND DISCUSSION

Figure 1 presents XRD analysis of cellulose ester and obtained hybrids. As it can be seen, the XRD profile of CAP showed its semi-crystalline nature [19]. The hybrid obtained with ETMS is amorphous while this one obtained with MTES is characterized by a number of amorphous halos probably corresponding to the presence of two or more separated amorphous phases.

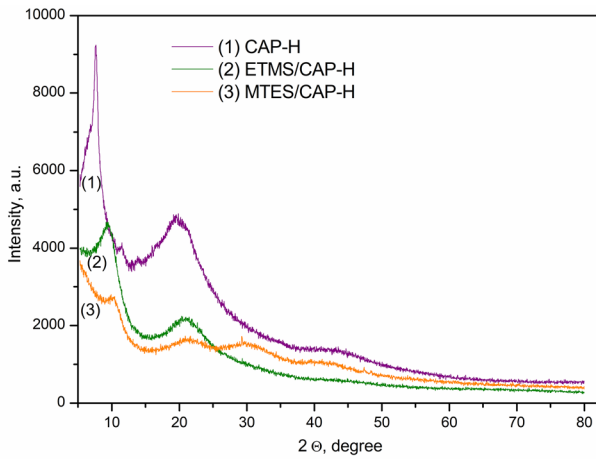


Fig. 1. XRD patterns of CAP-H and obtained hybrids.

The thermal behavior of cellulose ester and obtained hybrids is observed by DTA/TG analysis (Fig. 2). DTA curve of CAP (Fig. 2,a) corresponds to the simultaneous loss (Fig. 2,b) of acetyl and propionyl groups from the cellulose backbone in the temperature range 300–420 °C. The second exothermal peak in the range 450–570 °C can be associate with a subsequent pyrolysis of cellulose structure [20,21]. The hybrids obtained with MTES keeping the thermal profile of CAP precursor, are characterized by smaller mass losses, while the hybrids obtained with ETMS showed different thermal behavior due to silica precursor but retain the same temperature range and mass losses.

The surface morphology of obtained hybrids was investigated by SEM. In Fig. 3 SEM images

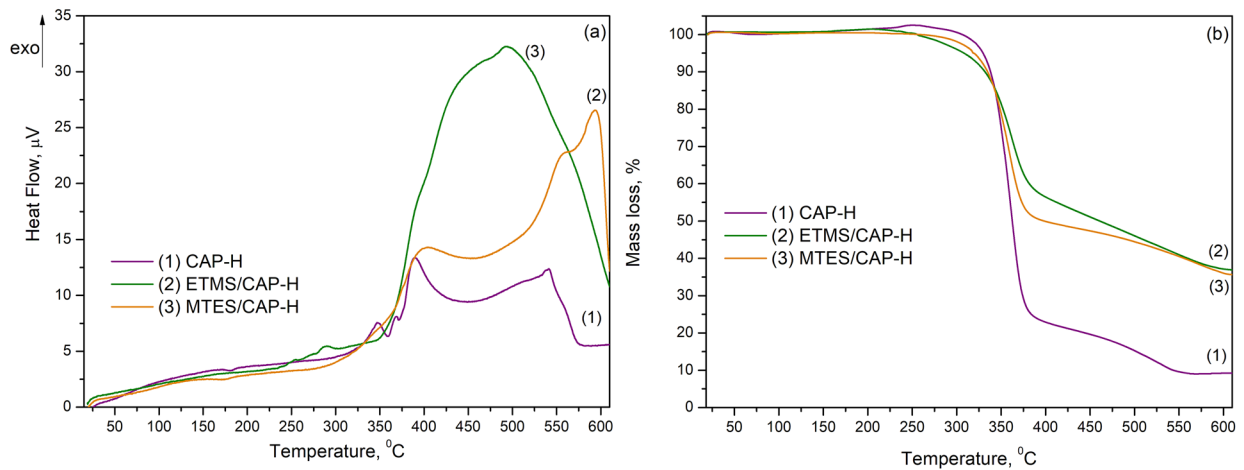


Fig. 2. DTA/TG analysis of CAP-H and obtained hybrids.

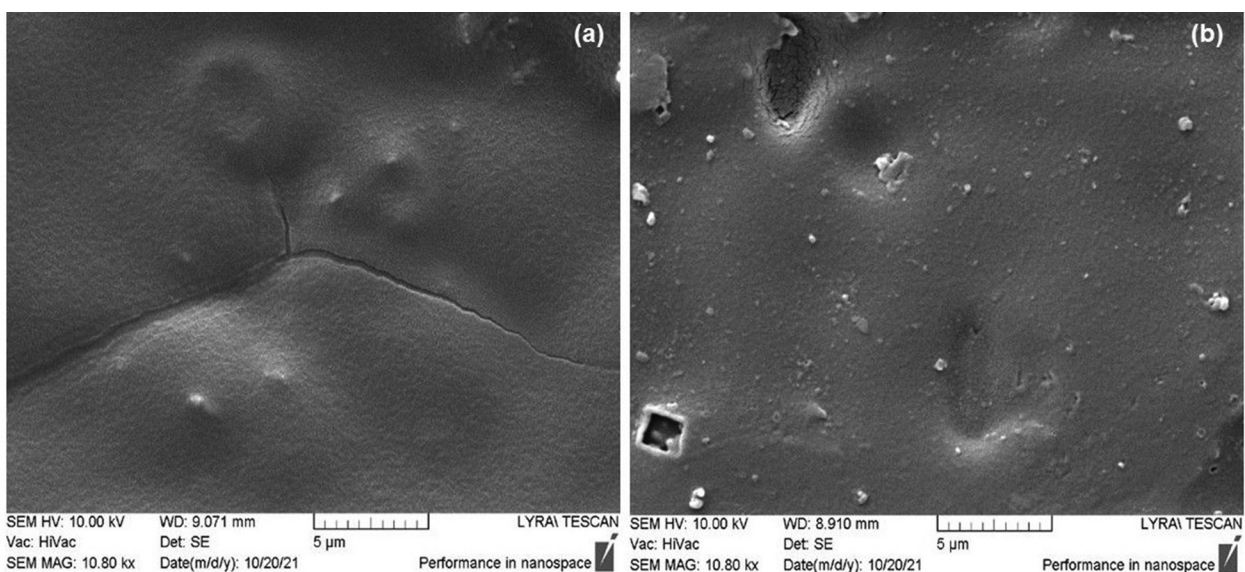


Fig. 3. SEM images of CAP-H obtained hybrids with ETMS (a) and MTES (b).

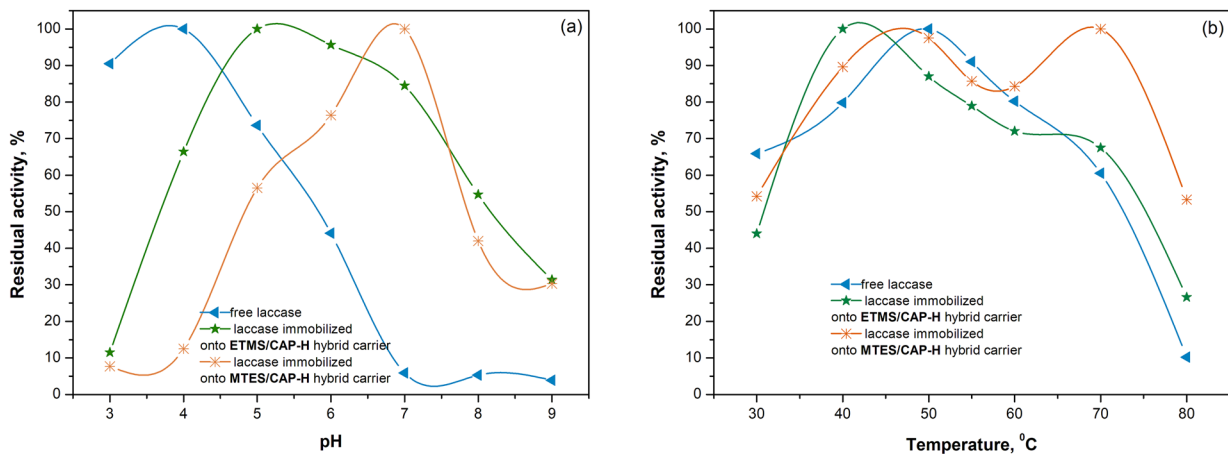


Fig. 4. pH (a) and temperature (b) profiles of free and immobilized laccase.

of hybrids at $\times 10\ 800$ magnifications are presented. Obtained hybrids are characterized by high density and low roughness. Unfortunately, by electron microscopy (SEM) is not possible to distinguish the presence of different amorphous states/phases and the results from XRD analysis for the presence of two or more amorphous phases are still questionable.

The pH profiles on the activity of free and immobilized laccase was also examined in the pH range 3.0–9.0 at 30 °C and the result is presented in Figure 4 (a). The optimum pH for free laccase was found at pH 4.0 which was similar to that reported from Mazlan and Hanifah [22]. All this gives us reason to continue to study this immobilized system at high temperatures, to track the loss of enzyme activity over time.

The optimum pH for immobilized laccase was shifted to pH 5.0 for ETMS and to pH 7.0 for MTES carriers. pH profiles of the immobilized laccase are broader than that for the free enzyme, which means that the immobilization method preserved enzyme

activity in a wider pH range. The matrix based on MTES with immobilized laccase shows higher temperature resistance at high temperatures and the unusual for laccase pH optimum equal to 7.0. The microenvironment of the immobilized enzyme and bulk solution usually has unequal partitioning of H^+ and OH^- concentrations due to electrostatic interactions with the matrix, which often leads to the displacements in the pH activity profile [22]. In Figure 4 (b) is presented temperature profile of the immobilized laccase improved the stability of the optimum temperature value in comparison to the free laccase. It means that the immobilization method preserved the enzyme activity. The temperature profile of immobilized laccase was also broader than free laccase. The optimum temperature for free laccase appeared at 50 °C and at 70 °C for immobilized laccase. It shows that immobilized laccase could withstand higher temperature conditions compared to free laccase.

Although the MTES-based matrix exhibits better pH and temperature behavior, the ETMS-based

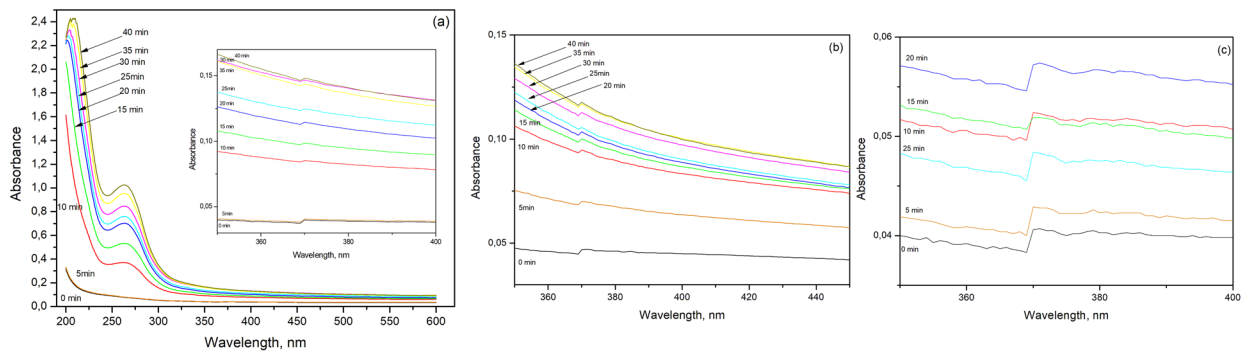


Fig. 5. Absorbance profiles of biosensor over time at different phenol concentrations, 1.10^{-3} M (a), 2.10^{-3} M (b) and 3.10^{-3} M (c).

matrix has better enzyme binding. Based on these results we choose ETMS matrix for the construction of the optical biosensor.

Figure 5 presents absorbance profiles of biosensor over time at different phenol concentrations.

As can be seen at each of the tested phenol concentrations, we registered characteristic peaks at 370 nm, which appear at the 5th minute of the measurement and persist until the 40th minute (Fig. 5 a). In the absorbance spectrum of the enzyme solution as well as the phenol, these peaks are not observed (not included in the figures). The enzymatic reaction of laccase with phenol produces intermediates with different spectroscopic properties [23], which is probably reason to appearance of the characteristic peak at around 370 nm. When we determine the response time of the biosensor, it is observed that there is a response at the 5th minute, but the signal is not stable at different phenol concentrations (Fig. 5 a small image graph). At concentrations below $1 \cdot 10^{-4}$ M and above $2 \cdot 10^{-3}$ M, a violation of the linearity of the biosensor response is observed (Fig. 5 b and c). The operating parameters of the biosensors, response time (10 min), life time (more than 20 days) and linear range ($1 \cdot 10^{-4}$ – $2 \cdot 10^{-3}$ M) were determined. The main advantage of the designed biosensor is that for the determination of phenol it is not necessary to add a dye such as 4-aminoantipyrine [24] to register the presence of phenol in the tested solution.

CONCLUSIONS

In this study sol-gel derived hybrid carriers based on two alkoxysilanes (ETMS, MTES) and cellulose ester (CAPH) were prepared and were used for laccase immobilization. The phase composition, thermal properties and surface morphology of hybrids were examined by XRD, DTA/TG and SEM analysis. The enzyme was immobilized by cross-linking. The enzyme activity, catalytic properties and amount of bonded protein for free and immobilized laccase were determined. An optical biosensor was designed for the detection of phenol with the best of the two matrices – ETMS. The operating parameters of the biosensors, response time (10 min), life time (more than 20 days) and linear range ($1 \cdot 10^{-4}$ – $2 \cdot 10^{-3}$ M) were determined.

Acknowledgments: *The authors are very grateful to the Project BG05M2OP001-1.001-0008 National Centre for Mechatronics and Clean Technologies, to Laboratory L2 „Bio-Mechatronics and micro/nano engineering for mechatronic technologies, elements and systems“, Section S4 „Biomimetic mechatronic systems“.*

REFERENCES

1. C. Malandain, F. Fayolle, H. Bedouelle, *IFP*, **60**, 6, 887 (2005).
2. C. Hou, L. Fu, Y. Wang, W. Chen, F. Chen, S. Zhang, J. Wang, *Carbohydrate Polymers* **273**, 118548 (2021).
3. A. Baldassarre, N. Mucci, L. Lecca, E. Tomasini, M. Rosario, *Int. J. Environ. Res. Public Health*, **17**, 2461 (2020).
4. H. Bagheri, A. Saber, S. Reza Mousavi, *Journal of Chromatography A*, **1046**, 27 (2004).
5. V. Strashilov, G. Alexieva, V. Velichkov, R. Mateva and I. Avramov, *Sensor Lett.*, **7**, 2, 203 (2009).
6. I. Youseff, F. Sarry, B. Nysten, G. Alexieva, V. Strashilov, I. Kolev, H. Alem, *Talanta* **153**, 145 (2016).
7. G. Nikoleli, D. Nikolelis, C. Siontorou, S. Karapetis, *Advances in Food and Nutrition Research*, **84**, 1 (2018).
8. C. Chen, J. Wang, *Analyst*, 145, 1605 (2020).
9. A. Zerva, Ch. Pentari, E. Topakas, *Molecules*, **25**, 2221 (2020).
10. J. Sanz, S. de Marcos, J. Galbán, *Anal. Bioanal. Chem.* **404**, 351 (2012).
11. M. Portaccio, D. Tuoro, F. Arduini, D. Moscone, M. Cammarota, D.G. Mita, M. Leporea, *Electrochimica Acta*, **109**, 340 (2013).
12. S. Mazlan, Y. Lee, S. Hanifah, *Sensors*, **17**, 2859 (2017).
13. S. Caballero, M. Guerrero, L. Vargas, C. Ortiz, J. Castillo, J. Gutiérrez, S. Blanco, *IOP Conf. Series: Journal of Physics: Conf. Series* **1119**, 012009 (2018).
14. S. Yaneva, N. Rangelova, L. Aleksandrov, D. Danalev, *Journal of Chemical Technology and Metallurgy* **53**, 6, 1203 (2018).
15. N. Rangelova, S. Yaneva, I. Stoykova, L. Aleksandrov, *Nanoscience & Nanotechnology: Nanostructured materials applications and innovation transfer*, **17**, 1, 23 (2017).
16. L. Yotova, S. Yaneva, Bulgarian Chemical Communication, 45, 4, 516 (2013).
17. S. Yaneva, Tz. Velinov, L. Yotova; *Journal of Chemical Technology and Metallurgy* **53**, 5, 791 (2018).
18. O. Lowry, N. Rosebrough, A. Farr, R. Randall, *J. Biol. Chem.* **193**, 1, 265 (1951).
19. S. Nobukawa, A. Nakao, K. Songsurang, P. Pulkerd, H. Shimada, M. Kondo, M. Yamaguchi, *Polymer*, **111**, 53 (2017).
20. J. Kujawa, E. Rynkowska, K. Fatyeyeva, K. Knorzowska, A. Wolan, K. Dzieszowski, G. Li, W. Kujawski, *Polymers*, **11**, 1217 (2019).
21. E. Rynkowska, K. Dzieszowski, A. Lancien, K. Fatyeyeva, A. Szymczyk, J. Kujawa, S. Koter, S. Marais, A. Wolan, W. Kujawski, *J. Membr. Sci.*, **544**, 243 (2017).
22. S. Mazlan, Sh. Hanifah, *International Journal of Polymer Science*, 5657271 (2017).
23. G. Zoppellaro, T. Sakurai, HW Huang *J Biochem* **129**, 6, 949 (2001).
24. M. Ettinger, C. Ruchhoft, R. Lishka, *Anal. Chem.*, **23**, 12, 1783 (1951).

Adsorption studies of a material based on the medicinal plant yarrow for the removal of Cu²⁺ ions from aqueous solutions

P. S. Vassileva*, L. P. Ivanova, A. K. Detcheva

*Bulgarian Academy of Sciences, Institute of General and Inorganic Chemistry,
Acad. Georgi Bonchev Str., Bl. 11, 1113, Sofia, Bulgaria*

Received October 12, 2021; Accepted January 09, 2022

Biosorption is process for the removal of toxic metals using a passive binding process with nonliving organisms. Medicinal plants are of great interest as biosorbents, because they contain numerous active phytochemicals which are prone to metal binding.

In the present study the feasibility of a material based on the widely used herb yarrow (*Achillea millefolium L.*) for the removal of Cu²⁺ ions from aqueous solutions was investigated. For its characterization XRD, FTIR and SEM analysis as well as low-temperature nitrogen adsorption were used. The estimation of optimal parameters influencing the Cu²⁺ removal such as solution acidity, contact time, temperature and initial metal concentration was studied by means of the batch method. Optimum pH value was found 3.0–5.0. Kinetic of Cu²⁺ adsorption for was very fast. Experimental data were fitted to Langmuir, Freundlich and Dubinin-Radushkevich models. It was established that the Langmuir isotherm most adequately described the adsorption process. The Langmuir maximum adsorption capacity for studied material was calculated. The results showed high adsorption capacity of the investigated biosorbent towards copper ions, hence it has good potential for removal of Cu²⁺ from contaminated wastewaters. The possibility for desorption was also studied.

Keywords: yarrow (*Achillea millefolium L.*), biosorption, copper ions, XRD, SEM, FTIR.

INTRODUCTION

Rapid industrialization has led to tremendous increase in the use of toxic elements over the past few decades and inevitably resulted in an increased flux of metallic substances in the aquatic environment. The heavy metals reach tissues through the food chain and accumulate in the human body [1].

Copper is one of these elements which constitute a real health hazard. Though essential for human health, it can be very harmful above specified concentrations limits, causing anemia, kidney damage, stomach intestinal distress, coma and eventual death [2, 3] In fact, copper is one of the most toxic metals for aquatic organisms, significantly more toxic than for mammals[4]. The most bioavailable and therefore most toxic form of copper is Cu²⁺. Fish and crustaceans are 10 to100 times more sensitive to the toxic effects of copper than are mammals. Algae especially blue-green algae species, are1,000 times

more sensitive to the toxic effects of copper than are mammals, as several authors, including Forstner andWittman [5] and Wrightand Welbourn [6] have demonstrated.

The effective removal of metal ions from wastewaters still remains to be a problem needing solution. There are many methods for removal of hazardous ions, such as emulsion pertraction, ion exchange, electrochemical precipitation, membrane separation and adsorption [7, 8]. These technologies are not only expensive, but they also create another problem with metal-bearing sludge [3]. Adsorption is one of the most cost-effective treatment technologies, but the adsorbents used can be very expensive, thus cheap and efficient materials are needed to be used as suitable adsorbents. Recently, biosorption is increasingly applied for the removal of toxic metals using a passive binding process with nonliving organisms. It is a good alternative compared with conventional wastewater treatment techniques as it is an efficient, clean and cheap method. In this aspect, different kinds of unexpensive easily available and effective biosorbents have been studied for the removal of toxic metals from polluted wa-

* To whom all correspondence should be sent:
E-mail: pnovachka@svr.igic.bas.bg

ters [9–13]. Medicinal plants are of great interest as biosorbents, because they contain numerous active phytochemicals which are able to attach metal ions. They are also low-cost and non-hazardous materials, abundant in nature, require little processing, are specifically selective for heavy metals and easily disposed by incineration. Another advantage of the biosorbents is their biodegradability [14, 15].

Yarrow (*Achillea millefolium* L.) is a widespread and well-known species amongst the members of Achillea. The plant is native to Eurasia and is found widely from the UK to China. It is also grown commercially for use in herbalism and traditional medicine. [16] No data concerning the biosorption of copper ions on yarrow have been reported in the literature so far.

The objective of this work was to investigate the feasibility of using a material based on the widely used herb yarrow as natural biosorbents for the removal of Cu²⁺ ions from synthetic aqueous media. The possibility for regeneration of the used biomaterial was also studied.

EXPERIMENTAL

Materials and methods

A commercially available product containing leaves and blossoms of yarrow (*Achillea millefolium* L.) was washed several times with distilled water to remove surface adhered and water soluble compounds and dried at 60 °C in an electric oven for 48 h. The material (denoted as AM) was then milled in an electric grinder. No other physical or chemical treatment was performed on the material thus obtained.

For pH determination, sample suspensions (0.5 g of sample in 50 mL of deionized water) were prepared in stoppered 100-mL glass bottles. The mixtures were stirred for 2 h on a mechanical stirrer and after filtration, pH values of the aqueous solutions were measured on a pH meter model 211, Hanna instruments (Germany).

X-ray diffraction (XRD) pattern was obtained on a D8 Advance System from Bruker Inc. (Germany) using CuK α radiation (40 kV and 40 mA; $\lambda = 1.5404$ nm).

The Fourier transform-infrared (FTIR) spectra were measured on a Thermo Nicolet 6700 FTIR-spectrometer. Spectra were collected in the region (4000–400 cm⁻¹). Samples were prepared by the standard KBr pellet method.

The surface morphology of the biosorbent was observed on a scanning electron microscope (SEM) – Tescan instrument model SEM/FIB Lyra I XMU.

The porous structure of the studied material was investigated by low-temperature (–196 °C) nitrogen adsorption using a Quantachrome Nova 1200 apparatus (Quantachrome Instruments, USA).

Adsorption studies

Batch experiments were carried out to determine the adsorption properties of the plant material. Experiments were performed using stoppered 50-mL Erlenmeyer flasks containing about 0.2 g of sample and 20 mL of aqueous solution of Cu²⁺ ions. The mixture was shaken at room temperature (20 °C) by an automatic shaker. The initial solution pH was adjusted using 0.1 M HCl or 0.1 M NaOH. After the experiment the biomaterial was removed by filtration through a Millipore filter (0.2 μ m). The initial and equilibrium copper concentrations were determined by flame atomic adsorption spectrometry on a Thermo Elemental SOLAAR – M5 AA spectrometer (Thermo Fisher Scientific, USA). The amount of adsorbed copper ions per gram sorbents Q_e , were calculated using the following relationship:

$$Q_e = (C_0 - C_e) * V/m \quad (1)$$

where C_0 = initial concentration (mg L⁻¹), C_e = equilibrium concentration (mg L⁻¹), m = mass of adsorbent (g), and V = solution volume (L). All measurements were replicated and the average results were discussed.

Deionized water and analytical grade reagents were used. Working standard solutions of Cu²⁺ ions with concentrations of 50–500 mg L⁻¹ were prepared by stepwise dilution of a stock solution with concentration of 1 g Cu L⁻¹ (CuCl₂ in H₂O), Titri-sol® Merck, (Darmstadt, Germany).

RESULTS AND DISCUSSION

1. Sorbent characterization

The XRD pattern of the sample AM is presented on Fig. 1. The peak at around 22° 2 θ is assigned to the crystalline form of cellulose 1a [17]. The range between 15° and 25° 2 θ , corresponds to amorphous phases of lignin, hemicelluloses and cellulose [12, 18].

The nitrogen adsorption-desorption isotherm and the pore size distribution of the investigated plant material are presented on Fig. 2. The isotherm belongs to the type IV with hysteresis loop which resembles the H3 type in the IUPAC classification. The calculated textural parameters of AM are as follows: specific surface area – 0.9 m² g⁻¹; total

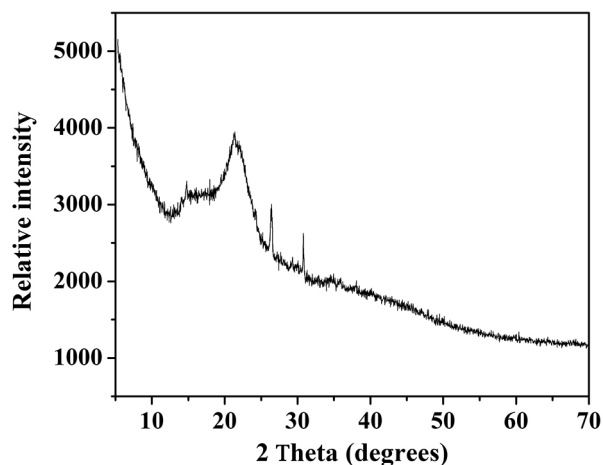


Fig. 1. X-ray diffraction pattern for AM.

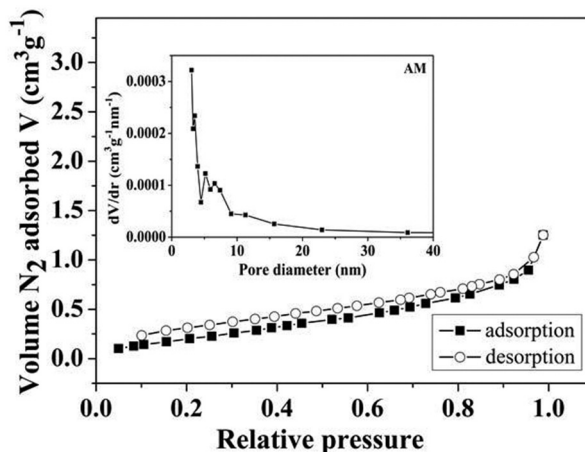


Fig. 2. Nitrogen adsorption-desorption isotherm and the pore size distribution of AM.

pore volume – $0.002 \text{ cm}^3 \text{ g}^{-1}$. The calculated average pore diameter for AM is 9 nm corresponding to mesoporous structure.

The measurements of slurry pH indicated that sample AM displayed pH values of about 5.7, which corresponds to the weakly acidic reaction of its aqueous suspension.

2. Adsorption studies

The pH of the aqueous solution has significant impact on the adsorption of metal ions on the adsorbents. The adsorption efficiency of the studied material as a function of pH of initial solutions is presented on Fig. 3. As expected, the removal of copper ions strongly depends on acidity of the initial solu-

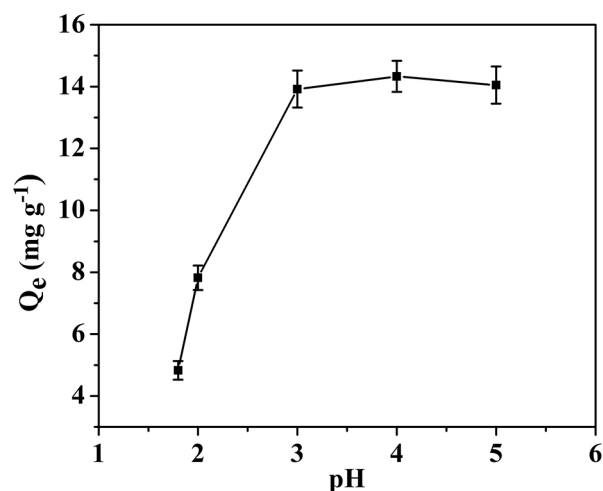


Fig. 3. Effect of pH on Cu^{2+} adsorption on AM.

tions. Upon increasing the pH values the amounts of adsorbed ions increased and the optimum pH range was found to be about 3.0–5.0. The adsorption can be explained on the basis of the competitive adsorption of H^+ and OH^- ions, on one side, and the copper ions on the other. The removal of Cu^{2+} ions could, therefore, be the combined result of ion exchange and surface complexation phenomena occurring on the surface of the investigated biomaterial.

The effect of contact time was studied at pH 4.0, initial Cu^{2+} concentration 200 mg L^{-1} . It was observed that the adsorption capacity increased rapidly with increasing of agitation time and reached equilibrium for less than 2 min, which shows a very fast adsorption rate. The short time for reaching equilibrium indicates that the biosorbent reveals high affinity towards Cu^{2+} ions.

The adsorption isotherm describes the distribution of the adsorbed species between the liquid and solid phases at equilibrium state. The elucidation of isotherm data by fitting them to different isotherm models is a substantial step in the adsorption study. Experimental isotherm of the investigated material is presented on Fig. 4.

The adsorption data were analyzed with the linearized forms of Langmuir, Freundlich and Dubinin-Radushkevich isotherm models.

The linear form of the Langmuir isotherm is expressed by the following equation:

$$C_e/Q_e = 1/K_L Q_0 + C_e/Q_0 \quad (2)$$

where C_e is the concentration of metal ions in the equilibrium solution (mg L^{-1}), Q_e is the amount of ion adsorbed (mg) per unit mass of adsorbent (g),

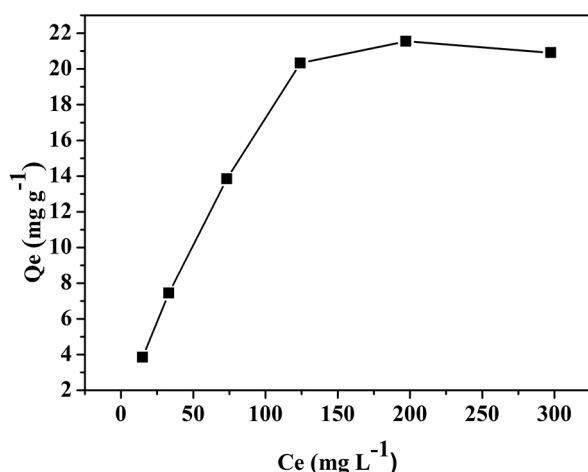


Fig. 4. Experimental adsorption isotherm for AM.

Q_0 , the maximum adsorption capacity (mg g^{-1}), K_L is the Langmuir constant related to enthalpy of the process.

The Langmuir model supports the following hypothesis: the adsorbent has a uniform surface: absence of interactions between the solid molecules; the sorption process takes place in a monolayer.

The linear form of the Freundlich model is expressed by the following equation:

$$\ln Q_e = \ln k_f + (1/n) \ln C_e \quad (3)$$

where k_f is a constant related to the adsorption capacity and n is an empirical parameter related to the intensity of adsorption.

The Freundlich model is valid for heterogeneous surfaces and predicts an increase in the concentration of the ionic species adsorbed onto the surface of the solid when increasing the concentration of certain species in the liquid phase.

The Dubinin–Radushkevich isotherm reveals the adsorption mechanism based on the potential theory. The linear form of the Dubinin–Radushkevich isotherm is described by the following equation:

$$\ln Q_e = \ln Q_m - \beta \varepsilon^2 \quad (4)$$

where Q_e is the amount of metal ion (mg) adsorbed per unit mass of adsorbent (g), Q_m is the maximum adsorption capacity (mg/g), β is the adsorption energy constant ($\text{mol}^2 \text{J}^{-2}$), and ε is the Polanyi potential, described as:

$$\varepsilon = RT \ln (1+1/C_e) \quad (5)$$

where R is the gas constant ($\text{J mol}^{-1}\text{K}^{-1}$) and T is the temperature (K). The mean adsorption energy E (KJ mol^{-1}) can be calculated using the parameter β as follows:

$$E = 1/(-2\beta)^{1/2} \quad (6)$$

The calculated isotherm constants and the correlation coefficients for the three models discussed above are presented in Table 1. From the correlation coefficients r^2 (greater than 0.95) it is clear that Langmuir model is most adequate in describing the adsorption processes. The maximum capacity was calculated and it was found to be 28.11 mg g^{-1} . It is evident that the material AM displays good adsorption capacity for Cu^{2+} and it could be used as potential adsorbent for the effective removal of these ions from contaminated aqueous solutions.

SEM analysis was used for the characterization of the morphology and structure of the AM biosorbent before and after Cu^{2+} adsorption. The SEM micrograph of the initial material (Fig. 5a) indicates that the biomass is of rough and heterogeneous morphology, containing a large number of pores of different size, which enables the sorption of various metal ions in the different parts of the biosorbent. The SEM micrograph of the AM biosorbent loaded with copper is shown in Fig. 5b. The porous cavities occupied by the adsorbed copper are visible as dots on the SEM image. As can be seen, the adsorbed copper ions are distributed homogeneously on the biosorbent surface.

As discussed above, the investigated plant material mainly consists of cellulose, hemicellulose and lignin. They contain many functional groups such as hydroxyl, carbonyl, carboxyl and amino groups with characteristic chemical structures. To deter-

Table 1. Isotherm constants and correlation coefficients for the three models for Cu^{2+} adsorption onto AM

Langmuir parameters			Freundlich parameters			Dubinin–Radushkevich parameters		
Q_0 (mg g^{-1})	K_L (L mg^{-1})	r^2	k_f ($\text{mg}^{1-n} \text{L}^n \text{g}^{-1}$)	n (L mg^{-1})	r^2	Q_m (mg g^{-1})	E (kJ mol^{-1})	r^2
28.11	0.013	0.9521	0.89	1.66	0.9099	17.54	0.09	0.7908

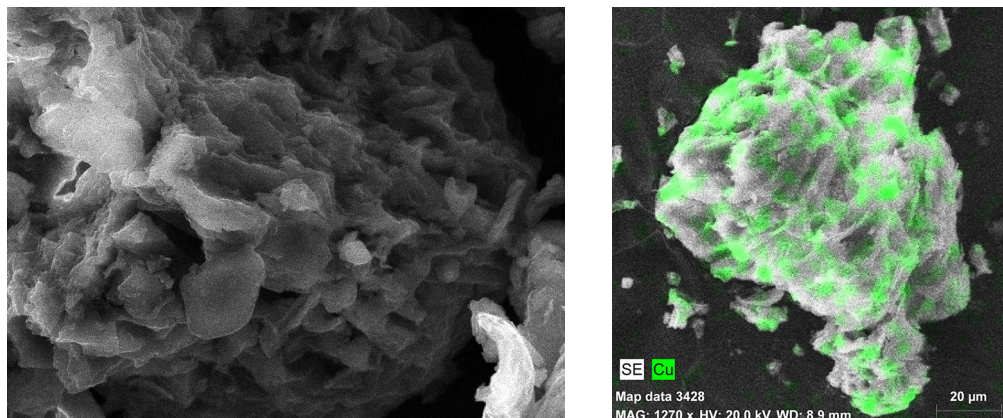


Fig. 5. Scanning electron micrographs of the surface of AM before (a) and after (b) Cu^{2+} adsorption.

mine the surface functional groups responsible for the adsorption properties of the studied plant, the FTIR spectra before and after Cu^{2+} -adsorption were recorded and shown in Fig. 6.

A very broad band between 3700 and 3000 cm^{-1} originates mainly from O-H stretching vibration of hydrogen bonded hydroxyl groups in phenolic and aliphatic structures. The group of bands around 2850 cm^{-1} belongs to the asymmetric and symmetric stretching C-H vibrations in methoxyl, methyl, methylene and methylidene groups in side chains aromatic and aliphatic structures. The bands and shoulders observed around 1730 cm^{-1} were attributed to carbonyl groups from the structures of ketones, esters, etc. The intensive band around 1640 cm^{-1} is a result of contributions from the stretching modes of C=C double bonds (isolated and conjugated), ring conjugated C=O bonds and C-O bonds in carboxylate groups [19, 20]. The multiple bands in the region of $1160\text{--}1040\text{ cm}^{-1}$ can be attributed to $\nu(\text{C-O-C})$ stretching mode in aliphatic ethers and

esters as well as $\nu(\text{C-O})$ stretching modes in alcoholic C-OH groups [17].

Looking at the spectra band shifting and possible involvement of hydroxyl and/or amino groups around the broad peak 3400 cm^{-1} is observed. Little change noticed in the carboxyl band at 1738 cm^{-1} and in the asymmetric C=O band at 1646 cm^{-1} indicates some carboxyl binding. The changes in the bands in the region of $1160\text{--}1040\text{ cm}^{-1}$ prove the participation of alcohols, ethers and esters in copper retention. If the shift is less than instrument resolution (4 cm^{-1}) it is not taken into account and cannot be discussed reliably. From the spectra it appears that carboxyl, hydroxyl groups as well as C-O and C=O groups (from ethers, esters and ketones) are involved in Cu binding to the AM which is in accordance with Khormaei et al [20]. Probably this plant contains components with functional groups which are readily available for coordination. The involvement of functional groups, containing hydrogen and oxygen atoms in the adsorption of Cu^{2+}

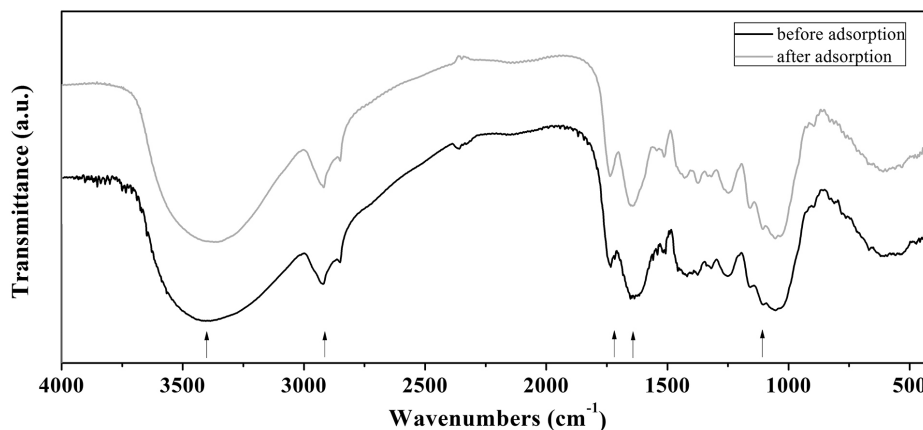


Fig. 6. FTIR-spectra of AM before and after Cu^{2+} adsorption.

ions is a proof that the process of copper retaining is a combination of ion exchange and surface complexation which is in accordance with the effect of pH study.

After adsorption of copper onto the investigated material, desorption studies have also been performed. The Cu²⁺ ions adsorbed onto the investigated biosorbent were eluted with 0.1M HNO₃, 1M HNO₃ and 0.1M EDTA. Diluted HNO₃ could not be used for desorption of Cu²⁺ ions (49% desorption). Both eluting agents 1M HNO₃ and 0.1M EDTA showed higher recovery efficiency, as follows: 98% for 1M HNO₃ and 87% for 0.1M EDTA, respectively, and are suitable for regeneration of both biosorbent and copper.

CONCLUSIONS

The present study deals with the adsorption properties of the medicinal plant yarrow (*Achillea millefolium* L.). XRD-patterns reveal peaks of cellulose 1 and amorphous phase due to lignin, hemicelluloses and amorphous cellulose. It was established from the FTIR spectra before and after Cu²⁺ adsorption that OH groups (from phenolic, alcoholic and COOH structures), as well as C-O и C=O groups (from ethers, esters and ketones) are involved in the biosorption process.

SEM analysis after metal loading revealed that the copper ions are distributed homogenously on the biosorbent surface. Langmuir model most adequately described the adsorption process and the maximum adsorption capacity was found to be 28.11 mg g⁻¹ which proved the good potential of the investigated material as a promising biosorbent for the removal of copper ions from aqueous solutions. 1M HNO₃ and 0.1M EDTA as eluting agents are suitable for regeneration of both biosorbent and copper.

Acknowledgements: This work is supported by the Bulgarian Ministry of Education and Science under the National Research Programme "Healthy Foods for a Strong Bio-Economy and Quality of Life" approved by DCM # 577 / 17.08.2018.

REFERENCES

1. Z-Y Yao, J. Qi, L-H Wang, *J. Hazard. Mater.*, **174**, 137 (2010).
2. M. Kanda, F. A. Abu Al-Rub, N. Al-Dabaybeh, *Adsorp. Sci. Technol.*, **21**, 501 (2003).
3. T. Benzaoui, A. Selatnia, D. Djabali, *Adsorp. Sci. Technol.* **36**, 114 (2018).
4. J. D. Cuppett, S. E. Duncan, A. M. Dietrich, *Chem. Senses*, **31**(7), 689–697 (2006).
5. U. Forstner, G. T. W. Wittmann, *Metal Pollution in the Aquatic Environment*, Springer-Verlag, Berlin, 1979.
6. D. A. Wright, P. Welbourn, *Environmental Toxicology*, Cambridge University Press, Cambridge, U.K., 2002.
7. F. Fu, Q. Wang, *J. Environ. Manag.*, **92**, 407 (2011).
8. P. Vassileva, A. Detcheva, D. Voykova, *Compt. Rend. Acad. Bulg. Sci.*, **67**, 497 (2014).
9. J. Wang, C. Chen, *Biotechnol. Adv.*, **27**, 195 (2009).
10. U. Farooq, J. Kozinski, M. Khan, M. Athar, *Bioresour. Technol.*, **101**, 5043 (2010).
11. I. Anastopoulos, A. Robalds, H. Tran, D. Mitrogiannis, D. Giannakoudakis, A. Hosseini-Bandegharrae, G. Dotto, *Environ. Chem. Lett.*, **17**, 755 (2019).
12. L. Ivanova, A. Detcheva, P. Vassileva, *Anal. Lett.*, **52**, 2650 (2019).
13. A. A. Redha, *Arab. J. Basic Appl. Sci.*, **27**, 183 (2020).
14. L. Ivanova, P. Vassileva, A. Detcheva, *Cellulose Chem. Technol.*, **54**, 1033 (2020).
15. L. Ivanova, P. Vassileva, G. Gencheva, A. Detcheva, *J. Environ. Prot. Ecol.*, **21**, 37 (2020).
16. E. Marian., P. Bianca, C. Zbarcea, M. Tigan, A. Puskas, N. Duteanu, *Analele Universității din Oradea, Fascicula Protecția Mediului*, **XXV**, 399 (2015).
17. C. Araujo, I. Almeida, H. Rezende, S. Marcionilio, J. Leon et al., *Microchem. J.*, **137**, 348 (2018).
18. G. Yuvaraja, N. Krishnaiah, M. Subbaiah, A. Krishnaiah, *Colloid Surface B*, **114**, 75 (2014).
19. M. Jarzębski, W. Smulek, H. M. Baranowska, Ł. Masewicz, J. Kobus-Cisowska, M. Ligaj., E. Kaczorek, *Food Hydrocoll.*, **104**, Article number 105748 (2020).
20. M. Khormaei, B. Nasernejad, M. Edrisi, T. Es-lamzadeh, *J. Hazard. Mater.*, 149, 269 (2007).

Manifestation of Vegard's law on the example of synthetic mixed Co-Mn alluaudite-type phases

V. Kostov-Kytin^{1*}, R. Stoyanova², D. Marinova²

¹ Institute of Mineralogy and Crystallography, Bulgarian Academy of Sciences, 1113 Sofia, "Acad. Georgi Bonchev" str., bl. 107, Bulgaria

² Institute of General and Inorganic Chemistry, Bulgarian Academy of Sciences, 1113 Sofia, "Acad. Georgi Bonchev" str. bld. 11, Bulgaria

Received October 12, 2021; Accepted January 15, 2022

Synthetic alluaudite-structure-type compounds have appeared to be promising cathode materials in electrochemistry. Results from Rietveld refinement of the crystal structures of six representatives of this group with the general formula $\text{Na}_{2+2\delta}(\text{Co}_{1-x}\text{Mn}_x)_{2-\delta}(\text{SO}_4)_3$ with chemical compositions falling within the range $0.12 \leq x \leq 0.52$, have been reported in this work. The manifestation of Vegard's law has been demonstrated as well as the opportunity to derive the transition metals' content directly from the values of lattice parameter b .

Keywords: Vegard's law, alluaudite-type phases.

INTRODUCTION

During the last few years, one of the fastest-growing directions in electrochemistry of cathode materials is targeting the double sulfates of sodium and transition metals with alluaudite-type structure as very perspective, cheaper, and environmentally compatible materials. Alluaudite sulfates are thought to be high-voltage electrodes for rechargeable-ion batteries (lithium and sodium), with structural matrix which is able to intercalate alkali ions quickly and reversibly [1, 2]. Recent investigations provided information for a quick and easy method for obtaining the foregoing salts with the general formula $\text{Na}_{2+2\delta}(\text{Co}_{1-x}\text{Mn}_x)_{2-\delta}(\text{SO}_4)_3$ ($0.12 \leq x \leq 0.52$). The synthesis procedure for these mixed sodium manganese-cobalt sulfates includes simple dehydration of the initially prepared hydrated salts with a blöndite-structure [3, 4]. The occupancy of the 8f crystal site in the structures of the run-products by Co and Mn leads to a lowering of the extent of cationic deficiency, which is thought to be an important factor affecting the Na^+ migration. This provides an opportunity to look for optimal compositions that lead to improved electrochemical behavior of these materials.

This work provides evidence for the validity of Vegard's law over a group of six alluaudite type compounds with chemical compositions falling within the above reported formula and ranges. It also demonstrates the opportunity to derive the transition metals' content for each particular phase directly from the value of the lattice parameter b of its crystal structure.

EXPERIMENTAL

Synthesis Procedure

The synthesis of these mixed sodium manganese-cobalt sulfates started with the preparation of hydrated salts $\text{Na}_2\text{Co}_{1-x}\text{Mn}_x(\text{SO}_4)_2 \cdot y\text{H}_2\text{O}$, $0 \leq x \leq 1.0$ and $y = 2, 4$, taking into account the solubility diagrams of the three-component systems Na_2SO_4 – CoSO_4 – H_2O and Na_2SO_4 – MnSO_4 – H_2O at 25 °C [5, 6]. The procedure next continued with isothermal decrease of the degree of supersaturation. Afterwards, the solutions were cooled down to room temperature under vigorous stirring. Equilibrium state was reached in about 2 to 5 days depending on the concentration of Mn^{2+} ions. All the reagents used were of analytical grade of purity (Sigma-Aldrich/Merck). The anhydrous double salts were obtained by thermal decomposition at up to 350 °C between 24 to 48 hours where the temperature and

* To whom all correspondence should be sent:
E-mail: vkytin@abv.bg

the heating time interval were dependent on the composition.

Analytical Procedures

The powder X-ray diffraction (PXRD) patterns were collected within the range from 5° to 80° 2θ with a scanning step 0.02° 2θ on Bruker D8 Advance diffractometer with $\text{CuK}\alpha$ radiation and LynxEye position sensitive detector and 0.2 s/strip counting statistics (equal to 35s/step).

The Co/Mn ratio in the solid residue was determined with Optical Emission Spectroscopy Inductively Coupled Plasma (ICP) spectrometer PRODIGY 7 (Teledyne Leeman Labs). Concentrations of the elements were determined at 257.610 nm for manganese and 228.615 nm for cobalt chosen as the best analytical lines.

Phase Identification

The presence of two crystalline phases has been detected in all powder X-ray diffraction patterns of the considered here samples. One of them has been recognized as an alluaudite-type anhydrous sodium mixed cobalt-manganese sulfate material with a general composition $\text{Na}_{2+2\delta}(\text{Co}_{1-x}\text{Mn}_x)_{2-\delta}(\text{SO}_4)_3$ with chemical compositions falling within the range $0.12 \leq x \leq 0.52$. The crystal structures of its representatives have been refined using as a starting model the $C2/c$ space group structure of the previously reported pure manganese analogue of this materials [3]. The presence of the other one has been established as an admixture phase after a search has been undertaken in the ICDD database (PDF-4+ 2015 – PDF card 4-017-3170) using chemical criteria and the two strongest lines of this compound ($d=4.01 \text{ \AA}$ (210) and $d=3.44 \text{ \AA}$ (212)) that could not have been described by using solely the alluaudite structure model. It has appeared that this is a structure analogue of the mineral vanthoffite – $\text{Na}_6\text{Mg}(\text{SO}_4)_4$ (<https://www.mindat.org/min-4151.html#autoanchor6> [7]) where magnesium atoms have entirely been substituted by cobalt and/or manganese – $\text{Na}_6(\text{Co,Mn})(\text{SO}_4)_4$. Pure Co- and Mn-vanthoffites have firstly been prepared by a solid-state reaction [8]. They crystallize in S.G. $P2_1/c$, $Z=2$, and the lattice parameters values are: a (\AA) = 9.922, 9.965; b (\AA) = 9.246, 9.280; c (\AA) = 8.282, 8.248; $b(\circ)$ = 116.25, 116.25; and V (\AA^3) = 681.4, 684.1, correspondingly.

Rietveld Refinements

The Rietveld refinement procedures has been carried out with the GSAS program and EXPGUI [9, 10]. Both structures have initially been refined

with soft constraints, consisting of all S-O bond distances. After several attempts to include the atomic parameters of the Co-vanthoffite in the Rietveld refinement process it has become clear that the final results are quite unrealistic from a crystal chemical point of view regardless of the values of the restraint weighting factors involved. Subsequently for this phase only the profile parameters and never the atomic ones have been used in the refinement procedures. Later on, established gradual shifts of its strong reflections towards their lower d -values with increase of the Co/Mn ratio ($R^{\text{VI}}\text{Co}^{2+} - 0.745 \text{ \AA}$; $R^{\text{VI}}\text{Mn}^{2+} - 0.83 \text{ \AA}$, R -ionic radius for the corresponding coordination according to [11]) have suggested that both these elements enter its crystal structure in amounts corresponding to those set in the initial reaction batch. In the final refinement cycles the soft constraints have been released for the alluaudite type materials without causing any substantial structural distortions before reaching convergence. Neutral atomic scattering factors, as these are stored in GSAS, have been used for all atoms. No corrections have been made for absorption.

Visualization

The following programs have been used for graphic presentations:

- WinPLOT utilities as a Windows tool [12] (powder X-ray diffraction patterns);
- VESTA ver. 3.3.2 [13] (visualization of crystal structure).

RESULTS

Six representatives of alluaudite-type mixed cobalt-manganese sulfate phases have been prepared by the above described procedure and further on designated according to the Co-content in their composition (wt%) detected by the ICP analysis as: Co48, Co59, Co65, Co68, Co82, and Co88. The overall Co+Mn content of the octahedral position in the structure has been normalized to 100 (see next section text, Table 1, and Fig. 3).

Figure 1a presents a general view of the alluaudite-type structure of the studied title compounds. Figure 2 contains the Rietveld refinement plot of $\text{Na}_{2.68}(\text{Co}_{1.26}\text{Mn}_{0.59})_{1.85}(\text{SO}_4)_3$ – sample Co65, refined in the $C2/c$ space group together with the cobalt-and-manganese-containing vanthoffite phase – $\text{Na}_6(\text{Co,Mn})(\text{SO}_4)_4$. Some of the strongest vanthoffite lines are denoted by letter v). Inset a) demonstrates the gradual shift of the XRD (020)-reflections of the studied materials towards their lower d -values with increase of the Co/Mn ratio in their compositions. Powder data statistics and crystal-

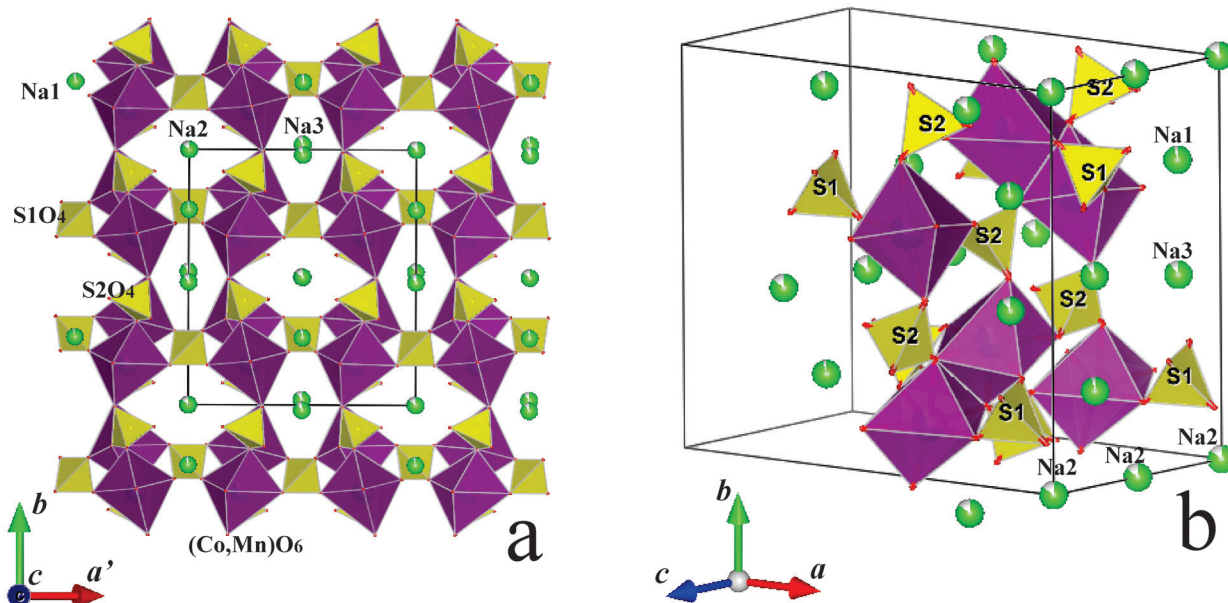


Fig. 1. *a* – General view of the alluaudite-type structure. The mixed $(Co,Mn)O_6$ octahedra are dark grey and the $S1O_4$ and $S2O_4$ tetrahedra are light gray; *b* – edge sharing $(Mn,Co)O_6$ units forming the $(Mn,Co)_2O_{10}$ dimers.

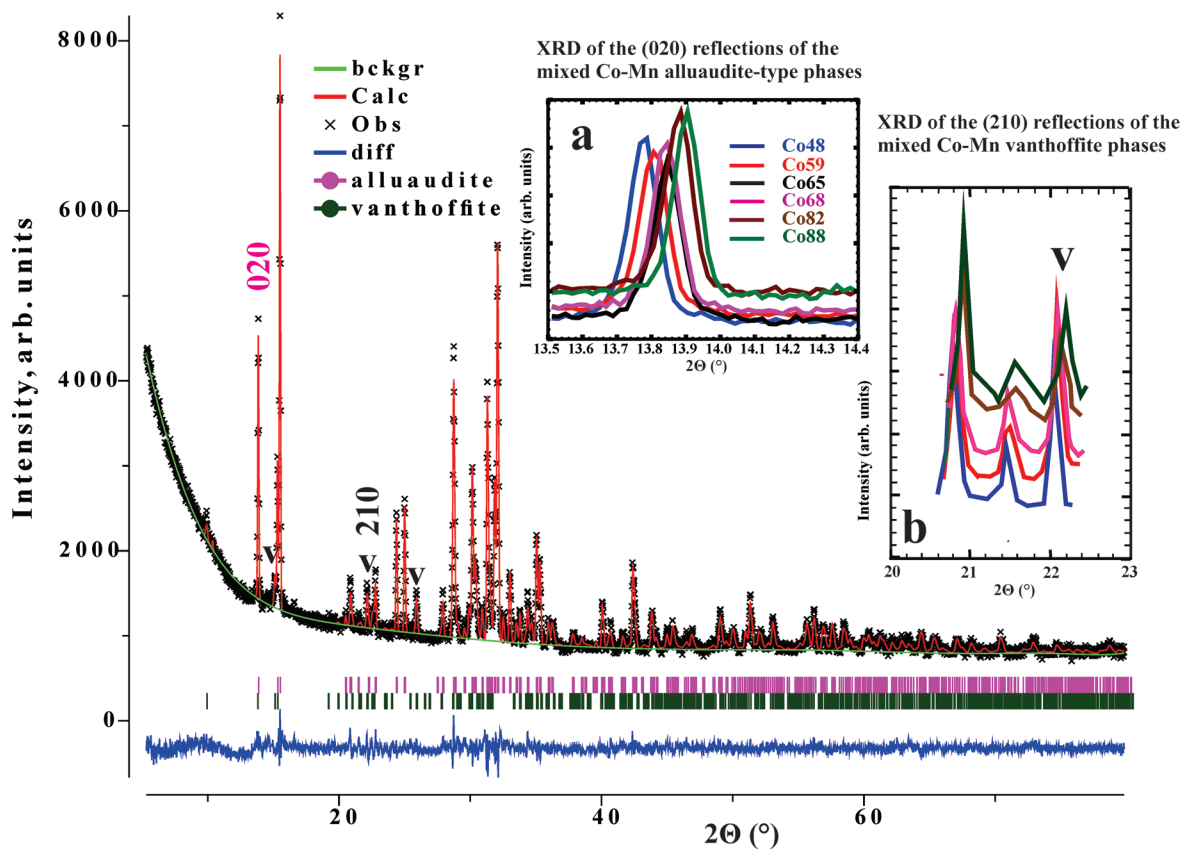


Fig. 2. Rietveld refinement plot of $Na_2(Co_{0.63}Mn_{0.37})_2(SO_4)_3$ solved in the $C2/c$ space group together with $Na_4(Co,Mn)(SO_4)_4$ (some of its strongest lines are denoted by letter *v*). The inset presents the gradual shift of the XRD (020)-reflections of the studied materials towards their lower *d*-values with increase of the Co/Mn ratio in their compositions.

Table 1. Lattice parameters and refinement details for the alluaudite-type mixed cobalt-manganese sulfate phases

	Co48	Co59	Co65*	Co68	Co82	Co88
<i>Space Group</i>	<i>C2/c</i>	<i>C2/c</i>	<i>C2/c</i>	<i>C2/c</i>	<i>C2/c</i>	<i>C2/c</i>
<i>a</i> (Å)	12.6799(4)	12.6787(5)	12.6455(7)	12.6564(5)	12.6261(4)	12.6168(4)
<i>b</i> (Å)	12.8231(4)	12.7946(4)	12.7730(6)	12.7699(4)	12.7347(4)	12.7220(3)
<i>c</i> (Å)	6.5303(2)	6.5200(2)	6.5113(3)	6.5108(2)	6.4989(2)	6.4967(2)
angles (°) α	90	90	90	90	90	90
angles (°) β	115.503(2)	115.440(2)	115.425(3)	115.4033(2)	115.3321(2)	115.307(2)
angles (°) γ	90.0	90	90	90	90	90
<i>V</i> (Å) ³	958.34(6)	955.11(7)	949.86(1)	950.53(6)	944.46(6)	942.72(5)
Formula unit	Na _{2.69} (Co _{0.88} Mn _{1.02}) _{1.90} (SO ₄) ₃	Na _{2.68} (Co _{1.09} Mn _{0.83}) _{1.91} (SO ₄) ₃	Na _{2.68} (Co _{1.26} Mn _{0.59}) _{1.85} (SO ₄) ₃	Na _{2.71} (Co _{1.27} Mn _{0.64}) _{1.91} (SO ₄) ₃	Na _{2.73} (Co _{1.52} Mn _{0.38}) _{1.90} (SO ₄) ₃	Na _{2.81} (Co _{1.68} Mn _{0.24}) _{1.92} (SO ₄) ₃
Calculated unit cell Fw	1831.876	1836.846	1826.762	1842.189	1845.420	1860.936
<i>Z</i>	4	4	4	4	4	4
Pcalc (g cm ⁻³)	3.174	3.194	3.194	3.219	3.245	3.278
Wavelength, Å	1.5419	1.5419	1.5419	1.5419	1.5419	1.5419
2 θ range (deg)	5-80	5-80	5-80	5-80	5-80	5-80
Step-scan increment (2 θ), deg	0.02	0.02	0.02	0.02	0.02	0.02
Step-scan time, s	35	35	35	35	35	35
Profile function	Pseudo-Voigt	Pseudo-Voigt	Pseudo-Voigt	Pseudo-Voigt	Pseudo-Voigt	Pseudo-Voigt
Rwp (%)	5.30	4.08	5.44	4.23	4.16	3.70
Rp (%)	4.14	3.32	4.85	3.43	3.17	2.98
Red- χ^2	2.153	1.813	1.168	1.98	1.687	1.853
RF ² (%)	10.04	9.42	11.14	12.54	11.26	13.00
Wt. Frac. %**	77	77	85	78	79	73

* Rietveld refinement results for the sample reported in [2]; The XRD experiment has been conducted at the new conditions applied for the representatives of the whole alluaudite series in the present work.

** The remaining up to one hundred percent belongs to the (Co,Mn)-vanthoffite phase – Na₆(Co,Mn)(SO₄)₄.

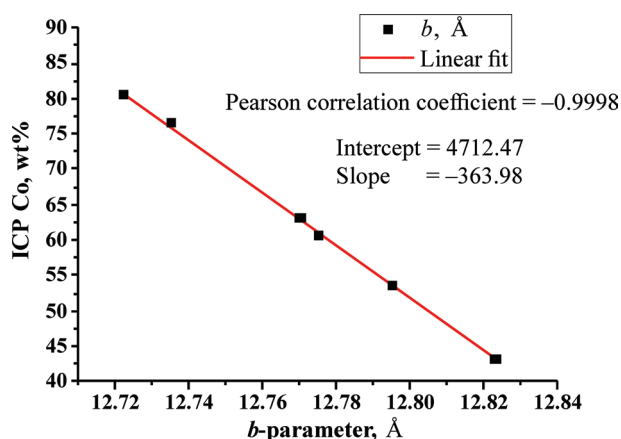


Fig. 3. Linear fit of the lattice b parameter values of the studied alluaudites set against the corresponding Co-contents provided by the ICP analyses. The overall Co+Mn content of the octahedral position in the structure has been normalized to 100.

lographic data from the refinements of the alluaudite-type compounds crystal structures based on the $C2/c$ space group are reported in Table 1. Figure 3 presents the linear fit of the obtained by the Rietveld refinement procedures six values for the b -parameters of the studied alluaudites set against the Co-contents provided by the ICP analyses (wt%), correspondingly.

DISCUSSION

Crystal structure of the mixed Co-Mn alluaudite-type phases

The crystallographically equivalent $(\text{Mn},\text{Co})\text{O}_6$ units are coupled by edge sharing to form $(\text{Mn},\text{Co})_2\text{O}_{10}$ dimers, which are in their turn connected by SO_4 tetrahedra to form three-dimensional framework with cavities and channels (Fig. 1b). The $(\text{Co}_{1-x}\text{Mn}_x)_{2-\delta}(\text{SO}_4)_3$ framework carries negative charge, whose compensation is achieved through the presence of sodium ions. The latter occupy three symmetrically independent positions. One of them resides in the cavities connected in a very narrow channel running along a -axis. The channels running along c axis in which the rest of the charge compensating ions are located are more interesting from practical considerations. As it has been discussed previously [3] their effective diameter is suitable for fast Na^+ diffusion during electrode reactions.

Compositional dependence of the values of the lattice parameter b

In general, the unit cell parameters of the studied phases respond adequately and consistently to any

changes in the Co/Mn ratio in their compositions due to the differences in the ionic radii of Co^{2+} and Mn^{2+} (see data in Table 1). Among them, the lattice parameter b is of special interest because its value can directly be derived from the X-ray diffraction experiment. The PXRD pattern presented in Fig. 2 clearly reveals the opportunity to measure the d -value of the (020)-reflection without any hindrance due to e.g. peak overlapping and this concerns all of the obtained phases. This is a second order reflection from the $\{0k0\}$ scattering planes. For the standard setting of space group $C2/c$ the distance between the (010) planes equals the lattice parameter b value. Thus, the magnitude of d -spacing measured for the (020)-reflection is twice less than that one of b (Å). The inset of the same figure indicates a gradual and regular shift of the XRD (020)-reflections of the studied materials towards their lower d -values consistent with the increase of the Co/Mn ratio in their compositions. Studies have shown that Co-Mn-vanhoffite also responds to changes in the ratio of these two metals in its composition. When comparing the experimental powder XRD patterns some of its reflections shift towards their lower d -values consistent with the increase of the Co content similar to the observed changes in the positions of the lines of the alluaudite materials (Fig. 2, inset b).

Before applying the procedure for establishing the compositional dependence of the values of the lattice parameter b , it is necessary to calculate the amounts of cobalt and manganese in the compositions of title compounds and their by-products. This is done assuming that the two transition metals enter the octahedral positions in the same ratio for both phases and also that all atomic positions in the vanhoffite structure are entirely occupied. The data from the quantitative analyzes performed by the Rietveld method (last row in Table 1) as well as the available crystal chemical information for both compounds have also been used.

The application of linear fit on a data set comparing the obtained by Rietveld refinement six values for the b -parameters of the studied alluaudites with the Co-contents of the corresponding alluaudite phases received by the ICP analyses (Fig. 3.) reveals a correlation coefficient of -0.9998 and the following linear equation can be derived:

$$Y_{\text{Co}} (\text{wt}\%) = 4712.47 - 363.98 \times d_{020}$$

Figures 2 and 3 clearly demonstrate manifestation and validity of Vegard's law [14, 15] on a set of alluaudite type compounds with the possibility of varying the content of cobalt and manganese in them, accompanied by regular changes in the values of lattice b parameter. Table 1 data reveal that

the Na content in the alluaudite phases slightly increases with the increase of the Co content. This, however does not withstand the overall shrinkage of the structure caused by the corresponding decrease of the larger in size Mn cations from the framework construction. Moreover, most of these species expected to provide the cationic mobility for these compounds are located in channels formed by the transition metal octahedra. Thus, the PXRD (020)-reflection proved to be a very convenient means for quantitative assessment of the cobalt/manganese content in the considered compounds. It can easily be obtained by passing the value of the measured interplanar distance – d_{020} in the above linear equation.

The preparation of pure sodium-manganian alluaudite phase has already been reported [3]. The entry of the experimentally measured value of d_{020} ($b = 12.943(1) \text{ \AA}$) for this compound in the above equation confirms the validity of the Vegard's rule in the direction of this end-member of the investigated series. Attempts to find any evidence supporting the manifestation of this rule towards the pure Co member in the available structural databases and literature sources failed. The increased amounts of the vanthoffite phases formed with increase of the Co-containing source in the reaction media (last row in Table 1) is an additional indicator that complete isomorphism between the two pure end members is hardly possible under the conditions of the here applied synthesis procedure. A maximum Co content of about 85 wt% can be judged from Figure 3 for thus prepared alluaudite phases.

CONCLUSIONS

This is a case study extending the validity of Vegard's rule on a group of alluaudite-type compounds characterised with various content ratios of the transition elements in them. It demonstrates as well the opportunity of obtaining information on their chemical composition based solely on powder X-ray diffraction data.

Acknowledgements: This work was supported by the Bulgarian Ministry of Education and Science under the National Research Programme "Low Carbon Energy for the Transport and Household (E+)" (approved by DCM # 577/17.08.2018).

REFERENCES

1. G. Rousse, J.-M. Tarascon, *Chem. Mater.*, **26**, 394 (2014).
2. Q. Ni, Y. Bai, F. Wu and C. Wu, *Adv. Sci.*, **4**, 1600275, (2017).
3. D. Marinova, V. Kostov, R. Nikolova, R. Kukeva, E. Zhecheva, M. Sendova-Vasilevac, R. Stoyanova, *J. Mater. Chem. A*, **3**, 22287, (2015).
4. D. M. Marinova, V. V. Kostov, R. P. Nikolova, R. R. Kukeva, E. N. Zhecheva, R. K. Stoyanova, *Chemical communications*, **54(43)**, 5466, (2018).
5. W. F. Linke, *Am. Chem. Soc.*, **Vol. II**, 1137, (1965).
6. [6] W. F. Linke, *Am. Chem. Soc.*, **Vol. II**, 566, (1965).
7. <https://www.mindat.org/min-4151.html#autoanchor6>. – Mindat.org – an outreach project of the Hudson Institute of Mineralogy, a 501(c)(3) not-for-profit organization.
8. K. L. Keester, W. Eysel, *Acta Crystallographica Section B: Structural Crystallography and Crystal Chemistry*, **33.1**, 306, (1977).
9. A. C. Larson, R. B. Von Dreele, General Structure Analysis System (GSAS), Report LAUR 86-748, Los Alamos National Laboratory, (2000).
10. B. H. Toby, EXPGUI, a graphical user interface for GSAS, *J. Appl. Crystallogr.*, **34**, 210, (2001).
11. R. Shannon, *Acta Cryst.*, **A32**, 751, (1976).
12. T. Roisnel, J. Rodriguez-Carvajal, in: Materials Science Forum (Proceedings of the Seventh European Powder Diffraction Conference (EPDIC 7), R. Delhez and E. J. Mittenmeijer (eds.), 118, (2000).
13. K. Momma, F. Izumi, VESTA 3 for three-dimensional visualization of crystal, volumetric and morphology data, *J. Appl. Crystallogr.*, **44**, 1272, (2011).
14. L. Vegard, *Zeitschrift für Physik*. **5(1)**, 17, (1921).
15. A. R. Denton, N. W. Ashcroft, *Physical Review A*, **43, 6**, 3161, (1991).

Phase characterization of glass-ceramics with high iron oxide concentrations

I. K. Mihailova^{1*}, R. G. Harizanova¹, N. I. Shtapleva¹,
G. V. Avdeev², C. Rüssel³

¹ *University of Chemical Technology and Metallurgy, 8 Kliment Ohridski Blvd., Sofia 1756, Bulgaria*

² *Institute of Physical Chemistry “Rostislaw Kaischew”, Bulgarian Academy of Sciences,
Akad. G. Bonchev Str., bl. 11, Sofia 1113, Bulgaria*

³ *Otto Schott Institute of Materials Research, University of Jena, Fraunhoferstr. 6,
07743 Jena, Germany*

Received October 30, 2021; Accepted January 11, 2022

Glass-ceramics containing iron oxides attract scientific interest due to their magnetic and electrical properties and the potential for various applications in electronics, biomedicine and catalysis. The synthesis of glass-ceramic materials in the system $\text{CaO}/\text{Na}_2\text{O}/\text{SiO}_2/\text{Fe}_2\text{O}_3$ with high concentrations of Fe_2O_3 (20, 25 and 30 mol%) is reported. The samples are obtained by melting-quenching technique. This led to spontaneous crystallization during pouring the melts and in the formation of magnetite and hematite, which are identified by X-ray diffraction analyses (XRD) and optical microscopy. Scanning electron microscopy (SEM) and elemental analysis by means of energy-dispersive spectroscopy (EDXS) are used to study the microstructure and the chemical composition of the crystalline and amorphous phases. The obtained results show an inhomogeneous microstructure of the glass-ceramics, composed of several different crystalline phases with different morphologies as well as of a glassy phase. Based on the data from EDXS measurements, a procedure is proposed by which the weight fraction of the two present iron oxide phases – hematite and magnetite – is evaluated. The weight percentage of the crystalline phases is estimated as a function of the iron oxide concentration and it is shown to vary between 13 to 29 wt% when the Fe-oxide concentration changes from 25 to 30 mol% (47–53 wt%) Fe_2O_3 .

Keywords: iron oxides, glass-ceramics, crystallization, SEM, EDXS.

INTRODUCTION

Glass-ceramics are functional materials which appropriately combine the properties of amorphous and crystalline phases and due to their variable properties, they find various applications. Typically, glass-ceramic materials are obtained by controlled crystallization of glasses with specially selected compositions. Glass-ceramics containing iron oxides have been the subject of numerous studies because the obtained materials could possess favourable catalytic activity, magnetic, optical and electrical properties [1]. Iron oxides occur in high concentrations in many wastes from mining and metallurgical industries. Hence, rational solutions have to be found for their utilization which explains the high interest of researchers in such systems. In

suitable combinations, they can be vitrified or converted into functional glass-ceramic materials. As an example, heat-shielding iron containing glasses [2] are to be mentioned. Glass containing more than 15 wt% iron oxides can be used to produce glass-ceramics with low resistivity and interesting magnetic characteristics. In analogy, glass-ceramics have been obtained which can find applications in semiconductor engineering, in household electric equipment and in civil engineering. They are proposed as promising materials for induction heating applications [3], as tiles for heated floors [4] and as fillers in composites absorbing high-frequency magnetic radiation [5]. The type and concentration of iron-containing phases is decisive for the properties of glass-ceramics and hence also for potential applications.

The crystallization of ferrimagnetic oxides from glasses has been extensively investigated for developing magnetic materials based on glass-ceramics [6]. It has been found that the magnetic properties

* To whom all correspondence should be sent:
E-mail: irena@uctm.edu

depend on the composition, processing temperature, annealing time, particle size, heat treatment and cooling rate [7–9]. Some investigations have also shown the influence of iron rich phases on electrical properties of glass-ceramics.

The presence of iron in silicate melts and glasses significantly affects their crystallization tendency, the type of crystalline phases formed and the microstructure of the obtained materials. The crystallization phenomena in iron rich silicate glasses are described by Karamanov and Pelino [10] and in Refs. [11, 12]. According to their research an initial liquid – liquid separation stimulates the magnetite formation. In addition, magnetite crystals serve as nuclei for the subsequent formation of silicate phases.

The quantity of the magnetic phase allows controlling the magnetic properties of glass-ceramics. Higher concentrations of iron oxides usually result in improved magnetic properties [13]. Iron oxides are often used as materials for biomedical applications due to their magnetic properties, low cost, and low cytotoxicity [14]. Many studies [13–20] have been performed in silicate systems containing iron oxides to develop glass-ceramics exhibiting suitable magnetic properties in order to use them as thermo-seed for hyperthermia and in bioactivity experiments.

In the present work, the phase composition of glass-ceramic materials in the system CaO/Na₂O/SiO₂/Fe₂O₃ with high concentrations of Fe₂O₃ (20, 25 and 30 mol%) further denoted as S2_20, S2_25 and S2_30, respectively are investigated by X-ray diffraction, optical microscopy and by EDXS/SEM. The main goal of the presented research is to evaluate the chemical composition and quantity of the crystalline and amorphous phases in an inhomogeneously crystallizing Fe-containing glass and to trace how the changing Fe-concentration from 25 to 30 mol% Fe₂O₃ influences the crystallization degree and morphology as well as phase composition of the occurring crystals.

EXPERIMENTAL PROCEDURE

In the present work, glass-crystalline materials obtained by the melt-quenching technique were investigated. These samples correspond to the system 16Na₂O/10CaO/(74-x)SiO₂/xFe₂O₃, x=20, 25, 30 (in mol%). For their synthesis, the following reagent grade raw materials were used: Na₂CO₃, CaCO₃, SiO₂ and Fe₂O₃. The compositions were melted in a Pt-crucible at a temperature of 1400 °C in air for 1.5 h. After pouring into a pre-heated C-mould, the melts were transferred to a muffle furnace and annealed for 10 min at 480 °C. Then the furnace is switched off and cooled down to room temperature.

Spontaneous crystallization occurred during pouring the melt.

X-ray diffraction (XRD) was applied for phase identification. The analyses were performed with an X-ray diffractometer Empyrean Panalytical using Cu-K α radiation in the 2 θ range from 7 to 95°, step size 0.06° and scan step time 1 s. In order to quantify the concentration of the crystalline phases and the amorphous phase, samples containing an additive of 30 wt% corundum, which acts as a reference were analyzed. The crystalline phases were identified using the powder diffraction files №:98-002-4005, 98-008-2434 and 98-008-8417 from database JCPDS – International Centre for Diffraction Data PCPDFWIN v.2.2. (2001). The quantitative phase analyses were performed with the High Score Plus, version 4.0 software.

Scanning electron microscopy (SEM) and optical microscopy on transmission were used to examine the microstructure of the samples. Thin sections with average thickness of about 50 μ m immobilized on a silica glass substrate were prepared and examined by an optical microscope Jenapol Interphako U MAP. SEM studies were performed on polished samples coated by sputtering a thin layer of carbon on the surface. The chemical composition of the crystalline phases and the residual glass in different points on the sample surface was investigated by energy dispersive X-ray spectroscopy (EDXS). Analytical Scanning Electron Microscope JEOL JSM-6010PLUS/LA with a fully integrated X-ray elemental analysis unit was used.

RESULTS AND DISCUSSION

X-ray diffraction data of the samples are presented in Fig. 1. The presence of a predominant amorphous phase (glass), as well as of two crystalline iron oxide phases: magnetite, Fe₃O₄ and hematite, Fe₂O₃ was found in all samples. The fraction of the crystalline phases is higher in the samples with a higher content of iron oxide in the initial composition and a lower iron content in the residual silicate glass. The results for the phase composition of the samples are summarized in Table 1. Sample S2_20 with 20 mol% Fe₂O₃ has a very small concentration of crystalline phases (approximately 2 wt%). Thus, the SEM/EDXS analyses were performed only on the samples with higher iron concentrations: S2_25 and S2_30.

The microstructure of the samples shows a number of similar features such as the presence of zoning and changes in the morphology from the bottom of the cast block to the upper surface. Nevertheless, the crystalline phases of the samples possess similar morphologies. The structural characteristics and

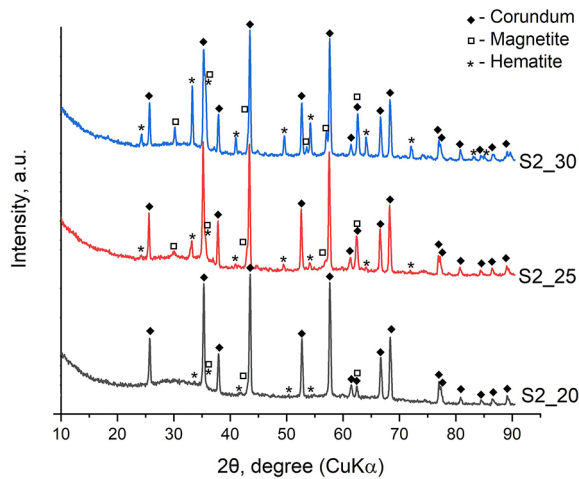


Fig. 1. XRD-pattern of the samples containing additive of 30 wt% corundum.

phase composition of the samples can be controlled by various factors: melt cooling rate, type of contact surface (with air, with graphite mold for annealing, etc.), chemical composition of the samples and respectively, amounts of iron oxide and silicon dioxide in the samples, the raw materials used, the quantity of the batch, etc. Here a platinum crucible and a high melting temperature as well as batch composition with high alkali and iron oxide concentration are used to achieve the crystallization of Fe-containing phases.

Typical microstructural features of the samples examined on polished surfaces of a cross-section of the cast blocks are presented in Fig. 2. At the periphery of the samples (i.e. this part of the cast block which is close to the mold walls), the solidifying melt cools fastest and this part is mainly amorphous (upper left corner of Fig. 2a). The microstructure

Table 1. Phase compositions of the samples, according to the X-ray diffraction data

Sample	Percentage of phases	
	Crystal phases [wt %]	Amorphous phase [wt %]
S2_20	Magnetite~ 1 % Hematite~ 1 %	98 %
S2_25	Magnetite 6.86 % Hematite 4.14 %	89 %
S2_30	Magnetite 5.11 % Hematite 7.57 %	87.28 %

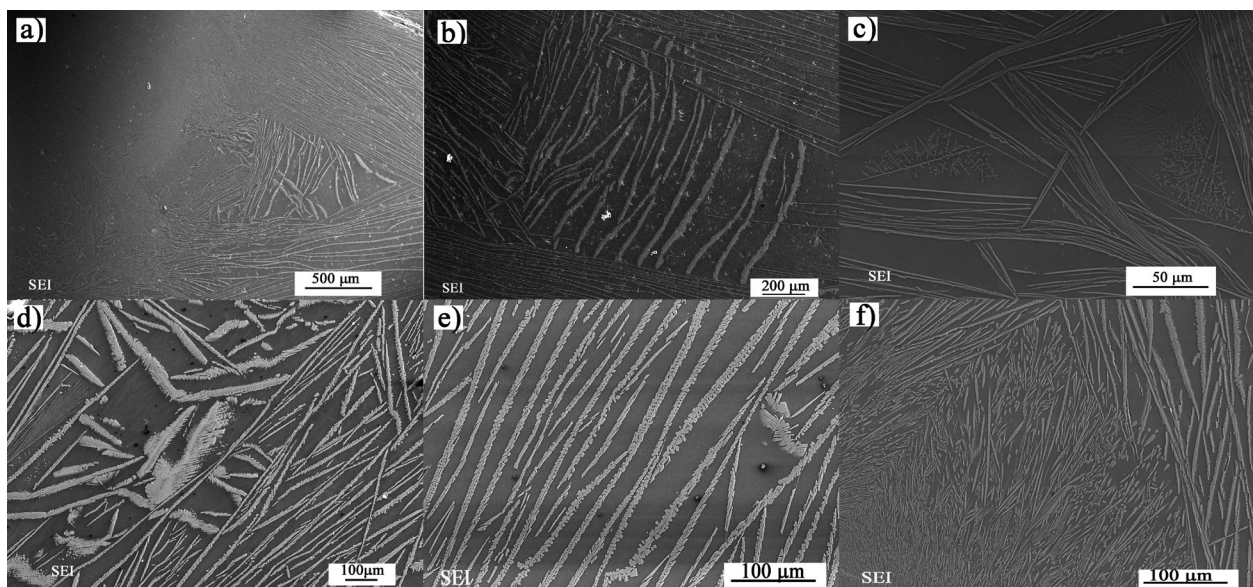


Fig. 2. SEM micrographs of the samples S2_25 (a, b, c) and S2_30 (d, e, f).

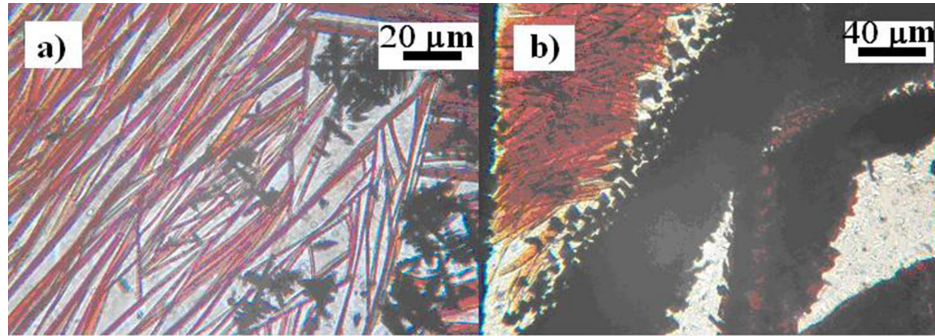


Fig. 3. Optical microscopy in transmission mode on the samples a) S2_25 and b) S2_30

gradually turns into fine crystalline when examining the surface corresponding to the inner parts of the cast block and near the center of the cast block, the size of the crystals and crystal aggregates increases. The highest degree of crystallization is observed in the central part of the sample. Closed pores formed as a result of the crystallization process are found in the samples. Crystal aggregates differ in color and appear brighter than the amorphous matrix. XRD patterns prove the presence of both magnetite and hematite. In an optical microscope, hematite and magnetite might be distinguished since they may differ in their transparency and color as witnessed by Fig. 3. In Figs. 3a and 3b the same morphology of the crystals imaged by SEM in Fig. 2 is seen,

however, here also the two types of Fe-oxides present could be discerned. It is observed in Fig. 3 that the sample S2_25 has smaller crystals compared to S2_30 and also, the hematite needles (red color) and magnetite mainly dendritic crystals (black color) may be distinguished. By contrast, in the SEM-micrographs, shown in Fig. 2, the crystalline phases of magnetite and hematite cannot be distinguished, but the analyses performed with energy dispersive spectroscopy render compositions close to those of hematite and magnetite, although the differences in the composition of the two phases are not large (Table 2). The crystalline aggregates that predominate the microphotographs have an elongated shape. At lower magnifications, they look like needles, but

Table 2. Chemical compositions of the crystalline phases in the glass-ceramics S2_25 and S2_30, according to EDXS, compared to the stoichiometric compositions of hematite and magnetite. The sample was taken from the center of the specimen.

Sample	Points	O[wt%]	Fe[wt%]	
Hematite	Stoichiometry	30.06	69.94	
	S2_25	He1	31.76	68.24
		He2	29.45	70.55
		He3	31.13	68.87
		Average	30.78	69.22
S2_30	He1	31.05	68.95	
Magnetite	Stoichiometry	27.64	72.36	
	S2_25	Mt1	26.74	73.26
		Mt2	28.82	71.18
		Average	27.78	72.22
		S2_30	Mt1	26.46
Mt2	27.27		72.73	
Mt3	26.54		73.46	
Mt4	27.11		72.89	
Mt5	27.82		72.18	
Mt6	26.27		73.73	
	Average	26.91	73.09	

at higher magnifications, it can be seen that these “needles” are not dense but are composed of many smaller crystals. On the other hand, some of the aggregates in a subparallel position with respect to the surface allow us to assume that the predominant shape of the aggregates is the lamellar one, and the needles are intersections of the lamellar aggregates with the studied surface. The Figures 2 and 3 illustrate the higher degree of crystallization of sample S2_30 compared to sample S2_25 under equal synthesis conditions. The higher Fe₂O₃ concentration and the lower concentration of SiO₂ lead to

lower viscosity and stimulate the crystallization in the melt.

The concentration of the crystalline phases can be calculated due to the fact that the crystallized phases are only iron oxides. Hence, the contents of calcium, sodium and silicon that are not included in the crystalline phases increase in the quantity of amorphous phase (glass) compared to the initial composition of the respective glass-ceramics. Accordingly, the glass phase is depleted in iron oxide, which is quantified in Tables 3 and 4 as well as in Fig. 4. The analysis points are ordered with respect

Table 3. Chemical compositions of the residual glass in the sample S2_25, according to EDXS

Points	Elements	Oxygen, O[wt%]	Sodium, Na[wt%]	Silicon, Si[wt%]	Calcium, Ca[wt%]	Iron, Fe[wt%]
1		36.28	9.47	19.22	4.55	30.49
2		35.44	10.63	17.95	5.5	30.48
3		36.3	8.83	20.08	5.31	29.48
4		36.84	8.82	20.28	4.67	29.38
5		34.39	10.71	19.85	5.69	29.37
6		37.59	9.43	20.1	5.35	27.53
7		37.6	9.09	21.16	6.29	25.86
8		38.63	9.27	21.03	5.61	25.46
9		37.44	11.18	20.89	6	24.5
10		37.93	11	21.1	5.62	24.35
11		37.44	10.96	22.42	5.94	23.25
Average		36.90	9.94	20.37	5.50	27.29
Chemical composition of S2_25		37.51	8.67	16.21	4.72	32.89

Table 4. Chemical composition of the residual glass in the sample S2_30, according to EDXS

Points	Elements	Oxygen, O[wt%]	Sodium, Na[wt%]	Silicon, Si[wt%]	Calcium, Ca[wt%]	Iron, Fe[wt%]
1		37.28	9.12	20.74	6.47	26.38
2		36.82	10.68	20.86	6.4	25.23
3		37.19	10.05	20.99	6.56	25.2
4		37.76	12.03	19.63	5.97	24.61
5		37.49	10.29	21.54	6.6	24.08
6		36.34	11.99	21.21	6.41	24.06
7		36.86	12.09	20.35	6.67	24.03
8		36.72	12.11	20.8	6.44	23.93
9		37.64	11.42	20.89	6.43	23.61
10		37.72	11.7	20.99	6.24	23.35
11		37.17	11.94	21.39	6.17	23.33
12		37.65	11.2	21.57	6.74	22.84
13		37.84	12.28	21.64	6.19	22.05
14		38.63	12.26	21.1	6.4	21.61
15		37.31	12.89	21.36	6.85	21.6
Average		37.36	11.47	21.00	6.44	23.73
Chemical composition of S2_30		36.32	8.19	13.75	4.46	37.29

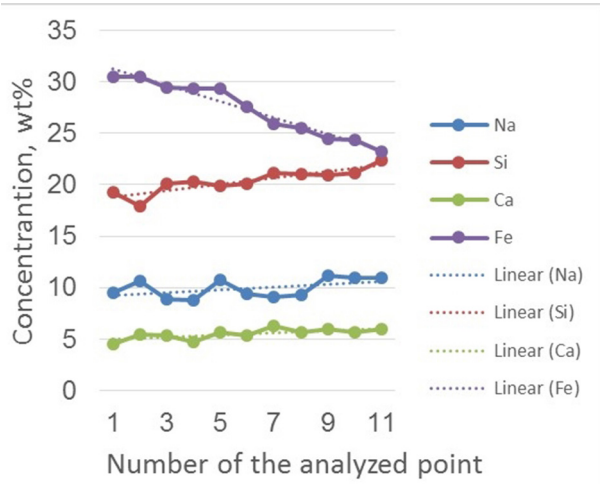


Fig. 4. Trends of change in the concentrations of Ca, Na and Si depending on the depletion of Fe in the residual glass in sample S2_25.

to the decreasing Fe concentration in order to illustrate the trends of change in the concentrations of Ca, Na and Si depending on the depletion of Fe in the residual glass in sample S2_25. The observed tendency for increase of the concentrations of Ca, Na and Si supports the hypothesis that the changes in the amorphous phase composition are the result from the different degree of crystallization of Fe-containing phases from a relatively homogeneous as chemical composition matrix and the depletion of the amorphous part in Fe. These differences between the concentrations of the elements in the total composition of the sample and the average composition of the residual glass phase can be used to calculate the amount of the precipitated crystalline phase and the residual glass phase. The following dependencies were used for the determination:

$$100 \cdot C_{\text{Na_total}} / (100 - C_{\text{FeOxide_crystal}}) = C_{\text{Na_glass}} \quad (1)$$

where: $C_{\text{Na_total}}$ – total sodium concentration in the glass-ceramics, wt%; $C_{\text{Na_glass}}$ – average concentration of sodium in the amorphous phase, wt%; $C_{\text{FeOxide_crystal}}$ – concentration of iron oxide crystalline phases (hematite and magnetite) in the glass-ceramics, wt%.

From eq. 1, we obtain:

$$100 \cdot C_{\text{Na_total}} / C_{\text{Na_glass}} = (100 - C_{\text{FeOxide_crystal}}) = C_{\text{glass phase}} \quad (2)$$

where $C_{\text{glass phase}}$ is concentration of amorphous phase in the glass-ceramics.

The dependencies of Si and Ca were calculated in analogy.

For iron, the dependence is different and is given by eq. 3:

$$(C_{\text{Fe_total}} - C_{\text{Fe_crystal}})100 / (100 - C_{\text{FeOxide_crystal}}) = C_{\text{Fe_glass}} \quad (3)$$

where: $C_{\text{Fe_total}}$ – total iron concentration in the glass-ceramics, wt%; $C_{\text{Fe_crystal}}$ – concentration of iron included in the crystalline phases (hematite and magnetite) in the glass-ceramics, wt%; $C_{\text{FeOxide_crystal}}$ – concentration of iron oxide crystalline phases (hematite and magnetite) in the glass-ceramics, wt%; $C_{\text{Fe_glass}}$ – average concentration of iron in the amorphous phase, wt%.

Having in mind that Fe_2O_3 and Fe_3O_4 are the only crystalline phases precipitated from the glass during casting of the melt and since the weight fraction of the two Fe-oxides is almost the same, we have calculated the average concentration of Fe in the crystalline phases according to $C_{\text{Fe_crystal}} = 0.7115 C_{\text{FeOxide_crystal}}$.

From eq. 3 we obtain:

$$C_{\text{FeOxide_crystal}} = 100 \cdot (C_{\text{Fe_total}} - C_{\text{Fe_glass}}) / (71.15 - C_{\text{Fe_glass}}) \quad (4)$$

Weight ratios between the total amount of crystalline phases and the amorphous phase in glass-ceramics samples determined by eqs. 1–4 are presented in Table 5.

The higher degree of crystallinity and crystallization tendency in the glass-ceramics S2_30 in comparison to S2_25 is illustrated in Fig. 5. It can be seen that in the experimentally established composition of the residual glass phase, designated as G_30, less iron and more silicon, calcium and sodium remain than in G_25. This difference is even more impressive, since in the initial compositions the ratios are the opposite, i.e. the sample S2_30 has more iron and less silicon, sodium and calcium than S2_25. The higher crystallization ability of this composition can be associated with the higher concentration of iron oxide in the batch composition, which leads to a decrease in the melt viscosity as well as in a decrease of the network connectivity in the respective glass.

On the other hand, significant differences are found in the quantitative (crystal/ amorphous phase) ratios as established by the quantitative X-ray diffractometry and the calculations based on the EDXS data. Especially large is this difference for the glass-ceramics S2_30 – 29–32 wt% crystalline phases, according to EDXS data and 13 wt% according to the X-ray diffraction analyses. This significant difference may be due to the following features of the samples and the studies performed. The glass-ceramics obtained by spontaneous crystallization

Table 5. Weight ratios between the total amount of crystalline phases and the amorphous phase in the glass-ceramic samples

Element*	Sample S2_25		Sample S2_30	
	Crystal phases	Glass	Crystal phases	Glass
Na	12.85	87.15	28.63	71.37
Si	20.42	79.58	34.53	65.47
Ca	14.20	85.80	30.71	69.29
Fe	12.78	87.22	28.59	71.41

* The weight fractions of the glass and of the crystalline phases in the glass-ceramics were estimated based on the established change in the determined concentrations of the elements (Na, Si, Ca and Fe) for the residual glass with respect to the nominal chemical composition of the sample.

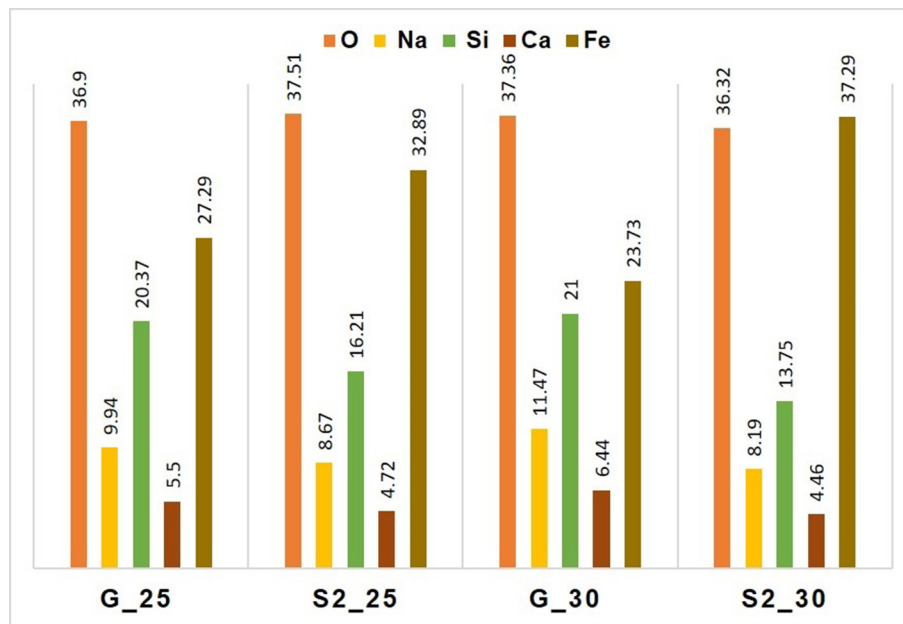


Fig. 5. Comparison of the initial chemical composition of the samples S2_25 and S2_30 with the average chemical composition of the residual glass after spontaneous crystallization G_25 and G_30.

of melts during their air-cooling show inhomogeneity with respect to their microstructure from the periphery, which is amorphous and a gradual increase in the amount and size of the formed crystals towards the center of the sample. The glass phase analyses were performed by EDXS mainly in areas with a higher degree of crystallization and they feature relatively small parts of the whole glass-ceramic surface, while for the same sample S2_30, the XRD analysis is representative for the whole sample. Although the results obtained by SEM-EDXS are not representative of the whole sample, we believe that they provide reliable information about the degree of crystallization of the sample in the studied areas and could in future be compared to the results of other methods, such as Mössbauer spectroscopy, suitable to characterize the local structure. Thus, the

difference in the obtained results for the degree of crystallization can be explained by the fact that the results of XRD refer to the whole glass-ceramics, while those of EDXS are related to special parts of the sample, in this case to zones with higher degree of crystallinity in the center of the sample.

CONCLUSION

XRD, optical microscopy and SEM/EDXS studies have been performed to characterize the phase composition and microstructure of glass ceramics in the $16\text{Na}_2\text{O}/10\text{CaO}/(74-x)\text{SiO}_2/x\text{Fe}_2\text{O}_3$ system with high Fe_2O_3 concentrations $-x = 20, 25$ and 30 mol%. Crystals of various sizes and morphology were found in the samples. Platelet-shaped

crystalline aggregates with different orientations are predominantly observed. These, however, were arranged subparallel, forming clusters in limited areas. The crystalline phases magnetite and hematite in the studied glass-ceramics were identified by XRD analyses and the quantitative ratio between the crystals and the amorphous phase in the samples was established. A procedure for determining the quantitative ratios of (crystals/glass) in the studied samples based on the difference in the concentrations of the elements in the glass phase (according to the EDXS results) and the average glass-ceramic sample compositions was proposed. The determined quantitative ratios of (crystals/glass) based on the difference in the concentrations of various elements (Na, Ca and Fe) in the samples showed good compliance. It was shown that using this approach, a successful estimation of the degree of crystallization in certain areas and, in case of inhomogeneous samples, with respect to the local crystal content can be achieved.

Acknowledgements: This work is financially supported by contract KII-06-H48/4 with the Bulgarian National Science Fund.

REFERENCES

1. R. K. Chinnam, A. A. Francis, J. Will, E. Bernardo, A. R. Boccaccini, *J. Non-Cryst. Solids*, **365**, 63 (2013).
2. N. I. Min'ko, I. N. Mikhal'chuk, M. Yu. Lipko, L. S. Komarova, *Glass Ceram.*, **58**, 7(2001).
3. M. Ponsot, Y. Pontikes, G. Baldi, R. K. Chinnam, R. Detsch, A. R. Boccaccini, E. Bernardo, *Materials*, **7**, 5565 (2014).
4. T. M. Zhdanova, A. V. Zemlyanuhin, S. N. Neumeecheva, *Glass Ceram.*, **4**, 24 (1991).
5. S. P. Solovev, M. A. Tsaritsyn, O. V. Vorobeva, G. P. Zamaev, Special Construction Glasses, Stroiizdat, Moscow, 1971(in Russian).
6. K. Tanaka, Y. Nakahara, K. Hirao, N. Soga, *J. Magn. Mater.*, **168**, 203 (1997).
7. A. A. Francis, R. D. Rawlings, A. R. Boccaccini, *J. Mater. Sci. Lett.*, **21**, 975 (2002).
8. A. A. Francis, R. D. Rawlings, R. Sweeney, A. R. Boccaccini, *Glass Technol.*, **43**, 58 (2002).
9. N. I. Min'ko, N. A. Koval'chenko, *Glass Ceram.*, **59**, 9 (2002).
10. A. Karamanov, M. Pelino, *J. Non-Cryst. Solids*, **281**, 139 (2001).
11. R. Harizanova, G. Völksch, C. Rüssel, *J Mater Sci* **45**, 1350 (2010).
12. C. Worsch, P. Schaaf, R. Harizanova, C. Rüssel, *J Mater Sci*, **47**, 5886 (2012).
13. K. Sharma, M. N. Deo, G. P. Kothiyal, *J. Non-Cryst. Solids*, **358**, 1886(2012).
14. R. Borges, L. Mendonça-Ferreira, C. Rettori, I. S.O. Pereira, F. Baino, J. Marchi, *Mater. Sci. Eng. C*, **120**, 111692 (2021).
15. Y. Ebisawa, F. Miyaji, T. Kokubo, K. Ohura, T. Nakamura, *Biomaterials*, **18**, 1277 (1997).
16. O. Bretcanu, E. Verne, M. Coisson, P. Tiberto, P. Allia, *J. Magn. Mater.*, **300**, 412, (2006).
17. Y. -K. Lee, S. -Y. Choi, *J. Amer. Ceram. Soc.*, **79**, 992 (1996).
18. Y. -K. Lee, S. -Y. Choi, *J. Mater. Sci.*, **32**, 431(1997).
19. Y.-K. Lee, K.-N. Kim, Se-Y. Choi, C.-S. Kim, *J. Mater. Sci.: Mater. Med.*, **11**, 511 (2000).
20. S.-H. Oh, S.-Y. Choi, Y.-K. Lee, K.-N. Kim, *J. Biomed. Mater. Res.*, **54**, 360 (2001).

Direct mechanochemical synthesis and optical properties of BaWO₄ nanoparticles

M. Gancheva^{1*}, R. Iordanova¹, G. Avdeev², P. Ivanov³

¹ Institute of General and Inorganic Chemistry, Bulgarian Academy of Science, Acad. G. Bonchev str., bl. 11, 1113 Sofia, Bulgaria

² Institute of Physical Chemistry, Bulgarian Academy of Sciences, Acad. G. Bonchev str., bl. 11, 1113 Sofia, Bulgaria

³ Institute of Optical Materials and Technologies, „Acad. Jordan Malinowski“, Acad. G. Bonchev str, bl. 109, 1113 Sofia, Bulgaria

Received November 29, 2021; Accepted January 11, 2022

Mono phase nanocrystalline BaWO₄ was successfully synthesized by direct mechanochemical reaction at room temperature. A stoichiometric mixture of BaCO₃ and WO₃ in a 1:1 molar ratio was subjected to intense mechanical treatment in air using a planetary ball mill for different period of time. The phases obtained and their transformations were monitored by X-ray diffraction (XRD) and infrared (IR) spectroscopy. The optical properties were investigated by ultraviolet visible (UV-Vis) and photoluminescence excitation/emission spectroscopy. The single phase BaWO₄ with tetragonal structure and with crystalline size of 19 nm was obtained after 3 h milling time at room temperature. The UV-vis absorption spectrum shows a strong peak at 210 nm and the calculated optical band gap is 5.09 eV. With excitation at 350 nm, the BaWO₄ powder exhibit broad PL emission in the blue wavelength range at 440 nm.

Keywords: ball milling, nanoparticles, optical properties.

INTRODUCTION

BaWO₄ is an important member of alkaline-earth metal tungstate family with scheelite type structure and exists in two polymorphs. At ambient conditions BaWO₄ crystallizes in the tetragonal scheelite-type structure which transforms into metastable monoclinic BaWO₄-II under pressure and temperature [1, 2]. In the scheelite structure, Ba ions are coordinated with eight oxygen atoms and W ions are connected to four oxygen atoms forming WO₄ groups [1]. This compounds finds applications as: microwave dielectric materials [3, 4], host matrix for doping of rare area active ions [5–7], catalysts [7, 8] and etc. In the literature there data exist the BaWO₄ powders possess violet, blue or green photoluminescence emission [9–15]. Different emission position mainly depends on the crystal structure, defects, particle size, morphology and methods of preparation. According to G. Blasse and M. Nikl, the blue emission is ascribed to the regular lattice, while the green one

originates from some defect centers relative to oxygen [11, 12]. L. Ma et al., established that at excitation source at shorter wavelength (210–280 nm) gives blue emission, while longer wavelengths yield green or red emission [13]. The same authors reported that the luminescence intensity depends on morphology of the particles as well as the method of preparation [13, 14]. Lima et al. explained that the structural disorder in the lattice is an important condition to obtain an intense and broad photoluminescence emission [15]. It is well known that the properties of the materials significantly depend of experimental conditions during the synthesis. A variety of different physics-chemical routes have been applied for the preparation of BaWO₄ as solid state reaction [5, 6, 8], hydrothermal synthesis [6, 9, 16], the microwave irradiation route [17, 18], coprecipitation [9, 10], combustion technique [19], sol-gel [20] and mechanochemical synthesis [3, 15, 21]. BaWO₄ powders obtained by the mechanochemical activation method possess good dielectric and luminescence properties. Mechanochemical activation is widespread in the synthesis of different solid state materials because very often it leads to direct synthesis, or to a decrease in time and temperature

* To whom all correspondence should be sent:
E-mail: m.gancheva@svr.igic.bas.bg

needed to obtain the final products [21–23]. A significant amount of crystalline defects as point and linear defects vacancies, dislocations and grain boundaries can be formed due to repeated ball-powder collision [24]. It is well known that the choice of milling conditions such as milling time, ball to powder weight ratio, rotation speed, and atmosphere plays an important role in the preparation of materials. The major parameter at mechanochemical treatment is milling speed and is a decisive factor for the rapid synthesis [22–26]. The lower milling speeds with extending the milling time usually are not sufficient for full synthesis. The milling time is other significant conditions. The longer milling time could lead to formation of undesirable phases [24, 27]. This work is a continuation of our investigation over mechanochemical synthesis of inorganic mixed oxides. The aim of this work is the preparation of nanocrystalline BaWO₄ from BaCO₃ and WO₃. The phase formation and the optical properties of the final product have been discussed.

EXPERIMENTAL

A mixture of BaCO₃ (Merck, purity 99.9%) and WO₃ (Merck, purity 99.9%) in the molar ratio of 1:1 was subjected to intense mechanical treatment in a planetary ball mill (Fritsch–Premium line–Pulversette No 7). Both vials and balls were made of stainless steel, the milling rotation speed was 500 rpm, milling time up to 3 h, and ball to powder mass ratio was 10:1. To minimize the temperature raise during the milling, the process was carried out for periods of 15 min, with rest periods of 5 min [26]. The influence of the ball milling on the phase and transformation of the samples was investigated by X-ray powder diffraction analysis (XRD), and infrared spectroscopy (IR). The powder X-ray diffraction study was performed with a Bruker D8 Advance instrument equipped with a copper tube (CuK α) and a position-sensitive LynxEye detector. The diffraction patterns were taken in the angular range 10–80.0 °2 θ with a step of 0.04 °2 θ and counting time of 0.1 second for each individual strip of the detector (total 17.5 s/step). The phase analysis, crystallite size and cell parameter evaluation was performed with HighScore plus 4.5 and ReX softwares [28]. Infrared spectra were registered in the range 1200–400 cm⁻¹ on a Nicolet-320 FTIR spectrometer using the KBr pellet technique. UV-Vis spectra were recorded on Evolution 300 UV-Vis spectrophotometer using Spectralon as a reflectance standard at wavelengths within the range 200–1000 nm. The emission and excitation spectra were measured on a Horiba Fluorolog 3-22 TCS spectrophotometer equipped with a 450 W Xenon Lamp as the exci-

tation source. All spectra were measured at room temperature.

RESULTS AND DISCUSSION

The XRD patterns of the mechanically activated sample are shown in Fig. 1. After 30 min milling time, the principal peaks of monoclinic WO₃ (PDF-01-072-0677) and hexagonal BaCO₃ (PDF-00-005-0378) were broadened and their intensity had decreased. This is a result of a reduction in particle sizes, destruction of the long-range order and partial amorphization. Increasing the milling time up to 1 h led to appearance of a set of new diffraction lines typical of tetragonal BaWO₄ (PDF-01-072-0746). The very low intensity peaks in the range from 22.00 to 25.00° characteristic for WO₃ were detected (marked in red square). It means that the full reaction between initial reagents is not finished. The additional mechanochemical activation up to 3 h led to preparation of a single phase of BaWO₄. The weight fraction of the phases, the unit cell parameters (*a*, *b*, and *c*), unit cell volume and the average crystallite size depending of milling time are calculated and presented in Table 1.

Mechanochemically synthesized BaWO₄ have a smaller the unit cell volume and the lattice parameters (*a*, *c*) as compared to PDF data. Similar values were reported from L. S. Cavalcante [18] obtained BaWO₄ by microwave synthesis realized at 140 °C at short irradiation times. The lattice parameters (*a*, *c*) and average crystallite size decrease with increasing of milling time. The energy induced during the mechanochemical activation led to obtain of the materials with high amount of point and linear de-

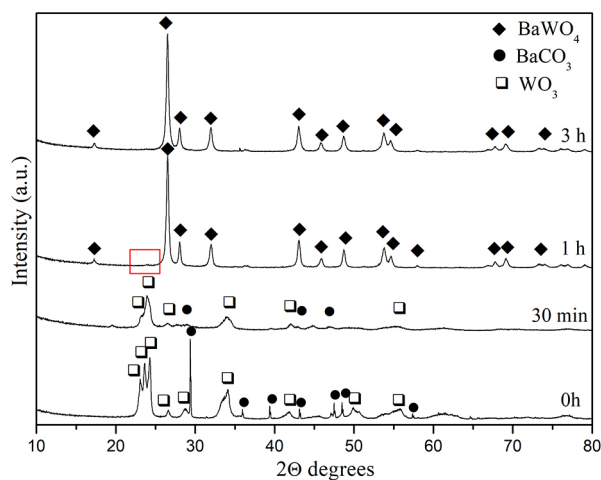


Fig. 1. XRD patterns of the sample obtained at milling speed of 500 rpm after different milling times.

Table 1. Weight fraction, lattice parameters, unit cell volume and crystallite size depending on milling time

Milling time, h	Weight fraction (%)	Lattice parameters			Unit cell volume, 10 ⁶ pm ³	Crystallite size, nm
		a(Å)	b(Å)	c(Å)		
1	BaWO ₄ – 95.6(5)	5.604(3)	5.604(3)	12.71(7)	399.02	30
	WO ₃ – 4.4(2)	5.39(2)	5.23(2)	7.51(3)	208.64	12
3	BaWO ₄ – 100	5.597(4)	5.597(4)	12.716(8)	398.37	19
PDF-01-072-0746	BaWO ₄	5.614	5.614	12.719	400.86	–

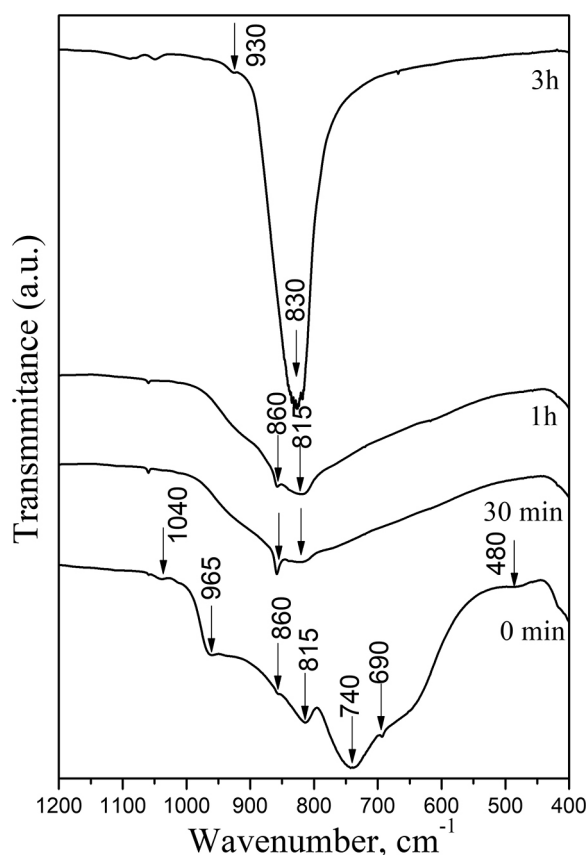
fects, which is observed by broadening of the peaks in diffraction pattern [24]. Probably, accumulation of the defects in the crystal lattice lead to the contraction of the unit cell volume and deformation in the [WO₄] groups.

The phase formation of BaWO₄ during the mechanochemical treatment was confirmed by IR spectroscopy. The IR spectrum the non-activated mixture exhibits absorption bands typical of structural units of WO₃ (bands at 965, 815 and 740 cm⁻¹) and of BaCO₃ (band at 1040, 860, 690 and 480 cm⁻¹) [29, 30]. The bands at 1040, 965, 740 and 690 cm⁻¹ disappeared after the early stages of the ball milling (30 min). The absorption band at 860 and 815 cm⁻¹ typical for initial reagents still remain after 1h milling time. This indicates that the full reaction has not finished. The noticeable changes in the IR spectrum were observed after 3h milling time which confirmed the phase formation of BaWO₄. The new absorption bands are in a good agreement with literature data [6, 17, 18, 31]. The strong band at 830 cm⁻¹ is attributed to the ν₃ stretching vibration of the WO₄ units. The weak shoulder at 930 cm⁻¹ is due to activation of ν₁ mode of the same structural groups. The presence of this shoulder probably is due to formation of more distorted structure during ball milling. The optical properties of the mechanochemical obtained BaWO₄ were studied by ultraviolet visible (UV-Vis) and photoluminescence (PL) spectroscopies. The UV-Vis reflectance spectrum of the BaWO₄ exhibits a strong band at 210 nm and shoulders at 240 and 320 nm, which is typical for wide-bandgap compounds. The peak at 210 nm is due to the ligand-to-metal charge transfer in the WO₄ group [32–34]. The optical band gap of the sample was calculated using Tauc's equation [35]:

$$\alpha h\nu = A(h\nu - E_g)^n,$$

where h is Planck's constant, α is the absorption coefficient, ν is the photon frequency, A is a constant, E_g is the optical band gap and n is a constant depending of the type of electronic transitions

($n = 0.5, 2, 1.5,$ and 3 for direct allowed, indirect allowed, direct forbidden, and indirect forbidden transitions, respectively). In our case the value of n is $= 1/2$. The optical band gap is determined through an extrapolation of the linear trend observed in the spectral dependence of $(\alpha h\nu)^{1/2}$ over a limited range of photon energies $h\nu$ and it is defined at the intercept of this linear extrapolation with the abscissa axis [36]. Based on this equation, the band gap of the mechanochemical obtained BaWO₄ was esti-

**Fig. 2.** IR spectra of the sample obtained at milling speed of 500 rpm after different milling times.

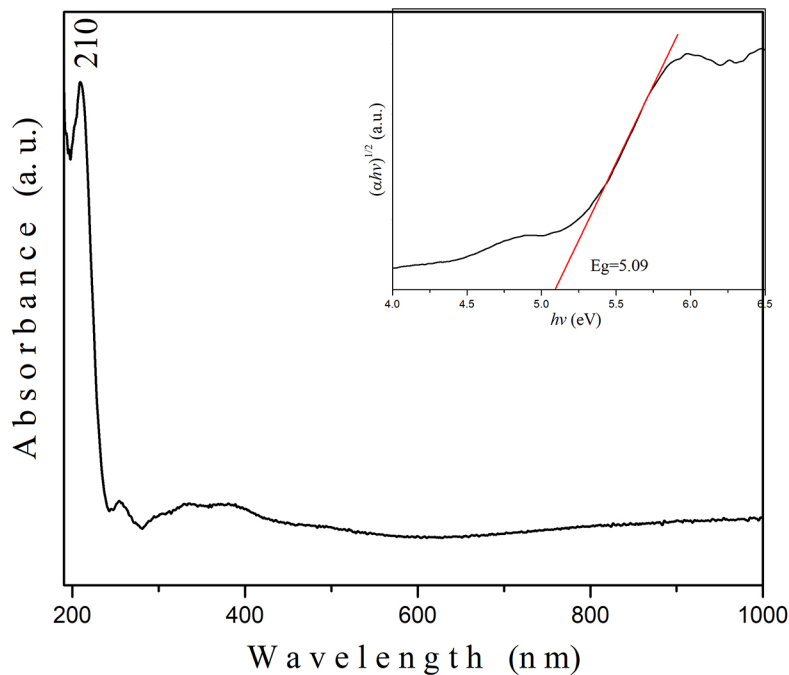


Fig. 3. UV-Vis diffuse reflectance spectrum and corresponding Tauc's plot for optical band gap of mechanochemically synthesized BaWO₄ powder.

mated to be 5.09 eV as illustrated in the inset of Figure 3. This value is similar to the optical band gap of BaWO₄ powders prepared by different methods as: the solid-state reaction ($E_g = 5.02$ eV) with average crystalline size of 26 nm [6], the hydrothermal method (5.07 eV) with the crystalline size of 75 nm [34] and the mechanochemical treatment ($E_g = 5.23$ eV) with the crystalline size of 20 nm [15].

The compounds with scheelite type structure are exhibit good emission luminescence at low and at

room temperature [6, 15, 37–39]. Fig. 4a and 4b show the photoluminescence excitation/emission spectra of mechanochemical obtained BaWO₄. The excitation spectrum was measured at emission wavelength of 380 nm. Only one intensity peak at 345 nm was observed, which is due to the charge transfer from O2p to W5d into WO₄ group [6, 21, 34]. No other peak was observed in the excitation spectrum of BaWO₄. Therefore, the emission spectrum was recorded at 350 nm and exhibited one

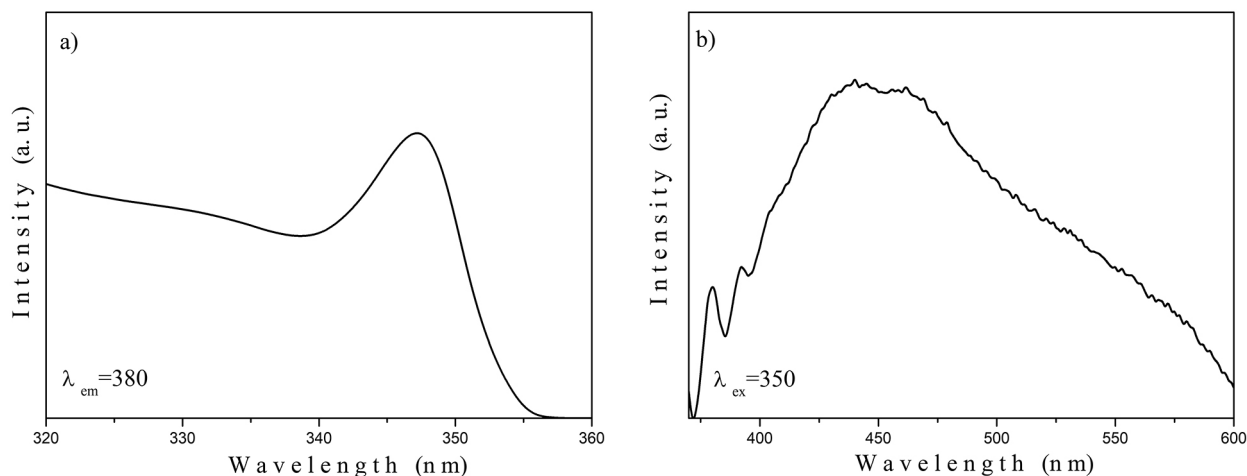


Fig. 4. (a) Excitation and (b) emission spectra of mechanochemically synthesized BaWO₄ powder.

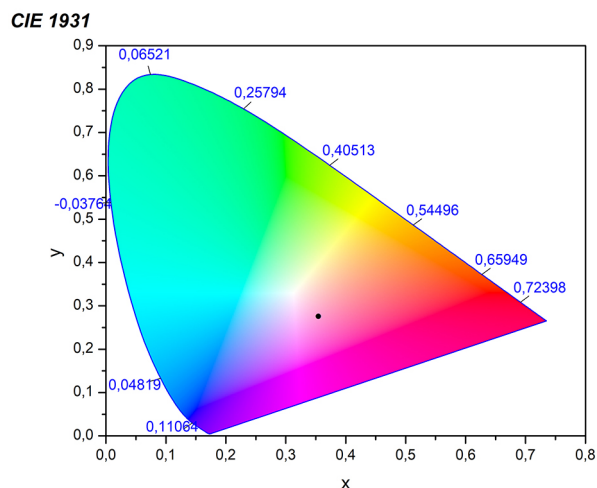


Fig. 5. CIE chromaticity diagram of mechanochemically synthesized BaWO₄ powder.

broad PL emission in the blue range of 380–500 nm. The main peak is observed around 440 nm. Having in mind the literature data for the photo luminescent materials, the blue emission we attributed to structural distortions of both WO₄ and BaO₈ groups [37, 38]. The CIE chromaticity coordinates (x, y) were calculated from the emission spectrum were found to be 0.35 and 0.28 and fall into the violet region of the diagram.

CONCLUSION

This article represents data on the mechanochemical synthesis, characterization and optical properties of BaWO₄ nanoparticles. The phase formation started after 1 h milling time and it was completely finished after 3 h milling time at 500 rpm. The calculated energy band gap value of as prepared BaWO₄ is 5.09 eV and exhibits photoluminescence emission in the blue range. The CIE chromaticity coordinate (x=0,35 and y=0,28) are located in the violet area. The optical properties suggest that mechanochemical obtained BaWO₄ can be used as efficient violet-emitting phosphor for LED applications.

REFERENCES

1. A. W. Sleight, *Acta Cryst.*, **B 28**, 2899 (1972).
2. I. Kawada, K. Kato, T. Fujita, *Acta Cryst.*, **B 30**, 2069 (1974).
3. L. Cheng, P. Liu, S. X. Qu, H.W. Zhang, *J. Alloys Comp.*, **581**, 553 (2013).
4. C. Anil Kumar, D. Pami, *Ceram. Inter.*, **41**, S296 (2015)
5. C. Bouzidi, M. Ferhi, H. Elhouichet, M. Feird, *J. Lumin.*, **161**, 448 (2015).
6. A.K. Kunti, N. Patra, S.K. Sharma, H.C.Swart, *J. Alloys Comp.*, **735**, 2410 (2018).
7. G. Jia, D. Dong, C. Song, L.Li, C. Huang, C. Zhang, *Mater. Letter.*, **120**, 251 (2014).
8. Z. Shan, Y. Wang, H. Ding, F. Huang, *J. Molec. Catal. A: Chem.* **302**, 54 (2009)
9. L. S. Cavalcante, F. M. C. Batista, M. A. P. Almeida, A. C. Rabelo, I. C. Nogueira, N. C. Batista, A. Varela, M. R. M. C. Santos, E. Longo, M. Siu Li, *RSC Advances*, **2**, 6438 (2012).
10. A. Phuruangrat, T. Thongtem, S. Thongtem, *Superlattices & Microstructures*, **52**, 78 (2012).
11. G. Blasse, *J. Lumin.*, **72**, 129 (1997).
12. M. Nikl, *Phys. Stat. Sol.*, **178**, 595 (2000).
13. L. Ma, Y. Sun, P. Gao, Y. Yin, Z. Qin, B. Zhou, *Mater. Letters*, **64**, 1232 (2010).
14. L. D. S. Alencara, A. Mesquita, C. A. C. Feitosa, R. Balzer, L. F. D. Probst, D. C. Batalha, M. G. Rosmaninho, H. V. Fajardo, M. I. B. Bernardi, *Ceram. Inter.*, **43**, 4462 (2017).
15. R. C. Lima, M. Anicete-Santos, E. Orhan, M. A. M. A. Maurera, A. G. Souza, P. S. Pizani, E. R. Leite, J. A. Varela, *J. Lumin.*, **126**, 74 (2007).
16. L. S. Cavalcante, J. C. Sczancoski, J. W. M. Espinosa, J. A. Varela, P. S. Pizani, E. Longo, *J. Alloys Comp.*, **474**, 195 (2013).
17. A. Phuruangrat, T. Thongtem, S. Thongtem, *J. Phys. Chem. Solids*, **70**, 955 (2009).
18. L. S. Cavalcante, J. C. Sczancoski, L. F. Lima, J. W. M. Espinosa, P. S. Pizani, J. A. varela, E. Longo, *Crystal Growth & Design*, **9**, 1002 (2009).
19. S. Vidya, S. Solomon, J. K. Thomas, *Advan. Conden. Matter Phys.*, 409620 (2013).
20. Y. Jia, X. M. Liu, G. Z. Li, M. Yu, J. Fang, J. Lin, *Nanotechnology*, **17**, 734 (2006).
21. P. Jena, S. K. Gupta, N. K. Verma, A. K. Singh, R. M. Kadam, *New J. Chem.*, **41**, 8947 (2017).
22. L. T. T. Vien, N. Tu, T. T. Phuong, N. T. Tuan, N. V. Quang, H. Van Bui, A. T. Doung, D. Q. Trung, P. T. Huy, *J. Lumin.*, **215**, 116612 (2019).
23. M. Mancheva, R. Iordanova, Y. Dimitriev, *J. Alloys Comp.*, **509**, 15 (2011).
24. C. Suryanarayana, *Intermetallics*, **3**, 153 (1995).
25. A. F. Fuentes, L. Takacs, *J. Mater. Sci.*, **48**, 398 (2013).
26. M. Gancheva, I. Szafraniak-Wiza, R. Iordanova, I. Piroeva, *J. Chem. Technol. Metall.*, **54**, 1233 (2019).
27. V. V. Boldyrev, *Russ. Chem. Rev.*, **75**, 203 (2006).
28. T. Degen, M. Sadki, E. Bron, U. König, D. Nénert, *Powder Diffraction*, 29 S13 (2014).
29. M. F. Daniel, B. Desbat, J. C. Lassegues, B. Gerand, M. Figlarz, *J. Solid State Chem.*, **67**, 235 (1987).
30. T. Shahid, M. Arfan, A. Zeb, T. BiBi, T. M. Khan, *Nanomater. Nanotechn.*, **8**, 1 (2018).
31. E. L. Gaiollo, R. P. Moreira, M. C. F. C. Felinto, H. P. Barbosa, Cássio C. S. Pedroso, E. E. S. Teotonio, O.L. Malta, H. F. Brito, *J. Braz. Chem. Soc.*, **31**, 2430 (2010).

32. M. M. J. Sadiq, A. S. Nesaraj, *J. Nanostruct Chem.*, **5**, 45 (2015).
33. P. Afanasiev, *Mater. Letters*, **61**, 4622 (2007).
34. M. Kowalkińska, P. Głuchowski, T. Swebosci, T. Ossowski, A. Ostrowski, W. Bednarski, J. Karczowski, A. Zielińska-Jurek, *J. Phys. Chem.*, **C125**, 25497 (2021).
35. J. Tauc, *Mater. Res. Bull.*, **5**, 721 (1970).
36. T. M. Mok, S. K. O'Leary, *J. Appl. Phys.* **102**, 113525 (2007).
37. S. Vidya, J. K. Thomas, *IOP Conf. Series: Mater. Sci. Engin.*, **73**, 012120 (2015).
38. C. Shivakumara, R. Saraf, S. Behera, N. Dhananjaya, H. Nagabhushana, *Mater. Res. Bull.*, **61**, 422 (2015).
39. S. Wang, H. Gao, G. Sun, Y. Li, Y. Wang, H. Liu, C. Chen, L. Yang, *Optical Mater.*, **99**, 109562 (2020).

Phase formation and dielectric properties of strontium-substituted barium titanate glass-ceramics

R. Harizanova^{1*}, M. Pernikov¹, W. Wisniewski², G. Avdeev³,
I. Mihailova¹, C. Rüssel²

¹ University of Chemical Technology and Metallurgy, 8 Kl. Ohridski Blvd., 1756 Sofia, Bulgaria

² Otto Schott Institute for Materials Research, Friedrich Schiller University, 07745 Jena, Germany

³ Institute of Physical Chemistry, Bulgarian Academy of Sciences, Bl. 11, Acad. G. Bonchev Str., 1113 Sofia, Bulgaria

Received October 13, 2021; Accepted January 10, 2022

Oxide glass-ceramics containing alkaline-earth and 3d-transition metal ions are of interest due to their advanced dielectric and magnetic properties and thus, their possible application in sensors and microelectronics. The work presented here features the synthesis of strontium-substituted barium titanate glasses in the system $\text{Na}_2\text{O}/\text{BaO}/\text{SrO}/\text{TiO}_2/\text{B}_2\text{O}_3/\text{SiO}_2/\text{Fe}_2\text{O}_3/\text{Al}_2\text{O}_3$. An appropriate thermal treatment leads to the crystallization of $\text{Ba}_{1-x}\text{Sr}_x\text{TiO}_3$ in these glasses according to X-ray diffraction analysis. The microstructure is studied by scanning electron microscopic methods and reveals the occurrence of a phase separation into one phase enriched in Ba, Sr and Ti, from which $\text{Ba}_{1-x}\text{Sr}_x\text{TiO}_3$ is formed during thermal treatment, while the other phase – the presumable amorphous matrix, is enriched in the remaining glass constituting elements. The dielectric properties of the prepared glasses and glass-ceramics with different thermal histories are analyzed by impedance spectroscopy and dielectric constants of about 100 at 1 kHz and 100 °C are determined. The degree of BaO/SrO substitution in the parent glass influences the dielectric constant. A maximum value for the dielectric constant is determined for the glass–ceramics containing 1 mol% SrO.

Keywords: strontium-barium titanate, crystallization, glass-ceramics, dielectric constant.

INTRODUCTION

The preparation of dielectric glass-ceramics from oxide glasses via a controlled crystallization is of great interest because the respective materials find application as electroceramics. They can be used as positive thermal coefficient elements (PTC) [1–6], dielectrics in multilayered capacitors [7], microwave dielectric ceramics [8], high-density optical data storage devices, phase conjugated mirrors and lasers, in optical computing, optical image processing and as optical waveguides [9]. Barium titanate, BaTiO_3 is a well-known dielectric phase of significant practical importance, which can be prepared from glass by controlled crystallization, [2–4, 6]. Depending on the polymorphs (cubic, tetragonal, etc.) in which BaTiO_3 may crystallizes from the glasses, the obtained glass-ceramic materials can find application as parts of piezoelectric devices, pyroelectric sensors, dielectric amplifiers, in microwave technology, as PTC devices, in dynamic

holography as well as in nanomedicine [7–19]. The BaTiO_3 modification with the most prominent ferroelectric, as well as piezoelectric and pyroelectric properties is the tetragonal one. According to the phase diagram, it is thermodynamically stable in the temperature range from 0 to 120–130 °C [7, 9, 12, 13, 15]. At 120–130 °C the tetragonal modification transforms to cubic BaTiO_3 which is paraelectric but also shows outstanding dielectric properties [3, 5, 7, 12, 13]. In some cases, it is convenient to have this phase transition at a temperature below 130 °C. This can be achieved by substituting the Ba^{2+} or Ti^{4+} ions with other elements such as Na^+ , K^+ , Ca^{2+} , Sr^{2+} , Zr^{4+} or Nb^{5+} [2, 8, 10, 14, 20, 21]. Depending on the degree of substitution and the substituting ion, the polymorphic modification stable at room temperature and the resulting electrical and optical properties of the obtained crystals can vary over a wide range [22]. Adding 3d-transition metals to BaTiO_3 allows the preparation of materials with tunable magnetic and even multiferroic properties [14, 15].

The main goal of the experiments presented here is to prepare glasses from which glass-ceramics with a controllable size and volume fraction of the

* To whom all correspondence should be sent:
Email: rharizanova@uctm.edu

crystalline phase and tunable dielectric and magnetic properties can be prepared using conventional melt-quenching followed by a thermal treatment. Hence glasses with high concentrations of alkaline, alkaline-earth and 3d-metals were synthesized in the system $20.1\text{Na}_2\text{O}/(23.1-x)\text{BaO}/x\text{SrO}/23\text{TiO}_2/7.6\text{B}_2\text{O}_3/17.4\text{SiO}_2/3\text{Al}_2\text{O}_3/5.8\text{Fe}_2\text{O}_3$ with $x = 0.5, 1$ and 2 mol% SrO. Their glass-transition and crystallization peak maximum temperatures (T_g and T_c respectively) are determined by differential scanning calorimetry (DSC). After subjecting the glasses to thermal treatments, the resulting glass-ceramics are analyzed by X-ray diffraction (XRD) to determine their phase composition and scanning electron microscopic methods to visualize their microstructure. Their electrical properties are investigated as a function of temperature and frequency using dielectric impedance spectroscopy and the dielectric permittivity, the ac-conductivity and the loss-angle tangent are determined.

EXPERIMENTAL

The glasses are melted from reagent grade raw materials: Na_2CO_3 , BaCO_3 , SrCO_3 , TiO_2 , $\text{Al}(\text{OH})_3$, $\text{B}(\text{OH})_3$, SiO_2 and Fe_2O_3 in 60 g batches for 1 h at 1250°C in air using a Pt crucible and a furnace with SiC heating elements. The melts are quenched on a copper block and transferred to a pre-heated graphite mould, held for 10–15 min at 450°C in a muffle furnace. Then, the furnace was switched off and allowed to cool to room temperature (RT). The characteristic temperatures, i.e. T_g and T_c , were determined by using a DSC (Linseis DSC PT-1600, LINSEIS Messgeräte GmbH, Germany). The powdered samples (fraction $\leq 350\ \mu\text{m}$) are heated in an Al_2O_3 crucible with 10 K/min in air. The phase composition of powdered samples was studied by XRD (Siemens D5000) using $\text{Cu-K}\alpha$ radiation ($\lambda = 1.5406\ \text{\AA}$) with a Ni filter in the $2\theta = 10\text{--}60^\circ$ range. The microstructures and the elemental composition of the glasses and the crystallized specimens were further analysed by scanning electron microscopy (SEM) using a Jeol JSM 7001F SEM equipped with an EDAX Trident analysing system. Energy-dispersive X-ray spectroscopy (EDXS) was performed without a standard using acceleration voltages of 15 kV.

Disc-shaped samples with a diameter of 10 mm and a thickness of about 3 mm were prepared for the electrical measurements. The plane parallel surfaces were roughly polished and Ag paste and Pt plates were used to prepare the electrodes. The Ag paste was dried at 400°C for 30 min to achieve a good contact between the metal electrode and the sample surface. Two contact point measurements and an ac-voltage with a 500 mV amplitude were used. The im-

pedance amplitude and the phase angle were measured as a function of the frequency (10 Hz–100 kHz) and temperature (from RT to 200°C) using a Zahner IM6 impedance analyser. The capacitances derived from the equivalent circuit, assuming resistance R and capacitance C in parallel, were determined at different frequencies and used to calculate the complex dielectric permittivity from the sample geometry. Furthermore, the ac-conductivity and the loss angle tangent were determined.

RESULTS AND DISCUSSION

The characteristic temperatures T_g and T_c of the investigated compositional series $20.1\text{Na}_2\text{O}/3\text{Al}_2\text{O}_3/(23.1-x)\text{BaO}/x\text{SrO}/23\text{TiO}_2/7.6\text{B}_2\text{O}_3/17.4\text{SiO}_2/5.8\text{Fe}_2\text{O}_3$, $x = 0, 0.5, 1$ and 2 (in mol%) are shown in Fig. 1. Adding SrO leads to a decrease of the T_g values from 450°C for the parent glass to about $433\text{--}439^\circ\text{C}$ for the SrO-substituted glasses while the T_c of the parent glass (560°C) and of the Sr-substituted glasses ($567\text{--}575^\circ\text{C}$) do not significantly differ.

XRD results obtained from Sr-doped glasses subjected to thermal treatments above T_g are shown in the Figs. 2 and 3. The crystallization behaviour of the parent glass ($x = 0$) has already been reported in Ref. [23]: the two crystalline phases cubic barium titanate, BaTiO_3 (JCPDS 98-002-7970) and hexagonal iron-containing barium titanate, $\text{BaTi}_{0.75}\text{Fe}_{0.25}\text{O}_{2.888}$ (JCPDS 98-002-7970) are always precipitated. The XRD analyses of the Sr-containing glass-ceramics reveal a different phase composition. In addition to the expected primary crystallization of $\text{Ba}_{1-x}\text{Sr}_x\text{TiO}_3$, barium fresnoite, $\text{Ba}_2\text{TiSi}_2\text{O}_8$ is detected for crystallization times longer than 3 h for all supplied temperatures. This is typical for the crystallization products in systems with a similar composition

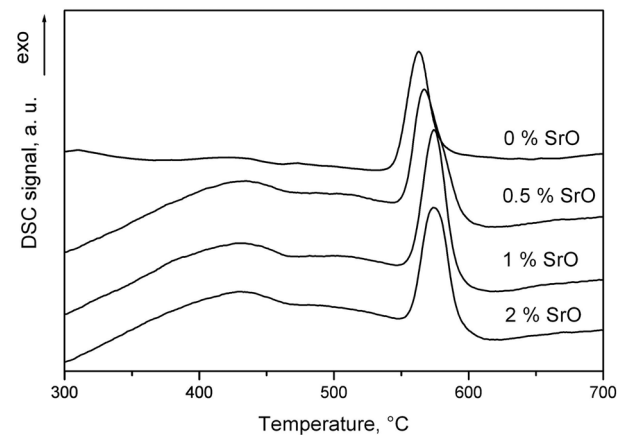


Fig. 1. DSC curves of glasses with batch composition $20.1\text{Na}_2\text{O}/(23.1-x)\text{BaO}/x\text{SrO}/23\text{TiO}_2/7.6\text{B}_2\text{O}_3/17.4\text{SiO}_2/5.8\text{Fe}_2\text{O}_3/3\text{Al}_2\text{O}_3$, with $x = 0, 0.5, 1$ and 2 mol%.

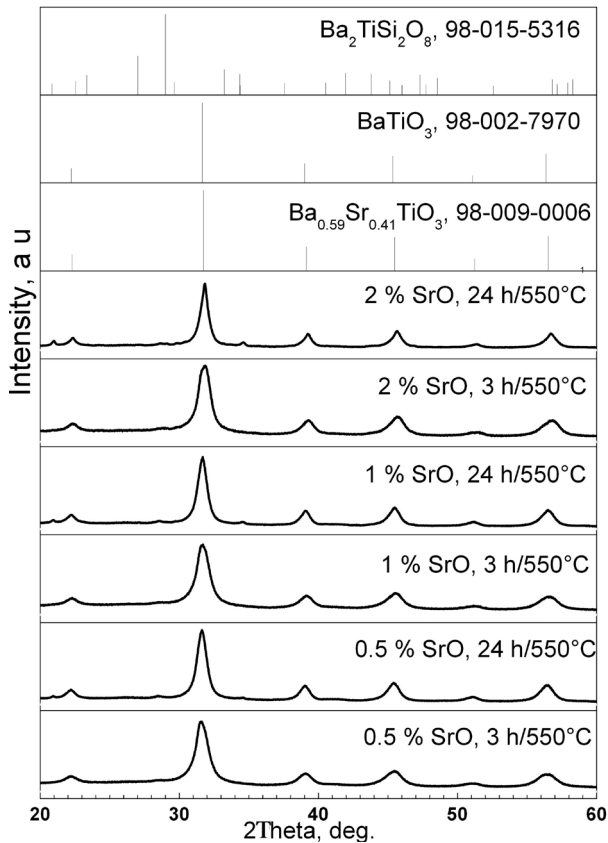


Fig. 2. XRD patterns of glass-ceramics with 0.5, 1 and 2 mol% SrO obtained after thermal treatment at 550 °C for different times.

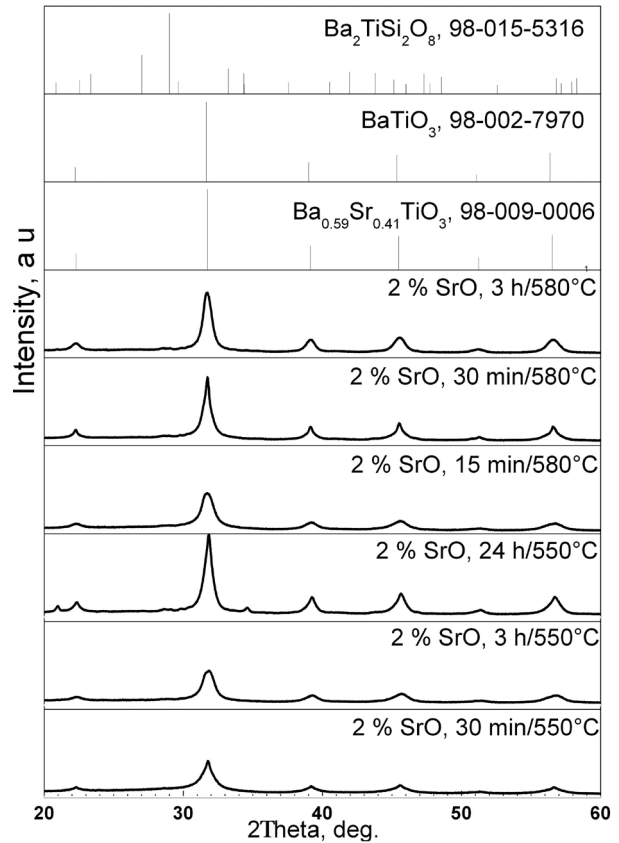


Fig. 3. Comparison of the XRD patterns of glass-ceramics with 2 mol% SrO obtained after thermal treatment at 550 and 580 °C for different times.

[6, 23]. A Rietveld refinement of the XRD patterns of the Sr-containing samples crystallized for 24 h at 550 °C showed that minor quantities of magnetic phases which match the peaks of BaFe_4O_7 (JCPDS 98-000-2529) and $\text{BaFeO}_{2.93}$ (JCPDS 98-016-7059) also precipitate. The occurrence of iron-containing barium oxide phases may have an interesting impact on the properties of the prepared glass-ceramics, due to their magnetic properties [24, 25]. The Rietveld analysis of the data in Fig. 2 shows that the changing SrO concentrations do not affect the size and type of the precipitating crystals. Only the temperature and the annealing time affect the crystallization behaviour significantly.

The microstructure of the obtained BaTiO_3 -containing glass-ceramics with $x = 0$ mol% SrO is presented in Fig. 4. This microstructure is typical for that formed in liquid/liquid phase separated materials as already reported for the present system [6, 23] and discussed in Ref. [26] for similar glass systems. The glass-ceramic samples with SrO concentrations of 0.5, 1 and 2 mol% in the composition exhibit the same phase separated microstructure and the occurrence of droplet-like structures with an average

size of 300-400 nm which tend to form interconnected aggregates for the longer annealing times, cf. Figs. 5a–c. This observation corresponds to the data from the XRD analyses as seen in Figs. 2 and 3. Ac-

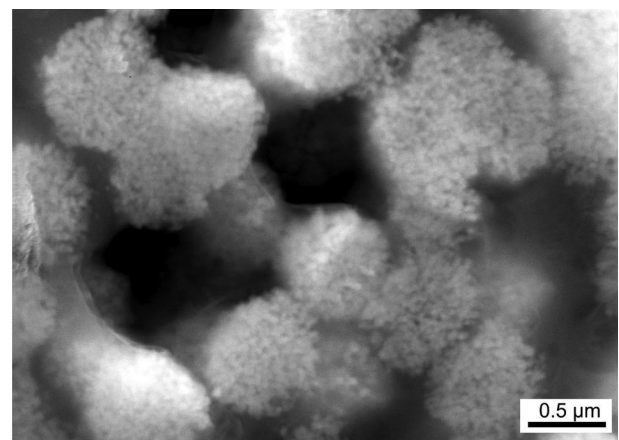


Fig. 4. SEM micrograph of the polished C-covered surface of a sample with 0 mol% SrO obtained after heat-treatment for 100 h at 600 °C.

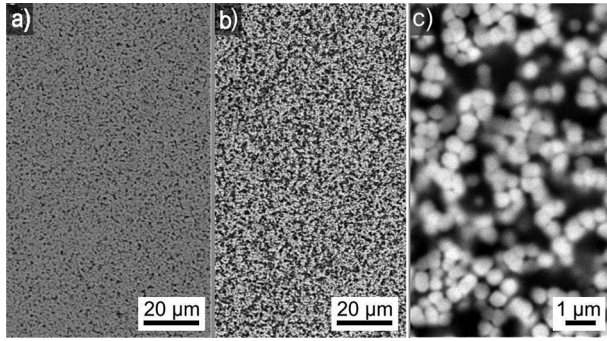


Fig. 5. SEM (BEC) micrograph of the polished C-covered surface of a sample with a) 0.5 mol% SrO obtained after heat-treatment for 3 h at 550 °C, b) 2 mol% SrO heat treated at 580 °C for 15 min and c) magnified micrograph of the microstructure of the sample from b).

According to Ref. [26], the microstructures of the obtained glass-ceramics for all SrO compositions are characterized by the presence of two phases. One is enriched in Ba, Sr and Ti from which barium-strontium titanate and fersnoite will crystallize later, while the other predominantly contains the remaining elements from the glass composition. Nevertheless, increasing the annealing temperature and the crystallization time do not lead to significant crystal growth. This could be caused by a phase separation which would result in many crystallization nuclei from which crystals will start to grow and will also limit crystal growth of at least one of the precipitating phases. Furthermore, the increase of both the crystallization temperature and time – as seen in the Figs. 6 and 7 will result in the presence of two types of crystal morphologies – those growing in the small droplet-like structures and larger ones with a different, dendritic morphology. Fig. 6 shows that the droplet-like microstructure contains superstructures reaching more than 20 μm in diameter (darker in the SEM micrograph) which are depleted of Fe and Na, enriched in Si and Al and share some morphological similarities with spherulites. Fig. 6c shows that they transcend the boundaries of the dominant microstructure, meaning they probably formed before phase separation occurred. If this is a crystalline aluminosilicate its volume concentration is probably below the detection threshold of XRD as no unexplained peaks occurred during XRD pattern evaluation. The EDXS results shown in Fig. 7 reveal that the probably amorphous matrix is enriched in Fe but depleted of Ti. As the crystal phases both contain Ti but no Fe, it may be concluded that the elements not included into the crystals form a residual glass.

Impedance measurements were performed on glasses and glass-ceramics with different SrO con-

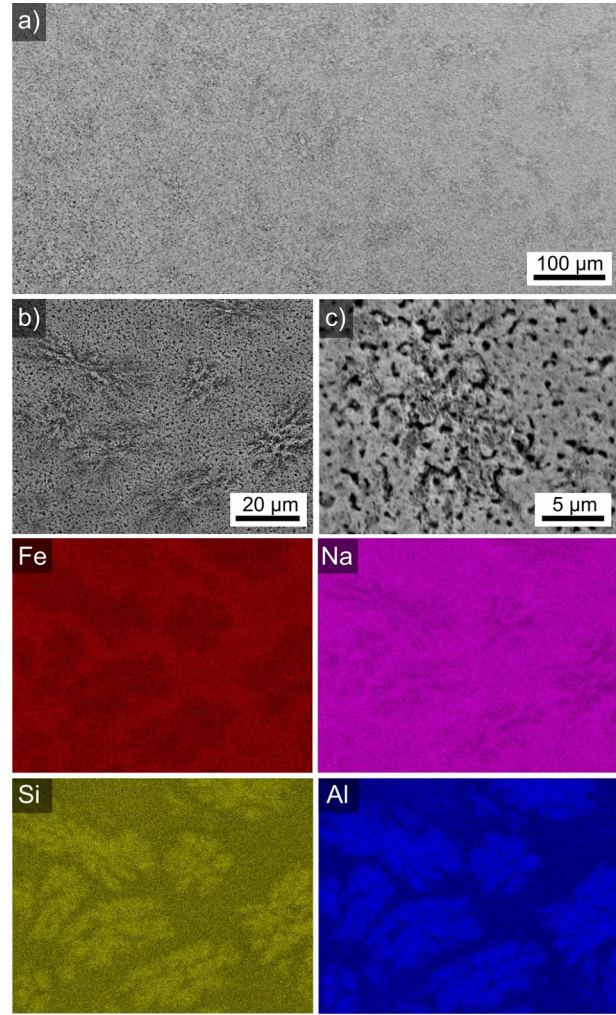


Fig. 6. SEM micrographs presenting a) an overview of a sample with 2 mol% SrO obtained after a heat-treatment for 24 h at 580 °C. b) shows the microstructure in greater detail while c) shows one of the darker structures amidst the phase separated microstructure. EDXS-maps of Fe, Na, Si and Al are presented below to illustrate the element distribution in b).

centrations to determine their dielectric properties. The impedance modulus and the phase angle of the glass-ceramics were measured as a function of the temperature and frequency. Then the real, Z' and the imaginary, Z'' parts of the impedance were separated. Furthermore, the real, $\epsilon' = \frac{Cd}{\epsilon_0 S}$ and imaginary, $\epsilon'' = \frac{d}{\omega R S \epsilon_0}$ parts of the complex dielectric permittivity were determined from the known sample geometry.

The tangent loss angle is calculated using $\tan \delta = \frac{\epsilon''}{\epsilon'}$.

The ac-conductivity was obtained, taking into account the sample geometry from $\sigma_{ac} = \omega \epsilon_0 \epsilon''$. The results from the data processing of the impedance measurements, i.e. the real part of the dielectric

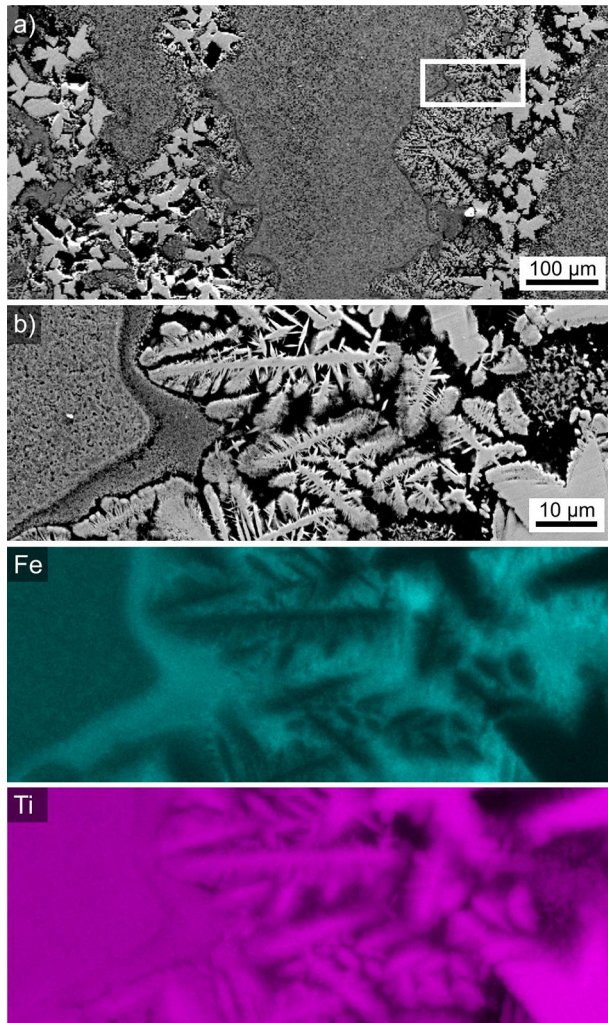


Fig. 7. a) SEM micrograph featuring a more inhomogeneous area in the same sample featured in **Figure 6**. The framed area in a) is presented in b) in greater detail to show that dendritic growth is implied for the larger crystals. EDXS-maps of Fe and Ti in this area are presented below.

constant, the tangent of the loss angle and ac-conductivity for samples with three different SrO concentrations thermally treated for 24 h at 550 °C are shown in the Figs. 8, 9 and 10 as a function of the temperature and frequency. The impedance measurements previously reported for glass-ceramics with a similar thermal history but containing no SrO [23] show that the dielectric constants ($\epsilon' \sim 70$ at room temperature and 1 kHz) are smaller at one and the same temperature and the loss tangents are also relatively low. The real parts of the dielectric permittivity for the samples containing SrO are generally higher than those for the samples without SrO. The data from the Figs. 8–10 show that the dielectric constant is highest for the sample containing 1 mol% SrO ($\epsilon' \sim 150$ at room temperature) and the loss tangent is smallest ($\text{tg}\delta \sim 0.3$ at 1 kHz). These changes in the dielectric constant and in the ability of the glass-ceramics with different SrO concentrations to absorb electromagnetic radiation should be due to the different type of incorporation of the Sr^{2+} ions in the samples and the resulting different structures. The ac-conductivities of the respective glass-ceramics with 1 mol% SrO are also highest: $\sim 10^{-7}$ S/m at RT and 1 kHz, while for the 0.5 and 2 mol% samples, the values are in the order of 10^{-8} S/m. The ac-conductivity of the SrO-free samples is about 10^{-6} S/m [23] which again can be explained by structural peculiarities of the respective glass-ceramics.

The frequency dependence of the dielectric constant for each temperature again shows that the decrease of the ϵ' -values is relatively fast which is also typical for other glass-ceramics as well as for glassy materials [27]. Otherwise, the temperature dependence of all Sr-containing glass-ceramics follows the theoretically predicted trend – the higher the temperature, the larger the dielectric constant.

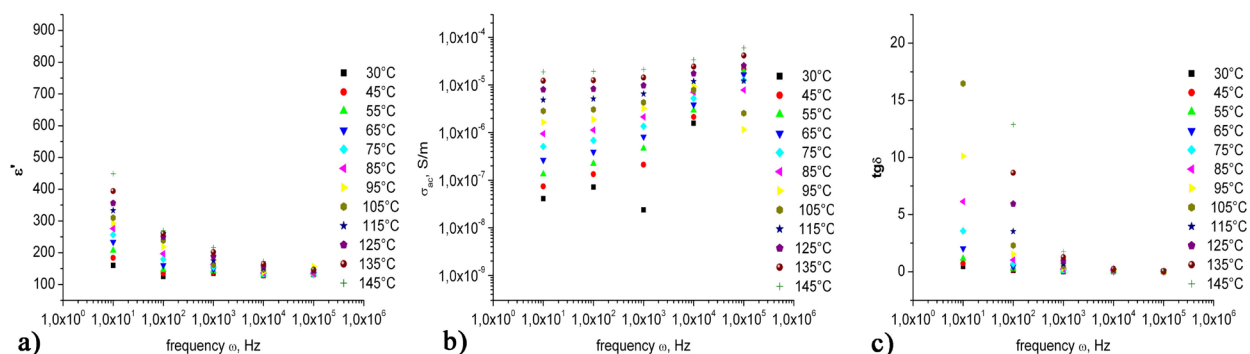


Fig. 8. Sample with 0.5 mol% SrO annealed 24 h/550 °C: Temperature and frequency dependence of the a) dielectric constant, b) ac-conductivity and c) loss tangent.

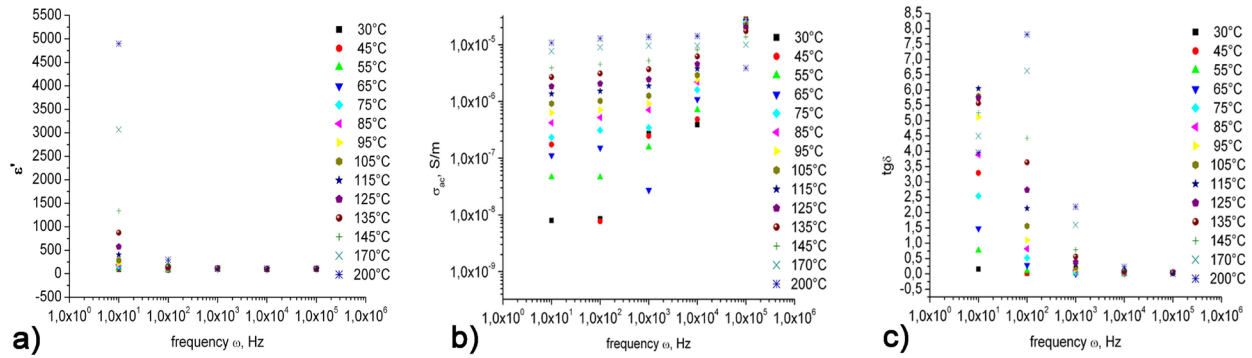


Fig. 9. Sample with 1 mol% SrO annealed 24 h/550 °C: Temperature and frequency dependence of the a) dielectric constant, b) ac-conductivity and c) loss tangent.

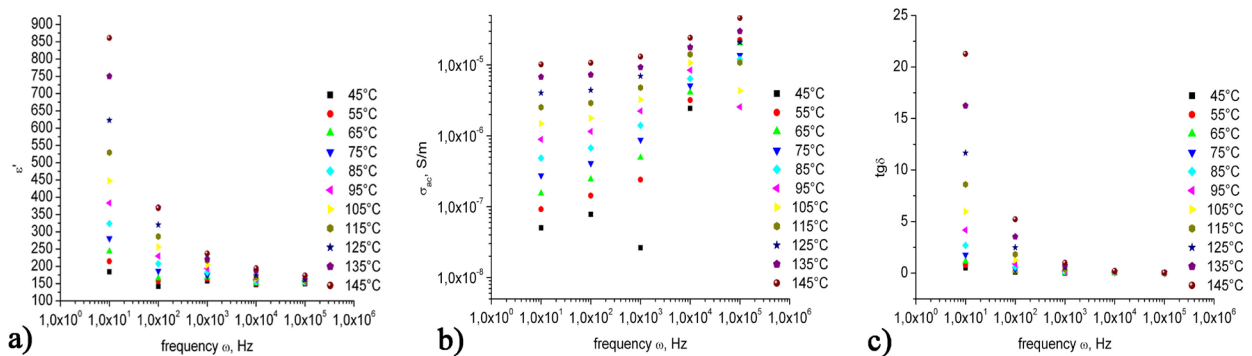


Fig. 10. Sample with 2 mol% SrO annealed 24 h/550 °C: Temperature and frequency dependence of the a) dielectric constant, b) ac-conductivity and c) loss tangent.

CONCLUSION

Bulk glasses are obtained with slight surface crystallization for SrO concentrations of $x = 0.5, 1$ and 2 mol% in the compositional series $20.1\text{Na}_2\text{O}/(23.1-x)\text{BaO}/x\text{SrO}/23\text{TiO}_2/7.6\text{B}_2\text{O}_3/17.4\text{SiO}_2/5.8\text{Fe}_2\text{O}_3/3\text{Al}_2\text{O}_3$. Independent of the applied time-temperature schedules, always cubic $\text{Ba}_{(1-x)}\text{Sr}_x\text{TiO}_3$ precipitates and for annealing times longer than 3 h, also, tetragonal $\text{Ba}_2\text{TiSi}_2\text{O}_8$ crystallizes.

An increase in the SrO concentration does not influence the $\text{Ba}_{1-x}\text{Sr}_x\text{TiO}_3$ solid solution composition but initially – up to 1 mol% SrO suppresses the crystallization of fresnoite and then for 2 mol% SrO further promotes it. The SEM and EDXS analyses hint on the presence of phase separation and after heat treatment and crystallization in the demixed regions of mainly $\text{Ba}_{1-x}\text{Sr}_x\text{TiO}_3$. Also, an unidentified phase enriched in Si and Al occurs in an in-

significant amount. The increasing heat treatment times and heat treatment temperatures lead to crystal growth, however, a significant effect of the SrO concentration on the average crystal size is not observed.

The dielectric constants as well as the dielectric losses of the SrO containing glass-ceramics are higher than those of the glass-ceramics without SrO at the same measuring conditions. The dielectric constant is highest for the 1 mol% SrO glass-ceramic while the loss tangent is smallest. Lower as well as higher SrO concentrations result in lower dielectric constants and higher losses for equal thermal history.

Acknowledgments: The authors appreciate the financial support of the Bulgarian National Science Fund under contract KII-06-H28/1.

REFERENCES

1. R. P. Maiti, S. Basu, S. Bhattacharya, D. Charkravorty, *J. Non-Cryst. Solids*, **355**, 2254 (2009).
2. A. K. Yadav, C. Gautam, P. Singh, *New J. Glass Ceram.*, **2**, 126 (2012).
3. M. S. Al-Assiri, M. M. El-Desoky, *J. Non-Cryst. Solids*, **358**, 1605 (2012).
4. A. Bhargava, R. L. Snyder, R. A. Condrate Sr., *Mater. Lett.*, **7**, 185 (1988).
5. V. Buscaglia, M. T. Buscaglia, M. Viviani, L. Mitoseriu, P. Nanni, V. Trefiletti, P. Piaggio, I. Gregora, T. Ostapchuk, J. Pokorny, J. Petzelt, *J. Eur. Ceram. Soc.*, **26**, 2889 (2006).
6. R. Harizanova, M. Abrashev, I. Avramova, L. Vladislavova, C. Bocker, G. Tsutsumanova, G. Avdeev, C. Rüssel, *Solid State Sci.*, **52**, 49 (2016).
7. J. F. Capsal, E. Dantras, L. Laffont-Dantras, J. Dandurand, C. Lacabanne, *J. Non-Cryst. Solids*, **356**, 629 (2010).
8. T. J. Jackson, I. P. Jones, *J. Mater. Sci.*, **44**, 5288 (2009).
9. R. Vijayalakshmi, V. Rajendran, *Digest Journal of Nanomaterials and Biostructures*, **5**, 511 (2010).
10. S. Sulekar, J. H. Kim, H. Han, P. Dufour, C. Tennailleau, J. C. Nino, E. Cordoncillo, H. Beltran-Mir, S. Dupuis, S. Guillemet-Fritsch, *J. Mater. Sci.*, **51**, 7440 (2016).
11. K. Yao, W. Zhu, *Thin Solid Films*, **408**, 11 (2002).
12. M. M. Vijatović, J. D. Bobić, B. D. Stojanović, *Sci. Sintering*, **40**, 155(2008).
13. U. Joshi, S. Yoon, S. Baik, L. S. Lee, *J. Phys. Chem. B*, **110**, 12249 (2006).
14. G. P. Du, Z. J. Hu, Q. F. Han, X. M. Qin, W. J. Shi, *J. Alloys & Comp.*, **492**, L79 (2010).
15. R. P. Borges, R. C. Silva, M. M. Cruz, M. Godinho, *J. Phys. Conf. Ser.*, **200**, 072014 (2010), doi: 10.1088/1742-6596/200/7/072014.
16. P. S. More, S. B. Deshpande, Y. B. Kholam, H. S. Potdar, R. N. Karekar, R. C. Aiyer, *Mater. Lett.*, **61**, 2891 (2007).
17. G.G.Genchi, A.Marino, A.Rocca, V.Mattoli, G.Ciofani, *Nanotechnology*, **27**, 232001 (2016).
18. P. Ren, H. Fan, X. Wang, *J. Mater. Sci.*, **48**, 7028 (2013).
19. Sh. Hossaina, A. M. Abdallah, S. Noor Azean, B. Jamaica, J. H. Zainia, A. K. Azada, *Renew. Sust. Energ. Rev.*, **79**, 750 (2017).
20. C. Kajtoch, W. Bak, B. Garbarz-Glos, K. Stanuch, W. Tejchman, K. Mroczka, T. Czeppe, *Ferroelectrics*, **463**, 130 (2014).
21. N. J. Ridha, M. Mat, W. Yunus, S. A. Halim, Z. A. Talib, F. K. M. Al-Asfoor, W. C. Primus, *Am. J. Eng. Appl. Sci.*, **2**, 661 (2009).
22. A. Kaur, A. Singh, L. Singh, S. K. Mishra, P. D. Babu, K. Asokan, S. Kumar, C. L. Chen, K. S. Yang, D. H. Wei, C. L. Dong, C. H. Wangi, M. K. Wu, *RSC Adv.*, **6**, 112363 (2016).
23. R. Harizanova, S. Slavov, L. Vladislavova, L. C. Costa, G. Avdeev, C. Bocker, C. Rüssel, *Ceram. Int.*, **46**, 24585 (2020).
24. O. Clemens, M. Gröting, R. Witte, J. M. Perez-Mato, C. Loho, F. J. Berry, R. Kruk, K. S. Knight, A. J. Wright, H. Hahn, P. R. Slater, *Inorg. Chem.*, **53**, 5911 (2014).
25. T. Ferreira, G. Morrison, W. M. Chance, S. Calder, M. D. Smith, H. C. zur Loye, *Chem. Mater.*, **29**, 2689 (2017), DOI: 10.1021/acs.chemmater.7b00580.
26. W. Vogel, *Glass chemistry*, 3 Edn., Springer, Berlin, Germany, 1992.
27. Y. Feldman, A. Puzenko, Y. Ryabov, Chapter 1: Dielectric relaxation phenomena in complex materials, in: *Fractals, diffusion and relaxation in disordered complex systems: a special volume of Advances in Chemical Physics*, T. Coffey, Y. P. Kalmykov and S. A. Rice (eds), vol. 133, Part A, W. John Wiley&Sons, 2006.

Analysis of structure factors (F_{hkl}) of meaningful XRD diffraction intensities for chemical determinations after ion-exchange and isomorphic substitutions in crystal structures

Ognyan Petrov*

*Institute of Mineralogy and Crystallography, Bulgarian Academy of Sciences,
Acad. G. Bonchev str., block 107, Sofia, Bulgaria*

Received November 25, 2021; Accepted December 20, 2021

The intensity changes of selected meaningful diffraction lines in the powder XRD patterns of sedimentary clinoptilolite modified by cation exchange are discussed and a crystal chemical analysis of the corresponding structure factors (F_{hkl}) is elaborated giving background for speedy quantification of the cation exchange in clinoptilolite. Similar approach is applied in the system of grown $\text{Ca}_{1-x}\text{Sr}_x\text{F}_2$ crystals for control of the Sr content. The study is based on mathematical calculations of structure factors (F_{hkl} , F_{hkl}^2) and the corresponding intensities (I_{hkl}), followed by crystal chemical discussion and quantification approaches. Such approach is promising for any crystal structure if detailed structural and crystal chemical knowledge is available and systematized.

Keywords: XRD, clinoptilolite, fluorite, structure factors, quantification

INTRODUCTION

A possibility exists to use intensities of peaks in the powder XRD patterns for chemical considerations for certain crystal structures characterized by ability for ion exchange as is the case of zeolites or in case of apparent isomorphic substitutions of elements with typical case being the $(\text{Ca}, \text{Sr})\text{F}_2$ fluorite series.

For example, ion-exchange of the zeolite clinoptilolite with heavy cations (Sr, Ba, Ag, Cs, Tl) results in large intensity changes in the powder XRD pattern, which can be interpreted using its known crystal structure [1–4]. After ion exchange with heavy cations the peak intensities in the powder XRD pattern of clinoptilolite change markedly due to changes in the structure factors F_{hkl} , which are related to the scattering factors (f_i) and the number (n_i) and positions (x, y, z) of the atoms in the structure. Structural channels are major characteristics of the microporous zeolite structures and can be occupied by alkaline and alkaline-earth cations surrounded by water molecules. The cation-water configurations are responsible for unique properties displayed by zeolites with potential for industrial applications. Ion exchange and sorption are among the most im-

portant ones. Thus, the chemical quantification of these effects is complicated, labor-intensive and time-consuming.

The powder XRD studies of $\text{Ca}_{1-x}\text{Sr}_x\text{F}_2$ single crystals are important to evaluate the influence of Sr-concentration in such single crystals, which are promising materials for optoelectronics [5]. In typical powder XRD patterns of grown $\text{Ca}_{1-x}\text{Sr}_x\text{F}_2$ crystals the inspection of the dependencies of the XRD intensity ratios of certain diffraction peaks (I_{111}/I_{222}) is a suitable crystal chemical parameter when studying the isomorphic substitutions in the fluorite structure. Single CaF_2 crystals are widely applicable in optical devices operating in the ultraviolet and visible spectral ranges due mainly to their isotropic optical properties and excellent transmission. In the case of $\text{Ca}_{1-x}\text{Sr}_x\text{F}_2$ crystals structural and optical studies concerned with materials with intermediate values of x are sporadic and have dealt only with very particular aspects of the effect of chemical composition on some properties of the material [6].

The present studies evaluate the significant intensity changes in the powder XRD patterns of sedimentary clinoptilolite modified by cation exchange. A crystal chemical analysis on these changes is elaborated giving background for speedy quantification of the cation exchange in clinoptilolite.

Analogically, similar approach is applied in the system of $\text{Ca}_{1-x}\text{Sr}_x\text{F}_2$ crystals for control of the Sr content.

* To whom all correspondence should be sent:
E-mail: opetrov@dir.bg

MATERIALS AND METHODS

Clinoptilolite case

Sedimentary clinoptilolite sample from Beli Plast deposit (Eastern Rhodopes, Bulgaria) was investigated. The sample was enriched to ~95 wt.% zeolite component by heavy liquids separation of the denser non-zeolitic minerals. The ion-exchange was performed at 90° C for 96 h in 1 N solutions of the nitrates of Sr, Ba, Ag, Cs, and Tl.

Fluorite case

The investigated $\text{Ca}_{1-x}\text{Sr}_x\text{F}_2$ crystals ($0.007 \leq x \leq 0.674$) were grown from natural raw fluorite mixed with suprapure SrF_2 (Merck) using a modified Bridgman–Stockbarger method either in a dynamic argon flow (for $0 < x < 0.307$) or in vacuum (for $0.383 < x < 0.674$) [7].

Powder XRD method

Powder X-ray diffraction (XRD) patterns were collected on a DRON 3M diffractometer in Bragg–Brentano geometry with Fe-filtered $\text{Co K}\alpha$ radiation (40 kV, 28mA) and on a D2 Phaser (Bruker) diffractometer using Ni-filtered $\text{CuK}\alpha$ radiation (30 kV and 20 mA).

The precise position and the integrated intensity of the peaks were determined by the WINFIT V1.2 package [8].

CRYSTAL CHEMICAL BACKGROUND

Clinoptilolite case

The unit-cell parameters of clinoptilolite change little after ion exchange with heavy cations (Sr_2^+ , Ba_2^+ , Pb_2^+ , Ag^+ , Cs^+ , Tl^+) but the intensities of the peaks in the powder XRD pattern change significantly [9]. These intensity changes are obviously due to the changes in the structure factors, $F(hkl)$, which are composed of atomic scattering factors (f_i) (for heavy cations these exceed several times the ones of lighter cations – Na^+ , K^+ , Ca_2^+ , Mg_2^+), and the number (n_i) and positions (x, y, z) of all atoms in the crystal structure.

The intensity of a given powder XRD line can be expressed as:

$$I(hkl) = K L_p |F(hkl)|^2 (\mu^*)^{-1} \quad (1),$$

where K is a constant of physical and experimental conditions; L_p is the Lorentz and polarization correction; μ^* is the mass absorption coefficient.

Structural studies on natural clinoptilolite confirm the C2/m centric space group [10–12] and the same same group was confirmed for Ba-exchanged [1] and Cs-exchanged [2, 12] clinoptilolites. Thus, the structure factor (F) for clinoptilolite can be expressed only with the real part (A) in the general formula $F = A + iB$:

$$F(hkl) = A(hkl) = \sum_i n_i f_i \cos 2\pi(hx_i + lz_i) \cos 2\pi ky_i \quad (2),$$

where hkl are Miller indices; $x, y,$ and z are fractional coordinates of atom i in the structure; f is the atomic scattering factor of atom i ; and n is the number of atoms in a given crystallographic position.

Further, for $(0k0)$ -type diffraction lines we have:

$$F(0k0) = \sum_i n_i f_i \cos 2\pi ky_i \quad (3)$$

In Eq. 3, $F(0k0)$ can be represented as a sum of the partial contributions by the framework atoms (F_f), water molecules (F_w), and exchangeable cations (F_c):

$$F(0k0) = F_f + F_w + F_c \quad (4)$$

Calculations of $F(020)$ from structural data for clinoptilolite and heulandite (iso-structural analogue) reveal that F_f and F_w have almost constant values: $F_f = -400$ (5) and $F_w = +150$ (7) with approximate sum of -250 . Thus, the variations in $F(020)$ should depend mainly and directly on F_c , and because exchangeable cations occupy the mirror plane of the clinoptilolite/heulandite structure with coordinates along b of $y=0, \frac{1}{2}$, F_c is given by:

$$F_c = \sum_i n_i f_i \quad (5),$$

i.e., the cationic part is always positive and depends on the type and quantity of the exchangeable cations.

Therefore, the equation to express $F(020)$ is:

$$F(020) = -250 + \sum_i n_i f_i \quad (6)$$

Eq. (6) can be used to calculate the square of $F(020)$ and after correction for absorption (μ^*) to relate the degree of cation exchange to the measured $I(020)$ changes. Eq. (6) allows $|F(020)|^2$ to be calculated for various compositions based on a model clinoptilolite with 6.5 tetrahedral Al in the unit cell, which should contain 6.5 monovalent or 3.25 divalent cations or their combination.

Fluorite case

Powder XRD studies of a material from $\text{Ca}_{1-x}\text{Sr}_x\text{F}_2$ single crystals ($0.007 \leq x \leq 0.674$) are important to evaluate the influence of Sr-concentration in such single crystals, which are promising materials for optoelectronics. The XRD intensity ratio I_{111}/I_{222} of the corresponding peaks is a suitable crystal chemical parameter when studying the fluorite structure (S.G. $Fm\bar{3}m$) [5].

Knowing the ion coordinates ($x, y, z = 1/4$ for F^- and $x, y, z = 0$ for Ca^{2+} (Sr^{2+})) in the fluorite structure one can calculate F_{111} and F_{222} : $F_{111} = 4f(M)$ and $F_{222} = 4f(M) - 8f(F)$, where ($M = \text{Ca}, \text{Sr}$) stands for cations occupying the (4a) Wyckoff position. It is clear that for $\text{Ca}_{1-x}\text{Sr}_x\text{F}_2$ compounds $f(M)$ depends strongly on x and, consequently, the ratio I_{111}/I_{222} should vary with x . The conclusion is that F_{111} and F_{222} (and respectively I_{111} and I_{222}) depend only on the isomorphous substitution of Sr^{2+} for Ca^{2+} and, as $f(\text{Ca}) < f(\text{Sr})$, the ratio decays exponentially with x . So, one can judge for the Sr^{2+} content in the fluorite structure based on the ratio I_{111}/I_{222} .

RESULTS

Clinoptilolite case

Powder XRD patterns of a natural clinoptilolite (Beli Plast deposit, Bulgaria) and several ion-exchanged forms are shown in Figure 1. Significant intensity changes in the diffraction lines exist and can be related to the atomic scattering factors of the heavy cations used for exchange, which are from 2 to 7 times greater than the original cations in the mirror plane of the structure, as well as to the different sites that are possibly occupied after ion exchange. Mass absorption coefficients also influence intensities.

Fluorite case

Figure 2 presents a powder XRD pattern for fluorite sample with $x=0.223$ (Sr content) and indexed peaks corresponding to the main reflecting crystal planes compared with pure CaF_2 . As seen, the most intensive peak is the reflex along 111-direction (this holds for all the XRD patterns measured).

As the ionic radius of Sr^{2+} (1.18 Å) is bigger than that one of Ca^{2+} (1.00 Å) then the XRD lines of $\text{Ca}_{1-x}\text{Sr}_x\text{F}_2$ will systematically shift to lower 2-theta angles. Namely, from $d = 3.16$ Å (CaF_2) to $d = 3.20$ Å for $\text{Ca}_{0.0777}\text{Sr}_{0.223}$ and for the case $\text{Ca}_{0.446}\text{Sr}_{0.554}$ for example this d-value is logically higher 3.298 Å.

Since to the best of our knowledge there are no refined XRD parameters for a number of members

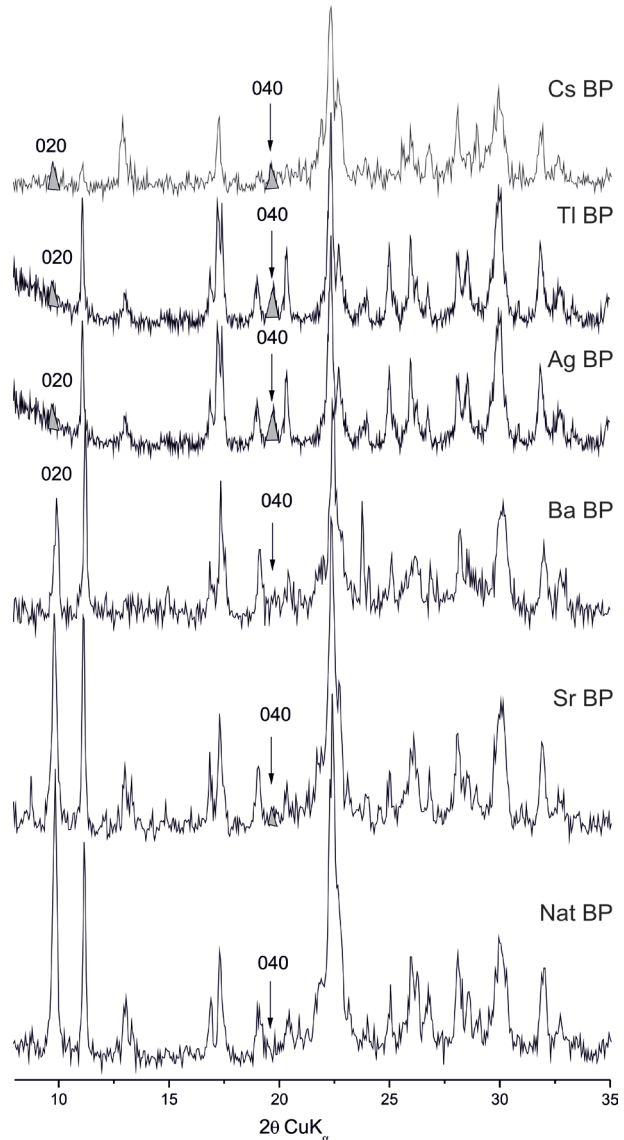


Fig. 1. Powder XRD diffraction patterns of natural and ion-exchanged clinoptilolite from Beli Plast deposit, Bulgaria.

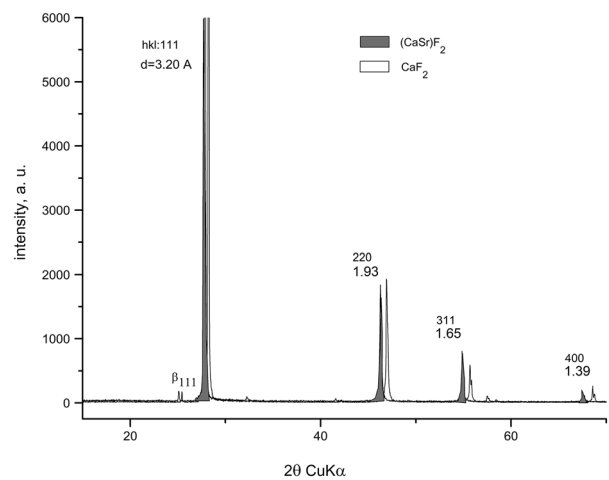


Fig. 2. Powder XRD pattern for fluorite sample with $x = 0.223$ (Sr content) and indexed peaks corresponding to the main reflecting crystal planes compared with pure CaF_2 .

Table 1. Unit cell parameter a and volume V for synthesized (Ca,Sr) fluorite samples with different Sr-content

Sr per unit cell	a (Å)	V (Å ³)
0.007	5.468(3)	163.5(5)
0.053	5.476(1)	164.2(1)
0.113	5.502(1)	166.5(2)
0.189	5.529(1)	169.0(1)
0.26a	5.544(1)	170.4(2)
0.383	5.589(3)	174.6(4)
0.500	5.660(2)	181.3(2)
0.509	5.641(2)	179.5(3)
0.554	5.658(2)	181.1(2)
0.674	5.688(1)	184.1(1)
0.760	5.714(1)	189.6(1)

of the $\text{Ca}_{1-x}\text{Sr}_x\text{F}_2$ system, we list for completeness in Table 1 the calculated values of both the unit cell parameter and volume.

DISCUSSION

Clinoptilolite case

Values of $|F(020)|^2$ calculated using Eq. (6) for various cationic combinations for a model clinoptilolite with 6.5 Al per unit cell (frequently met in nature) are graphically represented in Figure 3.

The curve shows the changes in the structure factor in relation to the number of electrons (N) of the atoms on the mirror plane of the clinoptilolite structure. Theoretically, a zero value of $F(020)$ can be reached if, e.g. 3.8Na^+ and 2.7Tl^+ ions are in the mirror plane of the structure. A $I(020)$ value, close to zero was obtained by Tl- and Cs-, combined with Na-exchange on clinoptilolite from Beli Plast deposit, Bulgaria (Fig. 4).

Some characteristic points and intervals can be specified on the curve in Figure 2. First, point “0” corresponds to about 268 diffracting electrons and in this case $|F(020)|^2$ should be zero ($I(020) = 0$).

The interval B–D on the curve represents all theoretically possible combinations of Ca, Na, and K, i.e., typical for natural clinoptilolite (6.5 tetrahedral Al for our case) exchangeable-cation compositions. Some natural samples are marked with x in Figure 4 according to their chemical content (Boles, 1972).

Further lowering of $|F(020)|^2$ can be achieved if clinoptilolite is ion-exchanged with heavy cations. Point “E” corresponds to 3.25 Ba atoms on the mirror plane. Such trend was used by Petrov [9] to evaluate directly the Ba content in clinoptilolite from Beli Plast using exchanged samples having different Na/Ba ratios and a Na-clinoptilolite reference sample following the intensity ratios after correction for μ^* (mass absorption coefficient) according to the equation:

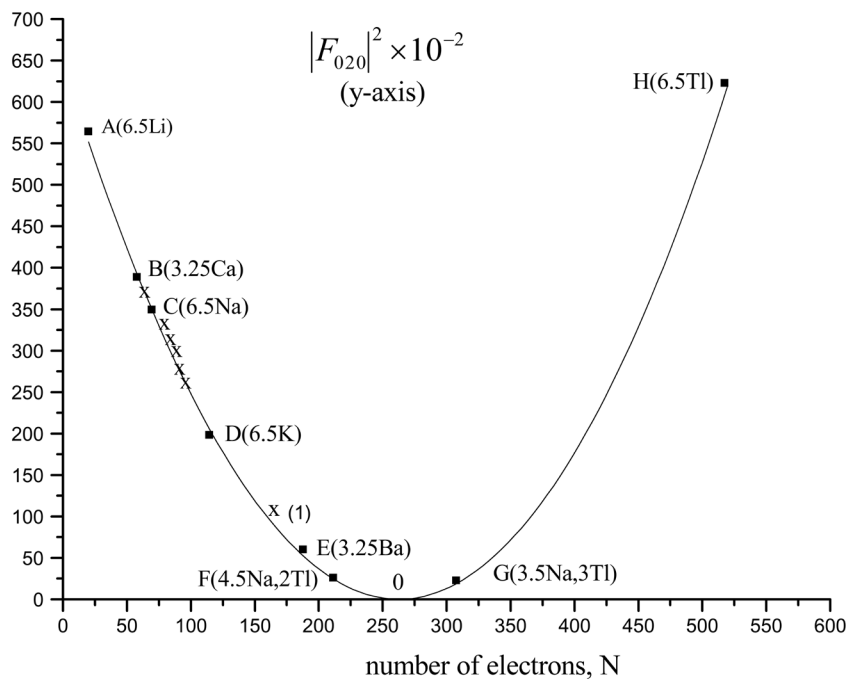


Fig. 3. Graphical representation of the behavior of $|F(020)|^2$ with an increase in the number (N) of diffracting electrons on the mirror plane of the clinoptilolite structure.

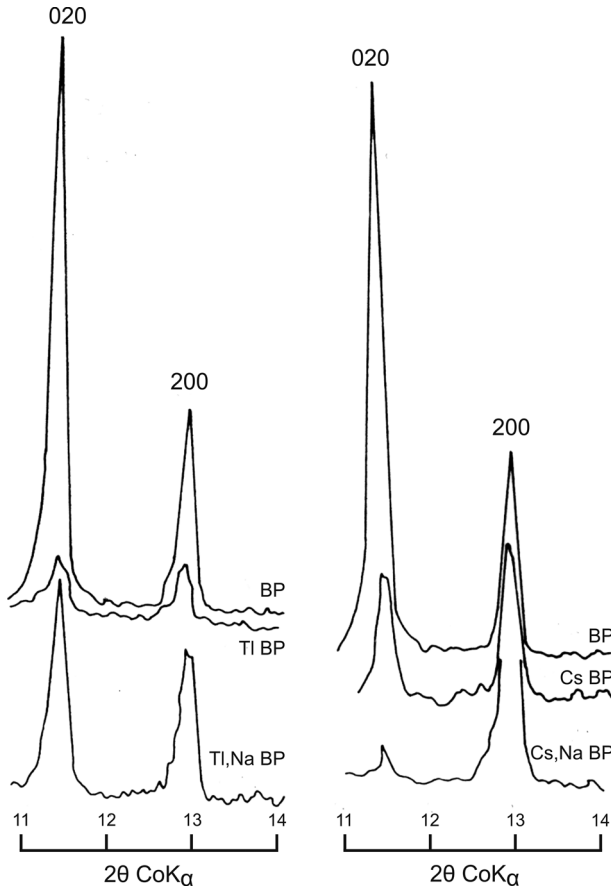


Fig. 4. Intensity changes in the 020 and 200 clinoptilolite reflections as a function of Tl, Cs, and subsequent Na-exchange.

$$I_{Ba} / I_{Na} = |F_{Ba}|^2 \cdot |\mu_{Ba}^*|^{-1} / |F_{Na}|^2 \cdot |\mu_{Na}^*|^{-1} \quad (7)$$

The right-hand side of Eq. 7 was used to construct a graphical curve of theoretical Ba-Na compositions; I_{Ba}/I_{Na} is experimentally measured. Figure 5 illustrates the good agreement between XRD and chemical analyses (in number of Ba atoms per unit cell).

Fluorite case

As described above from crystal chemical point of view one can judge for the Sr^{2+} content in the fluorite structure based on the ratio I_{111}/I_{222} .

The Sr-dependence (x) of the intensity ratio I_{111}/I_{222} in (Ca, Sr) fluorite is shown in Figure 6 by points, whereas the solid line presents the best fit to the data ($R^2 = 0.997$).

Additional parameter that can be used is the unit cell parameter of (Ca, Sr) fluorite, which is informative for the higher contents of Sr in the structure.

The x -dependence of the unit cell parameter a is given in Figure 7, where empty dots are the ex-

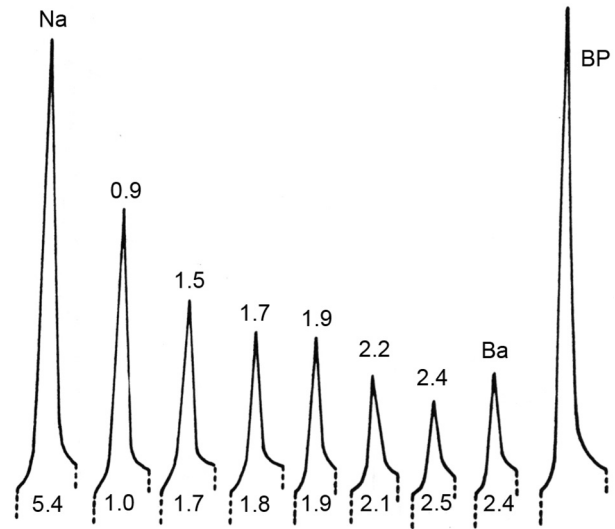


Fig. 5. Ba atoms determined by powder XRD (upper numbers) and wet chemical analysis (lower numbers) of natural sample BP (Beli plast deposit) its Na-exchanged form and Ba-exchanged series

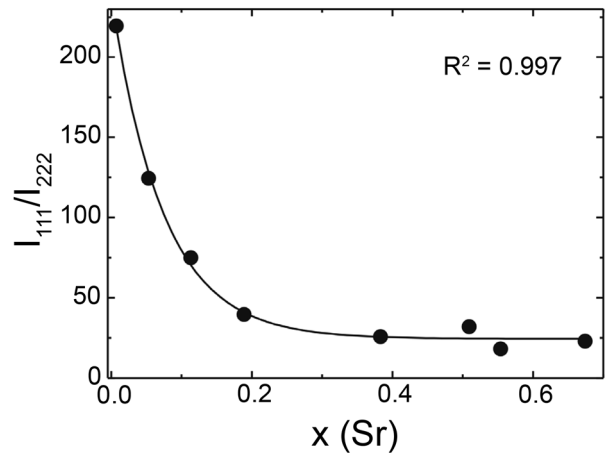


Fig. 6. x -dependence of the absolute change in the intensity ratio I_{111}/I_{222} . Circles are experimental data; the line presents the best fit to the data.

perimental data, while full squares are data from literature [4]. The straight line presents the linear regression best fit to the experimental data, $a = 5.453 + 0.342x$. This function describes very well the dependence of the unit cell parameter on the strontium concentration ($R^2 = 0.9975$).

The data in Table 1 for the unit cell parameters of (Ca, Sr) fluorite synthesized with controlled aliquots of strontium well represent the increase of a as well as of the volume (V) with the increase of the Sr content.

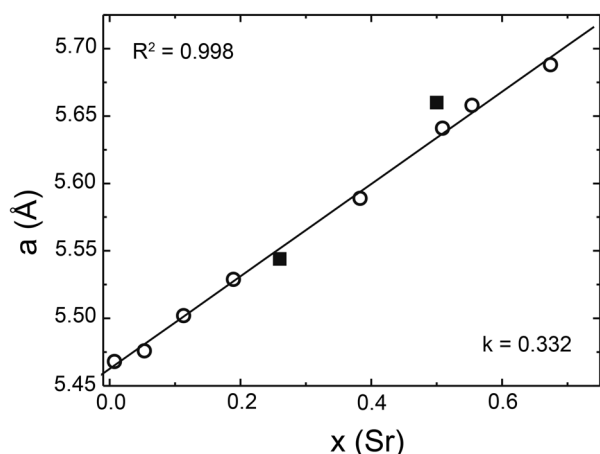


Fig. 7. x -dependence of the unit cell parameter a . (○) – experimental data, (■) – calculated data, the line is the linear regression best fit to the data.

CONCLUSIONS

The crystal chemical interpretation of changes in the structure factors of reflections in the powder XRD patterns allows chemical determinations of ion exchange processes on natural zeolite clinoptilolite using careful intensity measurements of peaks.

In the case of fluorite, as the XRD intensity ratio I_{111}/I_{222} was found to decay with the strontium concentration x , the latter can be easily followed out by a simple crystal chemical approach, which provides a means for determining the concentration of strontium in $\text{Ca}_{1-x}\text{Sr}_x\text{F}_2$ crystals based on XRD data only. For bigger concentrations of strontium the unit-cell

parameters additionally serve for the evaluation processes. Such approach is promising for crystal structures if detailed structural and crystal chemical knowledge is available and systematized.

REFERENCES

1. O. E. Petrov, L. D. Filizova, G. N. Kirov, *Compt. Rend. Acad. Bulg. Sci.*, **38** (5), 603 (1985).
2. O. E. Petrov, L. D. Filizova, G. N. Kirov, *Compt. rend. Acad. bulg. Sci.*, **44** (12), 77 (1991).
3. O. E. Petrov, in: Natural Zeolites '93, D. W. Ming and F. A. Mumpton (eds), Int. Comm. Natural Zeolites, Brockport, New York, 1995, p. 271.
4. L. Dimova, O. Petrov, M. Kadiyski, N. Lihareva, A. Stoyanova-Ivanova, V. Mikli, *Clay Minerals*, **46**, 197 (2011).
5. B. Kostova, J. Mouchovski, O. Petrov, L. Dimitrov, L. Konstantinov, *Mater. Chem. Phys.*, **113**, 260 (2009).
6. C. W. Ponader, R. E. Youngman, Ch. M. Smith, *J. Am. Ceram. Soc.*, **88** (9), 2447 (2005).
7. J. T. Mouchovski, K. A. Temelkov, N. K. Vuchkov, N. V. Sabotinov, *Bulg. Chem. Commun.*, **3**, 253 (2009).
8. S. Krumm, *Acta Universitatis Carolinae, Geologica*, **38**, 253 (1994).
9. O. E. Petrov, PhD Thesis, Sofia University "St. Kliment Ohridski", Bulgaria, 1988.
10. A. Alberti, *Tschermaks Min. Petr. Mitt.*, **22**, 25 (1975).
11. K. Koyama, Y. Takeuchi, *Z. Kristallogr.*, **145**, 216 (1977).
12. J. R. Smyth, A. T. Spaid, D. L. Bish, *Am. Mineral.*, **75**, 522 (1990).



Crystallography in Bulgaria and 10 years activities (2010–2020) of the Bulgarian Crystallographic Society

Ognyan Petrov

THE BEGINNINGS

Crystallography began in Sofia University in 1893 with the establishment of the Department of Natural History by Prof. Georgi Bonchev. He was PhD student in crystallography in Zagreb, Croatia, and taught geology, introduced a course in crystallography and published the first books on crystallography in Bulgaria in the 1890's. In 1905 he was appointed Chair of the Department of Mineralogy and Petrography.

Prof. Ivan Kostov graduated from the Natural Sciences Department of Sofia University. "St. Kliment Ohridski" in 1936. After studying at the Imperial College of Science and Technology in London

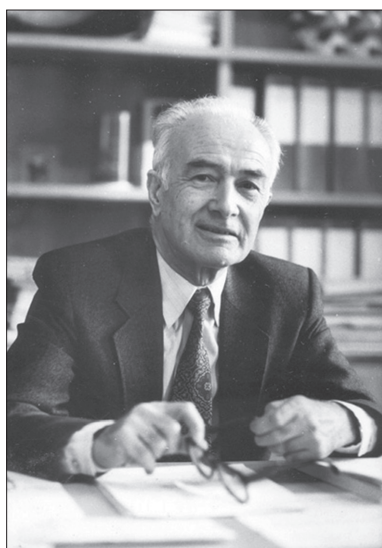


Fig. 1. Academician Professor Ivan Kostov.

(1940–1945), he returned to Sofia University. In 1953, as the first Head of the Dept. of Mineralogy and Crystallography, he taught crystallography, organized mineral collections, published Bulgarian, Russian and English editions of his textbooks on "Mineralogy and Crystallography" and supervised doctoral studies.

In 1967, Prof. Kostov was elected to Membership in the Bulgarian Academy of Sciences, (BAS) where he served as Head of the Geological Institute, Head of the Sector Mineralogy and Geochemistry, and Director of the National Museum of Natural History. He was a member of the German and Russian Academies of Sciences and Honorary member of the Bulgarian, Russian and Ukrainian Mineralogical Societies. His successor at the Department of Mineralogy and Crystallography Prof. Vesselina Breskovska, conducted crystallographic activities with Prof. Georgi Kirov, Assoc. Prof. Mihail Maleev and Assoc. Prof. Srebrni Petrov.

The Institute of General and Inorganic Chemistry of the Bulgarian Academy of Sciences was founded in 1960 by Prof. Georgi Bliznakov whose studies of the effects of impurities on the nucleation, growth and shape of crystals received international recognition. Crystallographic research was initiated in the 1960s with an electron microscope and Debye-Scherrer camera. In 1974, a DRON-1 diffractometer equipped with high and low-temperature chambers was installed. In 2006, the Institute obtained Bruker D8 equipment, which was successfully upgraded in 2010 with a linear LynxEye detector.

Between 1982 and 1985, Prof. Kostadin Petrov from the same Institute was Head of the Methodical

X-Ray Diffraction Lab at the Center of Chemical Sciences, which consisted of 10 institutes. His research activities were in the fields of preparative and applied inorganic solid state chemistry, structural perfection and texture of materials for electronics, superconductors, catalysts, refractory compounds, thin films, diffusion layers and galvanic coatings. He applied X-ray and neutron powder diffraction and Rietveld methods to materials identification, phase analysis and determination of crystallite sizes and microdeformations. His PhD thesis was concerned with polycrystalline inorganic catalysts and microstructure and topotactic synthesis of materials (later co-authors in this field of research were Kostadin Petrov, Nikolay Zotov and Daniela Kovacheva).



Fig. 2. Associate Professor Daniela Kovacheva with her staff and the new XRD diffractometer (2008) in the Laboratory of Solid State Chemistry & XRD analysis.

CRYSTALLOGRAPHY IN THE 1980s

In the 1980s, researchers from the Bulgarian Academy of Sciences and Sofia University held four meetings to discuss X-ray diffraction methods. The meetings evolved into National symposia

held in 1983, 1985, 1987 and 1991. These symposia were attended each time by over 80 scientists from 3 universities, research institutes and industrial laboratories in Bulgaria who gathered to share experiences and plan future studies. The interest in applying XRD-based methods for study grew among physicists, chemists, geologists, mineralogists and soil researchers. Resulting publications concerned small angle diffraction, X-ray topography, microdeformations of metal structures, thin layers, fiber composites, textures, and high-and low-temperature experiments.

INSTITUTE OF APPLIED MINERALOGY

The Institute of Applied Mineralogy of the Bulgarian Academy of Sciences was established in 1984 for research on minerals and their applications in industry and ecology. The Institute housed an XRD laboratory with an Enraf-Nonius CAD-4 single crystal diffractometer and two powder diffractometers, and Electron Microscopy and Crystal Growth laboratories. More than 100 structures of new crystalline materials were published under the leadership of Assoc. Prof. Josef Macicek who also supervised the PhD studies of Olyana Angelova, Todor Todorov, Rositsa Petrova and others.

In 1988, the research group of the XRD laboratory obtained a grant from the International Centre for Diffraction Data (ICDD) for production of PDF patterns of new crystalline phases. More than 200 new diffraction patterns were added to the PDF of ICDD (simple and double selenates, selenites, hydroselenites, adducts of inorganic salts with organic molecules, and perchlorates with nicotinic and isonicitric hydrazides). The research included synthesis and determination of structures and coordination numbers (RIRs), Computer programs were developed for calculating RIRs of powder patterns from known structures and characterization of the data according to IUCr guidelines.

INSTITUTE OF MINERALOGY AND CRYSTALLOGRAPHY

The Central Laboratory of Mineralogy and Crystallography (CLMC) of the BAS (successor of the Institute of Applied Mineralogy) was established in March, 1995, to conduct fundamental and applied investigations, provide consultation on and applica-

tion of analytical methods and training of specialists in mineralogy and crystallography. At the 5th General Assembly of the BAS, the Laboratory was renamed the Institute of Mineralogy and Crystallography “Acad. Ivan Kostov” (IMC-BAS). Today, IMC consists of well-equipped laboratories, offices and a library, it is supplied with an optical cable and Internet as well as PC for every research associate and specialist. Achievements are presented through Annual Reports (www.clmc.bas.bg), at scientific conferences and exhibitions, in periodicals, and *via* the mass media.

The laboratories of CLMC and IMC, have produced hundreds of scientific papers, conducted dozens of national and international projects, awarded PhD degrees and acquired a new scanning electron microscope (ZEISS EVO LS25), powder diffractometer (D2 Phaser BrukerAXS), single crystal dif-

fractometer (Oxford Supernova A 80-400 K Mo/Cu, with a temperature device from 80 to 400 K), a micro FTIR Spectrometer (TENSOR 37 Bruker) MIR and NIR with ATR accessories, and SETSYS Evolution TGA-DTA/DSC/MS up to 2400 K (Setaram).

Recently, the laboratory complex of IMC was substantially enriched with new modern apparatuses in the frame of projects of Center of Excellence and Center of Competence including single crystal XRD apparatus „D8 Venture“ – Bruker AXS and powder XRD apparatus „Empyrean“ – Malvern Panalytical.

BULGARIAN CRYSTALLOGRAPHIC SOCIETY

The Bulgarian National Committee for Crystallography (BNCC) was founded in 1992 as an adhering body of BAS. The members of BNCC were specialists in the fields of structural crystallography, crystal chemistry, crystal physics, mineralogy and materials sciences. BNCC coordinated the activities of the Bulgarian crystallographic community and maintained relations with IUCr and the European Crystallographic Association (ECA). Former Chairmen of BNCC were Andrey Apostolov (Sofia University, 1992–2000), Kostadin Petrov (Inst. of General and Inorganic Chem., BAS, 2000-2008), and Ognyan Petrov (Central Lab of Min and Cryst, BAS 2009–2010).

The 1st Bulgarian National Crystallographic Symposium

The 1st Bulgarian National Crystallographic Symposium organized by the NCCB in Oct. 2009 was attended by 98 participants presenting 68 oral and poster reports. Full papers were published in the Proceedings volume “1st National Crystallographic Symposium” (ISSN 1313-9991, Academic Publishing House Marin Drinov, online at http://clmc.bas.bg/symp09/docs/First_Cryst_Symp.pdf).

An assembly to establish the Bulgarian Crystallographic Society (BCS) was held on February 27, 2010, at the Institute of Mineralogy and Crystallography of BAS. 47 crystallographers from institutions throughout the country attended the assembly. The Bulgarian Crystallographic Society was officially registered in Bulgaria on **April 19, 2010** with a Board of seven Managers with Ognyan Petrov,



Fig. 3. The X-ray single crystal diffractometer Supernova A (Oxford Diffraction) in the Laboratory of X-ray diffraction analysis, IMC (2010).



Fig. 4. The staff of the Laboratory X-Ray Diffraction Analysis (IMC). From left to right: Boris Shivachev, Rositsa Petrova, Luiza Dimova Yana Tzvetanova, Ognyan Petrov, Vladislav Kostov-Kytin.

President of the Board, and Rositsa Nikolova, Vice-President. The initiative for this move started during the 1st National Crystallographic Symposium that took place on 22–23 October 2009 in the National Museum “Earth and Man”. The Board applied for membership of BCS in IUCr at the XXII General Assembly and Congress (IUCr) in Madrid, 2011. Bulgarian Crystallographic Society announces its decision to become a member of UICr (adhering body, category I) and **has been approved by the General Assembly on August, 25, 2011.**

The 2nd Bulgarian National Crystallographic Symposium

The 2nd Bulgarian National Crystallographic Symposium was announced by the already established Bulgarian Crystallographic Society.

The Second National Crystallographic Symposium (NCS’10) was organized by the University of Sofia, Faculty of Chemistry, and Organizing Committee headed by Prof. Tony Spassov with the support of the Earth and Man National Museum – Sofia, UNION project, Geological Institute – BAS, Institute of General and Inorganic Chemistry – BAS, Institute of Mineralogy and Crystallography – BAS. The 3-day event, held from 21st to 23th of October (2010) at the Earth and Man National Museum, Sofia, has gathered more than 100 participants from 6 countries. In accordance with the resolutions of the First Crystallographic Symposium (NCS’09), the event scope was extended with international participation. The organizers of NCS’10 invited leading researchers from abroad to inspire the interdisciplinary audience and attract young researchers to this important field of science. The invited speakers were Prof. Bernt Krebs (University of Münster, Germany), Prof. Mois Aroyo (University of the Basque Country, Bilbao, Spain), Prof. Borianna Mihailova (University of Hamburg, Germany), Prof. Ramiza Rastsvetaeva (Institute of Crystallography RAS, Moscow, Russia), Dr. Stanislav Ferdov (University of Minho, Portugal), and Dr. Milen Gateshki (Application Specialist, PANalytical).

Main purpose of the meeting was to create background for the crystallographic community in Bulgaria to meet and share knowledge and experience in modern crystallographic approaches of matter study achieved by scientists from national research institutes and universities in the fields of crystallography, crystal chemistry, crystal physics,

mineralogy and materials science. NCS’10 offered the opportunity for young scientists in various disciplines of Crystallography to present their research and exchange new ideas during the round table discussions. The most outstanding presentations from young scientists in all topics were awarded.

Special acknowledgements are due to the sponsors of the 2th National Crystallographic Symposium **PANalytical, Bruker AXS, TEAM OOD.**

The contributions presented at the Second National Crystallographic Symposium were given the opportunity to be published in a special issue (Proceedings of the 2nd National Crystallographic Symposium) of the Journal “Bulgarian Chemical Communications” (Bul. Chem. Comm. 43/2 2011). The acceptance of the papers was based on the Journal’s normal reviewing procedure with Guest editor Prof. Tony Spassov.



Fig. 5. Participants at the 2nd National Crystallographic Symposium

The 3rd Bulgarian National Crystallographic Symposium

The 3rd Bulgarian National Crystallographic Symposium took place on October 3–5 2011 in the National Museum “Earth and Man”. The constituted Organizing Committee was co-chaired by Prof. Daniela Kovacheva (Institute of General and Inorganic Chemistry, BAS) and Prof. Thomas Kerestedjian (Geological Institute, BAS).

The “Third National Crystallographic Symposium” (NCS2011) was organized by the Institute of General and Inorganic Chemistry – BAS, the Geological Institute – BAS and with the assistance of

the University of Sofia “St. Kl. Ohridski”, Faculty of Chemistry and the Institute of Mineralogy and Crystallography – BAS.

Along with invited distinguished lecturers in key fields of crystallography, the event was based also on the participation of Bulgarian scientists, working abroad and using the experience of crystallographic institutions. A testimony for the growing interest to the National Crystallographic Symposium is the fact that the Third symposium was attended by over 100 participants. With up to 14 hours of continuous face-to-face communication each symposium day, the attendees found out about the latest developments in research and industry, participated in workshops, improve their skills at hands-on demonstrations.

Again the Journal “Bulgarian Chemical Communications” gave the opportunity to published in a special issue the presented scientific results of the participating crystallographers (Bulgarian Chemical Communications, Volume 44, Special Issue, 2012).

During 2011 the International Union on Crystallography proclaimed an initiative for publishing materials about the development of Crystallography in the countries of South East Europe. Such invitation was submitted to the Bulgarian Crystallographic Society and the President at that time Assoc. Prof. Ognyan Petrov submitted the needed material for the history and present state of Crystallography in Bulgaria (**Newsletter – special issue volume 19, Number 4, 2011 Crystallography in South East Europe – Crystallography in Bulgaria – Ognyan Petrov**).

The 4th Bulgarian National Crystallographic Symposium

The successive Fourth National Crystallographic Symposium (NCS’12) was held in “Assen Zlatarov” hall of the University of Chemical Technology and Metallurgy, Sofia, November 1–3, 2012 and was organized under the auspices of the Bulgarian Crystallographic Society (BCS) by University of Chemical Technology and Metallurgy, Institute of Mineralogy and Crystallography – BAS, Institute of General and Inorganic Chemistry – BAS, Geological Institute – BAS, and Institute of Catalysis – BAS. The Organizing Committee chaired by Assoc. Prof. Ognyan Petrov invited leading researchers from abroad to inspire the interdisciplinary audience and attract young researchers. The organizers

of NCS’12 invited leading researchers from abroad to inspire the interdisciplinary audience and attract young researchers to this field of science.

A special issue of the “Bulgarian Chemical Communication” journal was kindly offered and included full texts of reports given at the 4th National Crystallographic Symposium. A testimony for the growing interest to the National Crystallographic Symposium was the fact that this special issue collected 37 papers – a number exceeding by about 60% the ones in previous NCS issues. They cover a wide interdisciplinary range – mainly synthesis, structure and properties of a variety of materials – “glaserite” type compounds, ion-exchanged natural zeolites and microporous titanosilicates, apatite, Ni-Al layered double hydroxides, ZnO powders, borate materials, ZnFe₂O₄, LiNbO₃ and LiTaO₃, TeO₂/TiO₂ powders, Fe-doped TiO₂ nanoparticles, magnesium chlorates, amorphous Ge–Te–In system, molybdenum modified aluminum bronze, bacteria and DNA samples, proteins, urea and thiourea adducts, orthodontic archwires, polycaprolactam, hybrid materials, organic dyes. Special attention is paid to the 100 years Anniversary of X-ray diffraction discovery.

Special acknowledgements are due to the sponsors of the 4th National Crystallographic Symposium – **ASTEL, PANalytical, Bruker AXS, RETSCH**, and Labexpert Ltd. for their help and making the symposium a success and this special issue possible.

The 5th Bulgarian National Crystallographic Symposium

The Fifth National Crystallographic Symposium with international participation (NCS’14) took place from 25th to 27th September, 2014, at the University of Chemical Technology and Metallurgy – Sofia and was organized under the auspices of the Bulgarian Crystallographic Society by an Organizing Committee chaired by Assoc. Prof. Irena Mihailova and was dedicated to the officially proclaimed by the General Assembly of the United Nations International Year of Crystallography. The year 2014 marked the centennial of the birth of modern crystallography and we hope to have used this opportunity to stimulate and ignite an interest in crystallography amongst students, scientists and the general public.

The UN adopted the resolution that 2014 should be the International Year of Crystallography at the Sixty-Sixth General Assembly on 3 July 2012.



Following the tradition, established in the previous symposia of the Bulgarian Crystallographic Society, the organizers invited leading researchers from abroad and from Bulgaria. The invited speakers were: Prof. Dr. J. Manuel Perez-Mato (University of Basque Country, Bilbao, Spain), Prof. Dr. Ulrich Bismayer (University of Hamburg, Germany), Prof. Dr. Georgi Kirov (Sofia University “St. Kliment Ohridski”, Bulgaria), Prof. Dr. Ross Angel (University of Padova, Italy), Prof. Dr. Maria Lalia-Kantouri (Aristotle University of Thessaloniki, Greece), Dr. Tonya Vitova (Karlsruhe Institute of Technology, Germany), Dr. Jörg Rothe (Karlsruhe Institute of Technology, Germany), Dr. Emre S. Tasci, (Middle East Technical University, Ankara, Turkey), Dr. Biliiana Gasharova (Karlsruhe Institute of Technology, Germany), Dr. Krassimir Grabev (Karlsruhe Institute of Technology, Germany), Assoc. Prof. Dr. Rossitza Pentcheva (University of Duisburg-Essen, Germany).

One of the sessions of the Fifth National Crystallographic Symposium, was dedicated to Prof. Georgi Kirov from Sofia University “St. Kl. Ohridski”. He was the first **scientist** awarded an honorary sign by the Bulgarian Crystallographic Society for his overall activity and his outstanding contribution to the development of crystallography in Bulgaria.

As expected in the International Year of Crystallography this edition of the symposium NCS'14 was marked by the largest number of participants compared to the previous ones. Bulgarian scientists from eight universities, eleven institutes of the Bulgarian Academy of Sciences and scientists from universities and institutes from Germany, Italy, Spain, Turkey, Greece, the Republic of Macedonia, USA and Egypt submitted 27 oral and 90 poster presentations. It is also a great achievement that over 30% of the participants in NCS'14 were students, PhD students and young scientists who actively participated in the poster sessions. An award for the Best Poster Contribution by young scientist was announced and given.

Already traditionally, a special issue of Bulgarian Chemical Communications Journal was offered to publish 66 studies, presented at the Fifth National

Crystallographic Symposium with international participation NCS'14.

Special acknowledgements are due to the sponsors of the 5th National Crystallographic Symposium – **PANalytical, Bruker AXS, Rigaku, AQUACHIM,, Oxford Cryosystems, FOT Ltd, Labexpert Ltd., Lab Technics Engineering, and the Ministry of Education and Science (Bulgaria).**

The 6th Bulgarian National Crystallographic Symposium

The 6th National Crystallographic Symposium (NCS2016), held in the Grand Hall of the Bulgarian Academy of Sciences, on 05–07 October 2016 was the successive initiative of the project started in the beginning of 2009 by a group of Bulgarian crystallographers – enthusiasts and it was again conducted under the auspices of the Bulgarian Crystallographic Society (BCS). NCS2016 was conducted by Organizing Committee co-chaired by Prof. Boris Shivachev and Assoc. Prof. Daniela Karashanova.

The organizers in conjunction with BCS have awarded a special honorary sign to Prof. Kostadin Petrov from the Institute of General and Inorganic Chemistry of Bulgarian Academy of Sciences. He was the first amongst the enthusiasts to start to act for the establishment of an independent Crystallographic Society in Bulgaria. The National Crystallographic Committee, which was chaired by Prof. Kostadin Petrov laid down the foundations for the appearance of the Bulgarian Crystallographic Society in 2009.

Invited lecturers of the NCS2016 were leading researchers in their respective fields: Svetlana Mintova, ENSICAEN, France, Prof. Katharina Fromm, University of Fribourg, Switzerland, Prof. Krzysztof Wozniak, University of Warsaw, Poland, Prof. Atul Khanna, Guru Nanak Dev University, India, Prof. Srebri Petrov, University of Toronto, Canada, Prof. Boriana Mihailova, University of Hamburg, Germany, Evdokiya Salamanova, Karolinska Institute, Sweden, Prof. Bogdan Rangelov, IC–BAS, Prof. Pavleta Shestakova, IOCCP – BAS, Prof. Radostina Stoyanova IGIC – BAS, Prof. Yuri Kalvachev, IMC-BAS, Ivanina Sergeeva, IG-BAS, Prof. Alexander Karamanov, IPCBAS, Liliya Vladislavova, Otto-Schott-Institut für Materialforschung, Friedrich-Schiller-Universität Jena, Germany, Prof. Tzonko Kolev, IMBBAS, Prof. Galina Gencheva, Sofia University.

The audience featured 110 registered scientists from seven Bulgarian universities, 16 institutes of the Bulgarian Academy of Sciences and scientists from universities and institutes from Poland, Switzerland, Germany, France, Sweden, Italy, Slovakia, Spain, Estonia, Turkey, the Republic of Macedonia, Czech Republic, Canada, USA and India. A total of 22 oral and 65 poster presentations involved more than 250 authors to present their investigations during the three days of the Symposium. It is worth noting that over 50% of the participants were students, PhD students and young scientists who actively participated in the poster sessions. For the second time the organizers were helped by the Ministry of Science and Education and the Bulgarian National Science Fund through a grant (DPMNF 01/13 – 27.09.2016) especially targeting the young scientists.

The progress in the level of experimental techniques – possibilities emerging from new, intense, tuneable and precisely focused X-ray beams, as well as from high resolution, sensitive, energy dispersive detectors were presented by our kind sponsors: **TA instruments, Jeol, Bruker, Panalytical, Zeiss, ELTA'90, Aquachim, Labexpert, InfoLab.**

The Symposium attracted the attention of several Bulgarian Official Institutions: the vice-president of the Bulgarian Parliament Ivan Ivanov, members of the Parliament's Commissions: for "Education and science", "Children, Youths and Sports", "Environment and Water", Parliament's Deputy Chair-

persons Borislav Velikov and Prof. Vili Lilkov, the Rector of the University of Chemical Technology and Metallurgy, Prof. Mitko Georgiev and the President of Bulgarian Academy of Sciences, represented by the vice-president Corresponding member Prof. Nikolay Miloshev.

Again a special issue of Bulgarian Chemical Communications Journal was offered to publish 17 full papers, presented at the Sixth National Crystallographic Symposium with international participation NCS'2016.

The 7th Bulgarian National Crystallographic Symposium

The 7th National Crystallographic Symposium (NCS'18), took place on 03–05 October, 2018 at the University of Chemical Technology and Metallurgy, Sofia, organized by the Board of The Bulgarian Crystallographic Society and conducted by Organizing Committee chaired by Prof. Zara Cherkezova-Zheleva. The presented investigations were focused on the current topics in material design and preparation, advanced characterisation techniques. 20 oral and 67 poster presentations focused on the crystallography were presented by 165 participants from 7 countries (see the photo). 39 of all 87 papers were presented by PhD students and young scientists.

An award for the best young scientist poster presentation was announced following the already



Fig. 6. Participants at the 7th National Crystallographic Symposium

existing tradition. The members of the international jury had the difficult task to select the winner. The NCS'18 award was given to Ekaterina Serafimova. In addition, Aleksandar Nikolov, Hristina Sbirikova-Dimitrova and Totka Todorova also received special certificates for the recognition of their achievements. The special honorary sign of the Bulgarian Crystallographic Society has been dedicated to Prof. Michail Maleev for his overall activity and his outstanding contribution to the development of crystallography in Bulgaria.

The lecturers of NCS'18 were leading researchers and experts from Europe and USA: David L. Bish, Indiana University, Bloomington, USA; Mira Ristic, Division of Materials Chemistry, Ruđer Bošković Institute, Croatia; Beatrix-Kamelia Seidlhofer, Helmholtz-Zentrum Berlin für Materialien und Energie GmbH, Germany, CALIPSOplus; Vladimir Stilinović, Department of Chemistry, University of Zagreb; George Tzvetkov, Sofia University; Angel Ugrinov, Department of Chemistry and Biochemistry, North Dakota State University, USA; Ana Proykova, Sofia University; Boris Shivachev, IMC-BAS; Hristo Kolev, IC-BAS; Vladislav Kostov-Kytin, IMC-BAS; Krastyo Buchkov, ISSP-BAS; Aleksandar Nikolov, IMC-BAS; Zara Cherkezova-Zheleva, IC-BAS.

Top presentation was given by Prof. David L. Bish – “**The Mars Science Laboratory Experience**” giving first results from the studies on the surface of the Planet Mars.

Special guests of the Symposium were Officials from Bulgarian Institutions: Rector of the University of Chemical Technology and Metallurgy, Prof. Mitko Georgiev represented by the Vice-Rector for Research Prof. Emil Mihailov, General Scientific Secretary of the Bulgarian Academy of Sciences Prof. Evdokia Pasheva, and Mrs. Zlatina Karova, Head of the Transnational Scientific Initiatives Unit at Science Directorate, Ministry of Education and Science.

The symposium NCS'18 has been organized with the financial support of the **National Science Fund, contract № DPMNF 01/37/2018**. We also acknowledge the financial support of sponsors of the 7th National Crystallographic Symposium – **Malvern-PANalytical, ROFA, Aquachim, Lab-expert, InfoLab and Eurotest Control**.

Also, as a tradition a special issue of the “Bulgarian Chemical Communication” journal was specified which gathered selected full text articles

(30 in number) from scientific investigations presented during the 7th National Crystallographic Symposium (NCS'18).

The 8th Bulgarian National Crystallographic Symposium

The 8th National Crystallographic Symposium with international participation (NCS'21), which took place from 1st to 4th September at the Creativity House of the Bulgarian Academy of Sciences, Varna. (Initially, this successive symposium was planned for 2020 but due to COVID19 pandemic it was postponed with one year).

Two colleagues and outstanding scientists – Prof. Andrei Apostolov and Assoc. Dr. Venelin Krastev from the Faculty of Physics, Sofia University “St. Kl. Ohridski” were decorated with the special honorary sign of the Bulgarian Crystallographic Society for their overall activity as co-founders of the Bulgarian Crystallographic Society and for their contribution to the development of crystallography in Bulgaria.

Lecturers at NCS'21 were leading researchers and experts from France, Germany and Canada as well as from Bulgaria: Christian Rüssel, Friedrich Schiller University, Germany; Valentin Valtchev, ENSICAEN, University of Caen – CNRS, France; Valentina Ivanova, Institut List, CEA Saclay Nano-INNOV, Commissariat à l'énergie atomique et aux énergies alternatives, France; Ognyan Petrov, IMC-BAS, Bulgaria; Svetoslav Stankov, Institute for Photon Science and Synchrotron Radiation, Karlsruhe Institute of Technology, Germany; Tanya Vitova, Institute for Nuclear Waste Disposal, Karlsruhe Institute of Technology, Germany; Snezana Bakardjieva, Institute of Inorganic Chemistry of the Czech Academy of Sciences, Czech Republic; Plamen Tchoukov, TCH NanoSolutions, Edmonton, Canada; Martin Fabián, Institute of Geotechnics, Slovak Academy of Sciences, Slovakia; Venelin Krastev, Sofia University “St. Kl. Ohridski”, Bulgaria; Liliya Vladislavova, EMPA, Switzerland; Silvana Dimitrijević, Mining and Metallurgy Institute Bor, Serbia; Zara Cherkezova-Zheleva, IC-BAS, Bulgaria; Ruzha Harizanova, UCTM-Sofia, Bulgaria.

The investigations presented at NCS'21 were focused on the current topics in materials design and preparation, as well as on various advanced characterization techniques. 18 oral and 59 poster presen-

tations encompassing different topics and aspects of crystallography were presented by 97 participants from 17 countries. 22 out of 77 papers were presented by PhD students and young scientists. They had the opportunity to disseminate their research results, to discuss problems, ask questions and to share their personal ideas and opinions. According to a well-established tradition, the organizers of NCS'21 encourage and support the initiation of successful scientific career of young researchers by awarding the best young scientist poster presentations as recognition of their achievements.

The symposium NCS'21 has been organized with the kind financial support of our traditional partners and sponsors – **Malvern-PANalytical, Aurubis-Bulgaria, Aquachim, Labexpert, InfoLab, ELTA'90 and Gravelita Ltd.**

Again a special issue of Bulgarian Chemical Communications journal was available for a selection of full text articles from scientific investigations presented at the 8th National Crystallographic Symposium with international participation (NCS'21).

International and National workshops, schools, and other activities of the Bulgarian Crystallographic Society

After the Fourth National Crystallographic Symposium (NCS'12) the Board of BCS decided to enlarge activities in direction of attracting students, PhD students and young scientists by organizing workshops, schools and lectures on basic crystallographic items and courses, which may ensure scientific background for their future scientific carriers.

International school on fundamental crystallography (2013)

The International school on fundamental crystallography: Introduction to International Tables for Crystallography, Vol. A: Space-group symmetry and Vol. A1: Symmetry relations between space groups was at Gulechitza winter resort, Bulgaria, in the period 30 September – 5 October, 2013, and organized by the BCS, the Institute of Mineralogy and Crystallography – BAS and the IUCr Commission on Mathematical and Theoretical Crystallography and the European Crystallographic Association. Chair of the Organizing Committee was Prof. Rositsa Nikolova.

Invited lecturers were **Prof. Mois Aroyo** and **Prof. Massimo Nespolo** from the IUCr Commission on

Mathematical and Theoretical Crystallography. 31 young researchers took part coming from Bulgaria, Spain, Italy, Israel, Turkey, and Macedonia.

In this period the given lectures were: **Massimo Nespolo**: Introduction, symmetry in two and three dimensions; Symmetry operations with a screw or glide components. **Mois Aroyo**: Matrix algebra; Point groups; Symmetry operations; Space groups; Structure tools. **Mihail Abrashev**: X-ray diffraction. **E. S. Tasci**: Tools for Phase Transitions. **Boris Shivachev**: Refinement strategies.

International Year of Crystallography – seminar organized by BCS in honor of this world wide recognition (2014)

The seminar was conducted in the Institute of Mineralogy and Crystallography, Bulgarian Academy of Sciences (24 May, 2014). The given lectures were: Transmission Electron Microscopy in morphological and phase analyses of modern materials (**Prof. Daniela Karashanova**, IOMT-BAS); Indexing using powder XRD patterns (**Prof. Vladislav Kostov-Kytin**, IMC-BAS), and demonstration of apparatus for Electron Microscopy and preparation of samples for study (Medical Technics Engineering).

International Year of Crystallography – European night of Scientists (2014)

This event was organized by the Bulgarian Academy of Sciences on 26 September, 2014, devoted to its 145 Anniversary. It was conducted in the frame of the Project **K-TRIO 2**, financed by the European Commission on the activities of Maria Skłodowska Curie and the Program “Horizon 2020”.

One of the topic lectures “**International Year of Crystallography**” was given by Prof. Rositsa Nikolova (Institute of Mineralogy and Crystallography-BAS) – President of the Bulgarian Crystallographic Society. Also, Assoc. Prof. Rositsa Titorenkova from this institute has organized and presented a Cabinet on curiosity “**Growing the Crystal**”.

Special presentation was given by Dr. Milen Kadyiski from the Institute of Mineralogy and Crystallography-BAS during the Night of Scientists organized by “ANGEL KANCHEV” UNIVERSITY OF RUSE. In the Café scientifique “Crystallography in the Scientific Debate” he gave the lecture – Importance of Crystallography for Science, Society and Business during 21 century”

Program “EUROPE 2014” – Contract “Yellow Bricks” between Sofia Municipality and the Bulgarian Crystallographic Society

The scientific project “Study of the composition, structure, properties and way of production of the yellow bricks in Sofia” was successfully finished by specialists from the Institute of Mineralogy and Crystallography-BAS, Institute of Physical Chemistry, the University of Mining and Geology, and the University of Architecture, Civil Engineering and architecture under the auspices of the Bulgarian Crystallographic Society. Multiple investigations were done on the original bricks and the samples prepared from **marl** material from Bulgarian deposit. The made conclusions concern possible ways for production of “authentic” bricks and recommendations were given for selecting of raw materials from Bulgaria for future production. Laboratory objects were synthesized equivalent to the original “yellow bricks” using different methods and raw materials.

The Final Report of this Project was officially defended and deposited in the Museum of Sofia.

International School on Introduction in the Rietveld structure refinement (2015)

The School was held in the hotel of the campus of the Bulgarian Academy of Sciences, Sofia 1113,

Bulgaria (28 September – 3 October 2015). The Organizing Committee was chaired by Prof. Daniela Kovacheva. This six day long school aimed to introduce participants to the way the information about crystal structure and sample microstructure is contained in X-ray powder diffraction patterns and how to get use of it. The school provided a **set of lectures**, devoted to the main aspects of crystal structure description and fundamentals of powder diffraction. Main concepts, that Rietveld structure refinement is based on, were covered as well. **Practical sessions** were designed to initiate and promote basic skills for working with powder diffraction data and respective data treatment software. Tutors were on disposal to help participants in the course of training.

As a whole 15 basic lectures were given by **Juan Rodriguez-Carvajal** (France), **Michael Evans** (Bruker–AXS, Karlsruhe, Germany), **Milen Gateshki**, PANALytical, Nederland, **Daniela Kovacheva** (Institute of General and Inorganic Chemistry, Bulgarian Academy of Sciences), **Ognyan Petrov** (Institute of Mineralogy and Crystallography, Bulgarian Academy of Sciences), **Boris Shivachev** (Institute of Mineralogy and Crystallography, Bulgarian Academy of Sciences), and **Peter Tzvetkov** (Institute of General and Inorganic Chemistry, Bulgarian Academy of Sciences).



Fig. 7. Group photo of the Participants

*School – Introduction to powder X-ray
Diffraction (2017)*

This school was conducted in Bulgarian and specially devoted to Bulgarian students and young researchers in the period 19–23 June, 2017 and hosted by the University of Chemical Technology and Metallurgy, Sofia. Prof. D. Kovacheva was chair of the Organizing Committee. Participated 40 young and even older researchers. During the 5 days of the school were given 20 lectures and conducted 20 trainings on the basic principles of crystals, crystal lattices and symmetry, X-rays and diffraction principles, powder XRD data and processing, phase identification and quantification, indexing, etc.

The Lecturers were: Assoc. Prof. Tsveta Stanimirova (FGG, Sofia University), Prof. Daniela Kovacheva (IGIC-BAS), Prof. Tomas Kerestedjan (GI_BAS). Prof. Srebri Petrov (University of Toronto), Assoc. Prof. Luiza Dimova (IMC-BAS), Assoc. Prof. Peter Tsvetkov (IGIC-BAS), and Prof. Ognyan Petrov (IMC-BAS).

*Second National School on Introduction
to Powder X-ray Diffraction (2019)*

This initiative was organized by BCS to continue the tradition to educate youngsters in crystallographic approaches and methods. The event was hosted by the Institute of Optical Materials and Technologies – BAS and took place on 19–21 June, 2019.

The main topics were covered by prominent scientists from institutes of BAS and concerned: CIF files, data conversion and software (Boris Shvachev); Small angle diffraction and thin films diffraction (Georgy Avdeev); Quantitative and semi-quantitative powder XRD analyses (Luiza Dimova); Line profile analysis and microstructure (Vladislav Kostov-Kytin)

*National School on Electron Microscopy and
its Application in Material Science*

Bulgarian Crystallographic Society also organized this event at the same place, which just followed (24–26, June, 2019) the previous one. The lecturers from institutes of BAS were D. Karashanova, B. Rangelov, B. Georgieva, M. Tarassov, S. Stoitsova, and Z. Paunova. They discussed the following main topics: principles of SEM and TEM,

element analysis and surface studies, ionic microscopy, preparation approaches for samples, study of biological objects, etc.

*Workshop for training specialists from Republic
of Kosovo on powder XRD methods (2017)*

In the period 5–11 November, 2017 the Institute of Mineralogy and Crystallography-BAS and the Institute of General and Inorganic Chemistry-BAS responded to the desire of representatives of the Geological Survey of the Republic of Kosova and the University “Isa Boletini” in Kosovska Mitrovitsa for organizing a “Intensive Practical Course on Powder X-ray Diffraction” with the help of the Bulgarian Crystallographic Society. They came and participated actively.

The given lectures by Prof. Daniela Kovacheva and Prof. Ognyan Petrov concerned basic items in the description of the solid substances, the properties of the X-rays and the principles for using them in the analyses of powder materials. The training included qualitative and quantitative analyses of geological samples. The colleagues from the Republic of Kosovo showed interest about collaboration and obtaining of methodical help in characterization of materials, education of PhD students as well as participation in scientific events in Bulgaria. This happened to be a good example for collaboration between scientists from countries in the Balkan region and the Bulgarian Crystallographic Society.

**Perspectives for sustainable development
of the Bulgarian Crystallographic Society**

Without no doubt it may be stated that the Bulgarian Crystallographic Society during this 10-Year existence has performed profound organizational, logistic, and popularization activities. One can only advise all this to continue with the same rhythm and consistency, namely, to continue organizing of subsequent Symposia in a row as well as international and national schools for young scientific personnel.

Sustainable popularization of Crystallography is also needed.

It is probably the time that came for strengthening the international relations with crystallographic societies, associations and groups from the neighbouring countries – Greece, Romania, Turkey, Serbia, North Macedonia, and possible others.

BULGARIAN CHEMICAL COMMUNICATIONS

Instructions about Preparation of Manuscripts

General remarks: Manuscripts are submitted in English by e-mail or by mail (in duplicate). The text must be typed double-spaced, on A4 format paper using Times New Roman font size 12, normal character spacing. The manuscript should not exceed 15 pages (about 3500 words), including photographs, tables, drawings, formulae, etc. Authors are requested to use margins of 3 cm on all sides. For mail submission hard copies, made by a clearly legible duplication process, are requested. Manuscripts should be subdivided into labelled sections, e.g. **Introduction, Experimental, Results and Discussion, etc.**

The title page comprises headline, author's names and affiliations, abstract and key words.

Attention is drawn to the following:

a) **The title** of the manuscript should reflect concisely the purpose and findings of the work. Abbreviations, symbols, chemical formulas, references and footnotes should be avoided. If indispensable, abbreviations and formulas should be given in parentheses immediately after the respective full form.

b) **The author's** first and middle name initials, and family name in full should be given, followed by the address (or addresses) of the contributing laboratory (laboratories). **The affiliation** of the author(s) should be listed in detail (no abbreviations!). The author to whom correspondence and/or inquiries should be sent should be indicated by asterisk (*).

The abstract should be self-explanatory and intelligible without any references to the text and containing not more than 250 words. It should be followed by key words (not more than six).

References should be numbered sequentially in the order, in which they are cited in the text. The numbers in the text should be enclosed in brackets [2], [5, 6], [9–12], etc., set on the text line. References, typed with double spacing, are to be listed in numerical order on a separate sheet. All references are to be given in Latin letters. The names of the authors are given without inversion. Titles of journals must be abbreviated according to Chemical Abstracts and given in italics, the volume is typed in bold, the initial page is given and the year in parentheses. Attention is drawn to the following conventions:

a) The names of all authors of a certain publications should be given. The use of "*et al.*" in

the list of references is not acceptable.

b) Only the initials of the first and middle names should be given.

In the manuscripts, the reference to author(s) of cited works should be made without giving initials, e.g. "Bush and Smith [7] pioneered...". If the reference carries the names of three or more authors it should be quoted as "Bush *et al.* [7]", if Bush is the first author, or as "Bush and co-workers [7]", if Bush is the senior author.

Footnotes should be reduced to a minimum. Each footnote should be typed double-spaced at the bottom of the page, on which its subject is first mentioned.

Tables are numbered with Arabic numerals on the left-hand top. Each table should be referred to in the text. Column headings should be as short as possible but they must define units unambiguously. The units are to be separated from the preceding symbols by a comma or brackets.

Note: The following format should be used when figures, equations, *etc.* are referred to the text (followed by the respective numbers): Fig., Eqns., Table, Scheme.

Schemes and figures. Each manuscript (hard copy) should contain or be accompanied by the respective illustrative material as well as by the respective figure captions in a separate file (sheet). As far as presentation of units is concerned, SI units are to be used. However, some non-SI units are also acceptable, such as °C, ml, l, etc.

The author(s) name(s), the title of the manuscript, the number of drawings, photographs, diagrams, etc., should be written in black pencil on the back of the illustrative material (hard copies) in accordance with the list enclosed. Avoid using more than 6 (12 for reviews, respectively) figures in the manuscript. Since most of the illustrative materials are to be presented as 8-cm wide pictures, attention should be paid that all axis titles, numerals, legend(s) and texts are legible.

The authors are asked to submit **the final text** (after the manuscript has been accepted for publication) in electronic form either by e-mail or mail on a 3.5" diskette (CD) using a PC Word-processor. The main text, list of references, tables and figure captions should be saved in separate files (as *.rtf or *.doc) with clearly identifiable file names. It is essential that the name and version of

the word-processing program and the format of the text files is clearly indicated. It is recommended that the pictures are presented in *.tif, *.jpg, *.cdr or *.bmp format, the equations are written using "Equation Editor" and chemical reaction schemes are written using ISIS Draw or ChemDraw programme.

The authors are required to submit the final text with a list of three individuals and their e-mail addresses that can be considered by the Editors as potential reviewers. Please, note that the reviewers should be outside the authors' own institution or organization. The Editorial Board of the journal is not obliged to accept these proposals.

EXAMPLES FOR PRESENTATION OF REFERENCES

REFERENCES

1. D. S. Newsome, *Catal. Rev.–Sci. Eng.*, **21**, 275 (1980).
2. C.-H. Lin, C.-Y. Hsu, *J. Chem. Soc. Chem. Commun.*, 1479 (1992).
3. R. G. Parr, W. Yang, *Density Functional Theory of Atoms and Molecules*, Oxford Univ. Press, New York, 1989.
4. V. Ponec, G. C. Bond, *Catalysis by Metals and Alloys* (Stud. Surf. Sci. Catal., vol. 95), Elsevier, Amsterdam, 1995.
5. G. Kadinov, S. Todorova, A. Palazov, in: *New Frontiers in Catalysis* (Proc. 10th Int. Congr. Catal., Budapest, 1992), L. Guzzi, F. Solymosi, P. Tetenyi (eds.), Akademiai Kiado, Budapest, 1993, Part C, p. 2817.
6. G. L. C. Maire, F. Garin, in: *Catalysis. Science and Technology*, J. R. Anderson, M. Boudart (eds), vol. 6, Springer-Verlag, Berlin, 1984, p. 161.
7. D. Pocknell, *GB Patent 2 207 355* (1949).
8. G. Angelov, PhD Thesis, UCTM, Sofia, 2001.
9. JCPDS International Center for Diffraction Data, Power Diffraction File, Swarthmore, PA, 1991.
10. *CA* **127**, 184 762q (1998).
11. P. Hou, H. Wise, *J. Catal.*, in press.
12. M. Sinev, private communication.
13. <http://www.chemweb.com/alchem/articles/1051611477211.html>.

CONTENTS

<i>Preface</i>	5
<i>V. Kurteva, R. Rusew, B. Shivachev, R. Nikolova</i> , Tandem hydroxymethylation-acetal protection of phenols under Eschweiler-Clarke conditions. The activation role of phenyl-azo moiety	7
<i>S.A. Yaneva, N.G. Rangelova, L.I. Aleksandrov, N.V. Savov</i> , Laccase-based optical biosensors for detection of phenol.....	15
<i>P.S. Vassileva, L.P. Ivanova, A.K. Detcheva</i> , Adsorption studies of a material based on the medicinal plant yarrow for the removal of Cu ²⁺ ions from aqueous solutions.....	21
<i>V. Kostov-Kytin, R. Stoyanova, D. Marinova</i> , Manifestation of Vegard's law on the example of synthetic mixed Co-Mn alluaudite-type phases.....	27
<i>I.K. Mihailova, R.G. Harizanova, N.I. Shtapleva, G.V. Avdeev, C. Rüssel</i> , Phase characterization of glass-ceramics with high iron oxide concentrations.....	33
<i>M. Gancheva, R. Iordanova, G. Avdeev, P. Ivanov</i> , Direct mechanochemical synthesis and optical properties of BaWO ₄ nanoparticles.....	41
<i>R. Harizanova, M. Pernikov, W. Wisniewski, G. Avdeev, I. Mihailova, C. Rüssel</i> , Phase formation and dielectric properties of strontium-substituted barium titanate glass-ceramics	
naerobic digester for generating bioenergy from an ethanol.....	47
<i>O. Petrov</i> , Analysis of structure factors (F_{hkl}) of meaningful XRD diffraction intensities for chemical determinations after ion-exchange and isomorphic substitutions in crystal structures.....	55
<i>O. Petrov</i> , Crystallography in Bulgaria and 10 years activities (2010–2020) of the Bulgarian Crystallographic Society.....	61
<i>INSTRUCTIONS TO AUTHORS</i>	72